Department Biologie I
Bereich Genetik
Ludwig-Maximilians-Universität München

Metabolic Signals and Pathways in Development of *Trypanosoma brucei*

Nicole Emmy Ziebart

Dissertation der Fakultät für Biologie,
Ludwig-Maximilians-Universität München
München, 2016

Erster Gutachter: **Prof. Dr. Michael Boshart**
Biozentrum der Ludwig-Maximilians-Universität München
Department Biologie I, Bereich Genetik

Zweiter Gutachter: **Prof. Dr. Kai Papenfort**
Biozentrum der Ludwig-Maximilians-Universität München
Department Biologie I, Bereich Mikrobiologie

Datum der Abgabe: 16.03.2016
Datum der mündlichen Prüfung: 06.10.2016

Eidesstattliche Erklärung

Ich versichere hiermit an Eides statt, dass die vorgelegte Dissertation von mir selbstständig und ohne unerlaubte Hilfe angefertigt wurde. Des Weiteren erkläre ich, dass ich nicht anderweitig ohne Erfolg versucht habe eine Dissertation einzureichen oder mich der Doktorprüfung zu unterziehen. Die folgende Dissertation liegt weder ganz, noch in wesentlichen Teilen einer anderen Prüfungskomission vor.

Nicole Emmy Ziebart
München, 15.03.2016

Statutory Declaration

I declare that I have authored this thesis independently, that I have not used other than the declared sources/resources. As well I declare, that I have not submitted a dissertation without success and not passed the oral exam. The present dissertation (neither the entire dissertation nor parts) has not been presented to another examination board.

Nicole Emmy Ziebart
Munich, 15.03.2016

Table of Contents

Abbreviations

2-HG	2hydroxyglutarate
α-KG	α-ketoglutarate
AAT	Animal African trypanosomiasis
ACH	acetyl-CoA thioesterase
ACL	ATP-dependent citrate lyase
ACN	acetonitril
ACO	aconitase
AK	adenylate kinase
AκCL	amino-ketobutyrate lyase
ALAT	alanine aminotransferase
ASCT	acetate:succinate CoA-transferase
ATP	adenosine triphosphate
BARP	brucei alanine-rich protein
BLAS	blasticidin resistance gene (blasticidin deaminase)
BLE	phleomycin resistance gene (phleomycin resistance protein)
BPS	bathophenanthroline disulphonic acid
BSF	bloodstream forms
CoA	coenzyme A
CS	citrate synthase
Cytc	cytochrome c
DHAP	dihydroxyacetone phosphate
DNA	desoxyribonucleic acid
EDTA	Ethylenediaminetetraacetic acid
EGTA	ethylene glycol-bis(2-aminoethylether)-*N*,*N*,*N′*,*N′*-tetraacetic acid
EMF	epimastigote forms
EtOH	ethanol
FAD	flavin adenine dinucleotide
FBPase	fructose 1,6-bisphosphatase
FCS	fetal calf serum
FHm	mitochondrial fumarase
Fig.	figure
FRDg	glycosomal fumarate reductase
FRDm	mitochondrial fumarate reductase
G6P	glucose 6-phosphate
G6PDH	glucose 6-phosphate dehydrogenase
G6Pase	glucose 6-phosphatase
GAPDH	glyceraldehyde 3-phosphate dehydrogenase
GC/MS	gas chromatography mass spectrometry
GCS	glycine cleavage system
GDH	glutamate dehydrogenase
Gluc	glucose
GlcNAc	N-acetyl D-glucosamine
GPDH	glycerol 3-phosphate dehydrogenase
GPI	glucose 6-phosphate isomerase
GPI	glycosylphosphatidylinositol
GSH	glutathione
HAT	Human African trypanosomiasis
HK	hexokinase
HYG	hygromycin resistance gene (hygromycin phosphotransferase)
ICL-like	isocitrate lyase-like
IDHg	glycosomal isocitrate dehydrogenase

IDHm	mitochondrial isocitrate dehydrogenase
IFA	immunofluorescence analysis
LB	lysogeny broth
LC/MS	liquid chromatography/mass spectrometry
LipDH	Lipoamide dehydrogenase
MDH	malate dehydrogenase
ME	malic enzyme
MeOH	methanol
MF	metacyclic forms
MS	malate synthase
MSP-B	major surface protease-B (metalloprotease)
MTS	mitochondrial targeting sequence
NADH/NAD^+	nicotinamide adenine dinucleotide (reduced/oxidized)
NADPH/$NADP^+$	nicotinamide adenine dinucleotide phosphate (reduced/oxidized)
NEO	neomycin resistance gene (aminoglycoside phosphotransferase)
OAA	oxaloacetate
OE	overexpression
OGDH	2-oxoglutarate dehydrogenase complex
P5CDH	pyrroline-5-phosphate carboxylate dehydrogenase
PAC	puromycin resistance gene (puromycin N-acetyltransferase)
PCF	procyclic forms
PDH	pyruvate dehydrogenase
PEP	phosphoenolpyruvate
PEPCK	phosphoenolpyruvate carboxykinase
PFA	paraformaldehyde
PFK	phosphofructokinase
PFR	paraflagellar rod protein
PGKB	phosphoglycerate kinase B
PPDK	pyruvate phosphate dikinase
PPP	pentose phosphate pathway
PRODH	proline dehydrogenase
PYK	pyruvate kinase
RBP6	RNA binding protein 6
$RBP6^+$	cells overexpressing RBP6
$RBP6^{Ti}$	cells tetracycline inducible for RBP6
RNA	ribonucleic acid
ROS	reactive oxygen species
RT	room temperature
SCS	succinyl-CoA synthetase
SDH	succinate dehydrogenase
SDS	sodium dodecylsulfate
SEM	standard error of mean
T7RNAP	T7-RNA-polymerase
TCA	tricarboxylic acid
TDH	threonine dehydrogenase
TETR	tetracycline repressor protein
Ti	tetracycline inducible
TPI	triose phosphate isomerase
UQ	ubiquinol UTR
VSG	variable surface glycoprotein
WB	Western blot
WHO	World health organisation
WT	wild type

Summary

While passing through the parasitic life cycle, trypanosomes are challenged by environments prevailing either in the mammalian host or the arthropod vector. It is inevitable for the parasites´ survival to adapt to available carbon sources accompanied by extensive remodelling of metabolic fluxes. Procyclic form (PCF) trypanosomes express all enzymes of the tricarboxylic acid (TCA) cycle, but the way trypanosomes make use of them differs from the canonical TCA cycle. Previous publications show that proline degradation involves the TCA cycle, yet there is no measurable CO_2 production in the TCA cycle from glucose in PCFs under culture conditions. Moreover, citrate is not a precursor of *de novo* lipid biosynthesis and enzymes of citrate metabolism are dispensable in bloodstream and procyclic form trypanosomes The objective of this work was to trace the citrate metabolism and to investigate whether it has a role in stage development. We found that an isocitrate dehydrogenase (IDH) isoform compartimentalized in glycosomes, but not the mitochondrial IDH, is the major sink for isocitrate. We provide proof for a pathway routing citrate produced by mitochondrial citrate synthase (CS) to the cytoplasm, where it is converted into isocitrate by a cytosolic aconitase (ACO) isoform to feed glycosomal IDHg. Even though CS, ACO and IDHg are not essential for growth in glucose- and glycerol-depleted conditions, expression of these enzymes is upregulated in absence of glucose and glycerol. We show that glucose and glycerol block development of the forms populating the tsetse organs. This was shown in a culture differentiation system based on the overexpression of RNA-binding protein 6 (RBP6). The RBP6 culture differentiation system was applied to analyse a set of metabolic null mutants. The ΔIDHg null mutant fails to develop metacyclic forms, a phenotype agreeing with the previous fly infection experiments, where ΔIDHg did not establish salivary gland infections. The fructose 1,6-bisphosphatase null mutant also blocks metacyclogenesis attributing gluconeogenesis a role in fly-development. IDHg has dual coenzyme specificity for NAD^+ and $NADP^+$. We hypothesize a role of IDHg in the NAD^+/NADH balance to promote gluconeogenesis and glyceroneogenesis, which is currently being investigated. Upon RBP6 overexpression, CS deficient cells develop forms with metacyclic morphology. Based on this observation and the functional irreversibility of the mitochondrial IDHm reaction shown by stable isotope labelling with [U-^{13}C] proline, we postulate the existence of an alternative isocitrate producing pathway, independently of CS and IDHm and suggest a reverse isocitrate lyase reaction consuming threonine-derived glyoxylate.

Zusammenfassung

Während Trypanosomen ihren parasitischen Lebenszyklus durchlaufen, werden sie durch die Bedingungen, die im Säugetierwirt und dem arthropoden Vektor vorherrschen, herausgefordert. Die Anpassung an die verfügbaren Kohlenstoffquellen geht einher mit einer umfangreichen Umgestaltung der Stoffwechselflüsse. Prozyklische Trypanosomen exprimieren alle Enzyme des Citratzyklus, aber wie sie Gebrauch von ihnen machen unterscheidet sich von dem kanonischen Citratzyklus. In vorangegangenen Publikationen wurde anhand von prozyklischen Trypanosomen unter Kulturbedingungen gezeigt, dass Prolin über den Citratzyklus abgebaut wird; von Glukose jedoch konnte keine CO_2 Produktion im Citratzyklus nachgewiesen werden. Es wurde gezeigt, dass Citrat nicht als Baustein für die *de novo* Lipidbiosynthese dient und die Enzyme des Citratstoffwechsels entbehrlich sind. Ziel dieser Arbeit war es, den Citratstoffwechsel nachzuvollziehen und herauszufinden, ob dieser eine Funktion in der Differenzierung zwischen den verschiedenen Stadien erfüllt. Wir haben nachgewiesen, dass Citrat im Mitochondrium von der Citrat-Synthase (CS) produziert und in das Cytoplasma transportiert wird. Im Cytosplasma wandelt eine Aconitase (ACO) Isoform Citrat in Isocitrat um und versorgt so die glycosomale IDHg mit Isocitrat. Obwohl CS, ACO und IDHg nicht essentiell für das Glucose- und Glyzerin-unabhängige Wachstum sind, wird ihre Expression durch Glucose- und Glyzerinentzug hochreguliert. Anhand des RNA-binding protein 6 (RBP6)-basierten Differenzierungssystems konnten wir in Kultur zeigen, dass Glukose und Glyzerin die Entwicklung zwischen den Stadien, welche die Organe der Tsetse Fliegen besiedeln, blockieren. Auch metabolische Nullmutanten wurden mithilfe des RBP6-basierten Differenzierungssystems auf Phänotypen untersucht. Die ΔIDHg Nullmutante entwickelt keine metazyklischen Formen. Dieser Phänotyp stimmt mit einem vorangegangenen Fliegenexperiment überein, in dem gezeigt wurde, dass die ΔIDHg Nullmutante die Tsetse Speicheldrüsen nicht besiedelt. Das Fehlen der Fruktose-1,6-bisphosphatase blockiert ebenfalls die Metazyklogenese in Kultur, woraus sich schließen lässt, dass die Glukoneogenese eine Funktion in der Entwicklung in der Fliege annimmt. Wir vermuten, dass die IDHg das glycosomale NAD^+/NADH Gleichgewicht beeinflusst, um Glukoneogenese und Glyzeroneogenese zu begünstigen. Zellen mit fehlender CS entwickeln Formen mit metazyklischer Morphologie, wenn man RBP6 überexprimiert. Aufgrund dieser Beobachtung und der, dass die mitochondriale IDHm Reaktion irreversibel ist, nehmen wir an, dass es einen alternativen Isocitrat-produzierenden Stoffwechselweg gibt, der unabhängig von CS und IDHm ist. Hier vermuten wir, dass Isocitrat durch die reverse Reaktion der Isocitrat-Lyase aus Succinat und Glyoxylat gebildet werden könnte.

1 Introduction

1.1 African trypanosomiasis- Epidemiology

Trypanosomes are flagellated eukaryotic protozoans that harbour a single mitochondrion stretching through the whole cell. The mitochondrial DNA comprises multiple copies of catenated minicircles and maxicircles that are condensed to a disk-shaped structure at the flagellar basal body, the kinetoplast (Lukeš et al., 2002). This structure is eponymous for the class of kinetoplasitida. Among the nonparasitic *Bodo species*, the pathogens *Leishmania spp*, *Trypanosoma spp* and *Cryptobia spp* are members of the class of kinetoplastida.

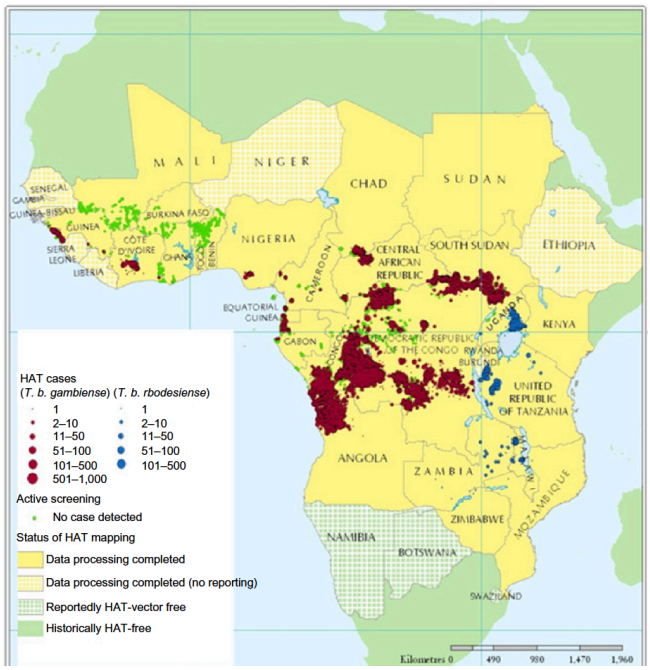

Figure 1 Geographic distribution of human African trypanosomiasis, recorded from 2000-2009 (Franco et al., 2014)

African trypanosomes are transmitted by tsetse fly species (*Glossina spp*), consequently, the geographical distribution depends on the presence of the vector. About 60 million human in 36 sub-saharan countries are at risk of getting human African trypanosomiasis (HAT) commonly known as "sleeping sickness" (WHO, 2012). Two *Trypanosoma brucei spp*, *T. b. rhodesiense* and *T. b. gambiense* are the causative agents of HAT each with distinct clinical symptoms. *T. b. gambiense* is responsible for about 98 % of the reported cases (WHO, 2015). This species cause a more chronic course of disease with patients being asymptotic over months or even years. *T. b. rhodesiense* infection is associated with an acute disease progression showing first symptoms after few month or even weeks. At late stage of infection, the parasites pass the blood brain barrier and the central nervous system is affected. Without medical treatment HAT is lethal. Current medications are often associated with severe side effects and hardly cure the disease at a late stage of infection (WHO, 2015). Animal African trypanosomiasis (AAT) is mainly caused by three species, *T. b. brucei, T. vivax* and *T. congolense* (WHO, 2015). As infected cattle produce less milk and meat, AAT is a big economical burden with an annual loss of

around 1.0 - 1.2 billion US$ (PAAT, 2015). In the human serum, the apolipoprotein L-I, also known as the trypanosome lytic factor, confers resistance to *T. b. brucei* (Vanhamme et al., 2003). Many species of wild life animals are trypanotolerant containing the disease progression and constitute a reservoir for AAT but also HAT (d'Ieteren et al., 1998). Macrophage migrating inhibitory factor (MIF) was identified in a comparative genetic analysis to be associated to prolonged survival of trypanotolerant animals. Low MIF levels are reported to be protective against anemia, a major cause of death of AAT (Stijlemans et al., 2014).

1.2 The parasite life cycle

In the course of a blood meal, an infected tsetse fly can transmit metacyclic trypanosomes through injection of its saliva. The metacyclic parasites differentiate into long slender forms, which replicate rapidly by binary fission. At late stage infection, bloodstream trypanosomes can traverse the blood-brain barrier and invade the central nervous system (Grab and Kennedy, 2008). After reaching a certain parasitaemia most of the trypanosomes differentiate into non-replicating short stumpy forms. The mechanism driving long-slender to stumpy form differentiation is based on parasitemia-dependent quorum sensing mediated by a yet unknown molecule termed stumpy inducing factor (SIF) (Dean et al., 2009; Reuner et al., 1997; Seed and Wenck, 2003). *In vitro* differentiation is triggered by *cis*-aconitate/citrate administration and cold shock (Brun and Schonenberger, 1981; Czichos et al., 1986; Engstler and Boshart, 2004; Ziegelbauer et al., 1990). Stumpy forms are pre-adapted to survival and differentiation in the tsetse midgut. The cell cycle arrest of stumpy forms decreases parasitemia limiting parasite virulence and prolonging host survival (Rico et al., 2013).

Various tsetse fly species serve as vector for the trypanosoma transmission cycle. Both male and female tsetse flies are hematophagous and can transmit the parasite. Even though the level of trypanosomiasis infection in mammals is high, the proportion of infected tsetse flies varies between 2 % and 20 %, depending on the tsetse fly species and trypanosoma species and focal area (Dyer et al., 2013). In the tsetse fly, trypanosomes are subjected to several bottlenecks and barriers reducing efficacy to establish midgut infection and restrict successful migration and maturation into infective metacyclic forms. Several traits promoting fly refractoriness have been reported, reviewed in (ROTUREAU and VAN DEN ABBEELE, 2013). Teneral tsetse flies at the day of eclosure are more susceptible to trypanosome infection than older flies (Walshe et al., 2011). In refractory flies, trypanosomes were cleared 5 days after ingestion of the infected blood meal (Gibson and Bailey, 2003).

It was shown that the microbiome has immunomodulatory effects on tsetse flies and influences the outcome of a trypanosome infection and thus vector competence (Weiss et al., 2013). The tsetse fly immune response is another obstacle that counteracts fly infection. The immunodefiency pathway (Imd) regulating antimicrobial peptide (AMP) production becomes activated upon trypanosoma infection (Lehane et al., 2003). Attacin, a member of AMP, was shown to be trypanocidal and constitutively expressed in refractory tsetse lines (Hu and Aksoy, 2005; Nayduch and Aksoy, 2007). Another tsetse protein affecting the outcome of infection was shown to be a glutamate-proline repeat protein (TsetseEP). Decreased TsetseEP levels result in elevated susceptibility to trypanosomal infection (Haines et al., 2010). However, the exact mode of action of TsetseEP is not known, yet. Further it was found that age and starvation influence the outcome of infection in the fly (Kubi et al., 2006).

Stumpy and long slender blood stream forms (BSFs) are ingested during infected blood meals. In the midgut, stumpy trypomastigotes differentiate into proliferating procyclic form (PCF) trypomastigotes, whereas long slender cells perish (Vickerman et al., 1988). After midgut colonization for about 6 days, a subpopulation of PCFs cross the peritrophic matrix (Gibson and Bailey, 2003). While migrating in the ectoperitrophic space along the digestive tract, trypanosomes develop into G0/G1 phase arrested mesocyclic forms (MCFs) with long flagella. MCF cells re-enter the alimentary canal at the proventriculus (ROTUREAU and VAN DEN ABBEELE, 2013). In the proventriculus, 4N post-mesocyclic trypomastigotes develop into a 4N epimastigote morphotype. Here, the soma becomes thinner and the relative position of the kinetoplast to the nucleus changes as the kinetoplast migrates from the posterior side to the anterior side of the nucleus. The proventriculus constitutes a barrier that only around 40 % of all established midgut infections can overcome (Peacock et al., 2012). In the paired ducts of the salivary glands, 4N epimastigote forms (EMF) complete a highly asymmetric division producing a long and a short epimastigote cell (Sharma et al., 2008; Van Den Abbeele et al., 1999). The long, more motile EMFs are thought to serve as shuttle to bring short EMF to the salivary glands (Van Den Abbeele et al., 1999). The journey from the proventriculus via foregut and mouthpart to the SG is forcing the EMFs through a bottleneck that only few cells and sometimes none can overcome. The resulting clonal expansion can support spread of rare genetic trypanosoma variants (Oberle et al., 2010). Short EMFs attach with their flagellum to the epithelium of the SGs to perform two distinct replication cycles (Vickerman, 1985). In the early phase, EMFs attached to the epithelium of the SGs proliferate symmetrically into identically progenies to colonize the SGs. Later, EMFs undergo asymmetric divisions. One progeny is similar to the mother

cell maintaining SG colonization. The other daughter cell is metacyclic (MF) and released into the SG lumen (Rotureau et al., 2012). Hundreds of infective MF cells are produced daily ready to be transmitted during the next blood meal (Otieno and Darji, 1979). Apart from this in SG, a meiotic life cycle has been described for haploid so-called promastigote-like cells. These gametes express homologues of meiotic genes and have the potential for cell fusion via interaction with the flagellum (Gibson, 2015; Peacock et al., 2014; Peacock et al., 2011).

So far, axenic cultivation of fly-stage trypanosomes was limited to PCFs (Brun and Schonenberger, 1979). Analyses of insect developmental stages required extensive fly infections. The parasite material gained from fly infection is limited restricting analytical methods within the bounds of possibility. Recently, Kolev and co-workers discovered an *in vitro* differentiation system. The system is based on inducible overexpression of a single RNA binding protein (*Tb*RBP6) in PCFs driving differentiation into developmental stages also found in tsetse flies (Kolev et al., 2012).

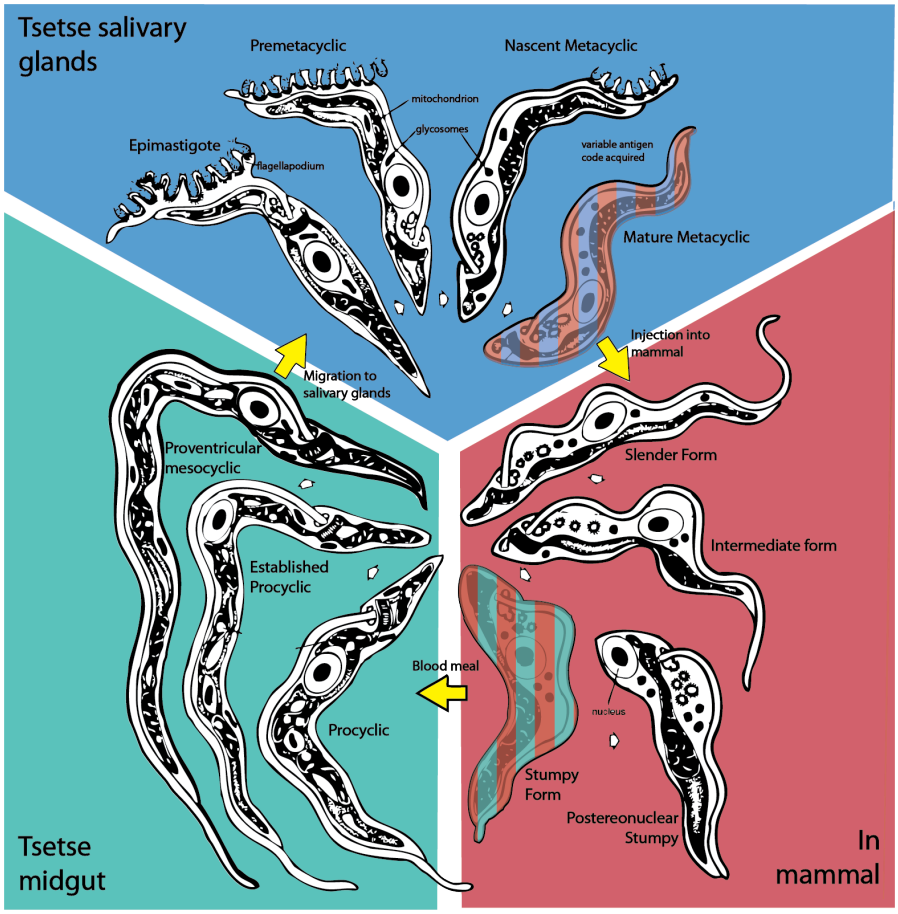

Figure 2 Life cycle *Trypanosoma brucei* (adapted and modified from (Vickerman, 1985)) Striped patterns indicate pre-adapted trypanosome forms for the transition from the mammalian host and tsetse fly vector and vice versa.

1.3 Changing of trypanosomes' coat in fly-stage

For bloodstream form (BSF) trypanosomes the glycosylphosphatidylinositol (GPI)-anchored variable surface glycoprotein (VSG) coat and its antigenic variation is well described (reviewed in (Horn and McCulloch, 2010)). BSF stumpy forms ingested during the blood meal differentiate into proliferating procyclic forms (PCF) in the tsetse fly midgut. This development requires substantial adjustments not only of cell morphology and metabolism but also in replacing the VSG coat by GPI-anchored procyclins. The present nomenclature of procyclins (formerly designated as procyclic acidic repetitive proteins (PARP)) is based on the single letter amino acid code of the C-terminal repeats. The name of the EP isoforms is based on the 21-27 repeats of the dipeptide glu-pro EP (Mowatt and Clayton, 1987; Roditi et al., 1987). Another isoform was designated GPEET as it consists of 5-6 repeats of the pentapeptide gly-pro-glu-glu-thr. GPEET is highly phosphorylated at 6 to 7 threonine residues of the GPEET motif and sensitive to proteolytic cleavage (Bütikofer et al., 1997; Mehlert et al., 1999). All EP1 (EP1-2) and EP3 (EP3-2, EP3-3 and EP3-4) isoforms are N-glycosylated ($Man5\text{-}GlcNAc_2$) and contain an asparagine-proline sequence being sensitive to hydrolysis by mild acid, whereas EP2 (EP2-1) lacks glycosylation and an asparagine-proline bond (Acosta-Serrano et al., 1999; Treumann et al., 1997). In the fly, the procyclin N-terminus is sensitive to proteolytic cleavage by fly proteases, whereas the repeat containing C-terminus is resistant. The C-terminus is thought to protect trypanosomes from fly proteases (Acosta-Serrano et al., 2001).

At the earliest stage of fly infection, co-expression of all procyclin isoforms replaces the VSG coat. After 24 h, the coat of early procyclics almost completely consists of GPEET and traces of EP. However, in late procyclic forms GPEET expression is suppressed and the glycosylated EP isoforms, mainly EP1 and lower amounts of EP3, form the surface protein coat (Urwyler et al., 2005; Vassella et al., 2001). Procyclin expression patterns vary among the different culture cell lines and depending on the number of *in vitro* passages (Bütikofer et al., 1997). Procyclins are arranged in polycistronic gene structures. *Cis*-acting secondary RNA structures at the 3'UTR regulate the stability of each mRNA after processing into monocistronic mRNAs (Furger et al., 1997; Hotz et al., 1997; Roditi et al., 1998). As procyclins are transcribed by RNA polymerase I in the nucleolus, it was found that proteins processing ribosomal RNAs also regulate GPEET expression on a post-transcriptional level (Schumann Burkard et al., 2013). Both glycerol and glucose control GPEET expression through the same glycerol response element (GRE), a 25 nucleotides long sequence in the 3'UTR (Vassella et al., 2000; Vassella et al., 2004). The differentiation of early to late PCF cells goes along with GPEET repression and migration into the ectoperitrophic space. GPEET repression is associated to enrichment of alternative GPEET mRNA species like

oligo(u)-tailed transcripts in late procyclic forms (Knusel and Roditi, 2013). Interestingly, procyclin expression is influenced by metabolic signals. Medium low in glucose as well as the presence of glycerol promote GPEET expression, whereas hypoxia negatively affects GPEET expression (Morris et al., 2002; Vassella et al., 2000). In the 3'UTR LII domain of the GPEET mRNA, the glycerol responsive element was identified destabilizing the mRNA in glucose-rich medium or upon glycerol withdrawal (Vassella et al., 2000; Vassella et al., 2004). Low glucose levels and silencing of enzymes involved in glucose metabolism results in a decrease of EP1 and EP3 surface expression and an increase of unglycosylated surface proteins (Morris et al., 2002). The acetate:succinate CoA-transferase / succinyl-CoA synthetase cycle (ASCT/SCS cycle) and the electron flow through the trypanosomal alternative oxidase, but not the Krebs cycle, promote GPEET expression on the surface (Vassella et al., 2004).

Mature epimastigote forms (EMFs) and metacyclic forms (MFs) residing in the salivary glands do not express procyclins (Acosta-Serrano et al., 2001; Urwyler et al., 2005). Instead, brucei alanine-rich protein (BARP) was identified on the surface of a subset of EMFs attached to the salivary glands (Urwyler et al., 2007). Initially, BARP was identified in BSF surface microdomains and termed bloodstream alanine-rich protein (Nolan et al., 2000). However, probing different BSF and PCF trypanosoma strains with BARP antiserum did not verify the presence of BARP in these stages (Urwyler et al., 2007). Metacyclic forms do not express BARP on the surface. Being the pre-stage for BSFs, metacyclic cells express one allele of a subset of variable surface glycoproteins (designated as M-VSG) on their surface (Graham and Barry, 1995).

Flagellar EF-hand calcium-binding proteins (calflagins) are differentially expressed. Calflagin exüression levels are 10-fold higher in BSF than in PCF *Trypanosoma brucei* and can be used as marker protein (Emmer et al., 2010). In contrast to EMFs, salivary gland metacyclic forms pre-adapted to survival in the mammalian host show a strong enrichment in calflagin (Rotureau et al., 2012). Three calflagin homologues (Tb24, Tb17 and Tb44) have been identified in *T. brucei* (Wu et al., 1994). The Tb24 association to lipid rafts in the flagellar membrane depends on a N-terminal dual acylation with a palmytoyl- and a myristoyl moiety (Emmer et al., 2009; Tyler et al., 2009). Organisation of calflagins in lipid rafts, as well as the presence of EF hand domains, suggest a role in calcium-mediated signalling. The course of *in vivo* infection with calflagin-deficient cells is milder, which seems to be associated to decreased resistance of the mutant to the adaptive immune response (Emmer et al., 2010). However, the molecular mechanism was not identified, yet.

1.4 External carbon sources utilized by insect-stage trypanosomes

Glucose is the primary energy source for mammalian cells and very abundant in the blood (Burgess, 2011). Initially it was published that blood stream form (BSF) trypanosomes have a simple carbon metabolism limited on carbohydrate consumption. The major end product of this aerobic-type glycolysis is pyruvate. Energy is produced by substrate level phosphorylation catalysed by pyruvate kinase in form of 2 mol ATP per 1 mol glucose in the cytosol (Durieux et al., 1991; Hannaert et al., 2003b; Michels et al., 2000). BSFs have a rudimentary mitochondrion, TCA cycle enzyme activities are barely or not detectable (Durieux et al., 1991). A functional cytochrome c-dependent respiratory chain is absent in BSFs although complex I is expressed but not essential (Priest and Hajduk, 1994; Surve et al., 2012). However, BSF mitochondrions harbour a unique electron transport chain involving FAD-dependent glycerol-3-phosphate dehydrogenase and the trypanosoma alternative oxidase (TAO). These enzymes together with the glycosomal glycerol 3-phosphate/dihydroxyacetone phosphate shuttle maintain glycosomal redox balance (Clarkson et al., 1989; Guerra et al., 2006). Unlike procyclic cells, the mitochondrial membrane potential is maintained by F_0F_1-ATP-synthase acting in reverse. This F_0F_1-ATPase pumps protons across the inner mitochondrial membrane under hydrolysis of ATP generated by glycolysis (Brown et al., 2006; Nolan and Voorheis, 1992; Schnaufer et al., 2005). Later it was found that BSF metabolism is more complex than initially expected. In the mitochondrion, acetate is produced from glucose and threonine to fuel essential *de novo* lipid biosynthesis. But still, pyruvate remains the major excretion product. Alanine, acetate and succinate are minor end products making 9 %, 5 % and 0.8 % of the exometabolome, respectively (Mazet et al., 2013). It was found that in BSFs glucose fuels the pentose phosphate pathway (PPP) and provides aspartate for pyrimidine synthesis. Interestingly, a very small proportion of glucose was incorporated into fatty acids and citrate (Creek et al., 2015).

In the tsetse fly, the nutritional situation is different from the mammalian host requiring substantial adaptations of the trypanosomal metabolism to available carbon sources. Glucose is present shortly after blood meals and gets sparse later (Vickerman, 1985). It has been published that the major amino acids in the haemolymphs of *Glossina morsitans* are proline, alanine and glutamine (Cunningham and Slater, 1974). Proline synthesized from fat bodies is known to be the key energy source for tsetse flies (Balogun, 1974; Bursell, 1977). Consequently, trypanosomes depend on amino acid catabolism, whereof proline is thought to be the major carbon source (Evans and Brown,

1972). However, when grown in glucose-rich medium procyclic form (PCF) trypanosomes favour glucose over proline. Proline uptake is 6-fold increased upon glucose withdrawal as glucose suppresses proline metabolism (Lamour et al., 2005). Interestingly, not the concentration of cytosolic ATP or the simple presence of glucose, but a reduction of the glycolytic flux promotes proline catabolism (Coustou et al., 2003; Deramchia et al., 2014). Even though threonine is taken up in high amounts, proline is the only amino acid that maintains proliferation in absence of glucose (Coustou et al., 2003; Lamour et al., 2005).

In insect stage trypanosomes, different carbon sources are metabolised in distinct pathways. Under culture conditions, aerobic fermentation of glucose yields partially oxidized end products mainly succinate and acetate as well as small amounts of lactate, malate and alanine (Bringaud et al., 2006). Phosphoenol pyruvate (PEP) generated in the cytosol in the course of glycolysis is at a branching point where metabolic flux is split into three different pathways. First, PEP can enter the succinic fermentation pathway in the glycosome producing malate and succinate (Besteiro et al., 2002). Second, after conversion into pyruvate it can feed the acetate branch in the mitochondrion. With the acetate:succinate CoA transferase (ASCT) /succinyl-CoA synthase (SCS) cycle as central part, the acetate branch is an important producer of ATP in the mitochondrion (Riviere et al., 2004; Van Hellemond et al., 1998a). Third, PEP can enter the mitochondrion as malate to produce succinate via fumarase and mitochondrial fumarate reductase (FRDm) (Coustou et al., 2005). However, glucose is not further oxidized via the Krebs cycle for energy generation (van Weelden et al., 2003). Glycerol is considered to be one of the major carbon sources of early PCF cells as it is taken up and metabolised with high efficiency (van Weelden et al., 2005). Similar to glucose, glycerol is oxidized mainly to succinate as well as acetate and CO_2 in the pyruvate dehydrogenase reaction (Ryley, 1962; van Weelden et al., 2005). Threonine is converted into acetate and glycine in the mitochondrion. Acetate is excreted and used as building block for *de novo* lipid and sterol biosynthesis in trypanosomes (Cross et al., 1975; Linstead et al., 1977; Millerioux et al., 2013). It has been reported that glycine is incorporated into glutathione to produce trypanothione or excreted (Millerioux et al., 2013). The presence of the components of the glycine cleavage system has been predicted by sequence homology (Berriman et al., 2005; Roldán et al., 2011). In contrast to *Leishmania*, trypanosomes lack serine hydroxymethyl transferase and serine dehydratase candidate genes (Berriman et al., 2005; Opperdoes and Coombs, 2007). Proline feeds as anaplerotic substrate into the TCA cycle entering as α-ketoglutarate. It has been reported that in the presence of glucose, proline flux through the TCA cycle is blocked at succinate, as

glucose enters the Krebs cycle as malate to produce succinate via fumarase and FRDm in the reverse direction. In glucose-rich conditions, proline mainly yields glutamate and succinate and small proportion of acetate, alanine and lactate are excreted (van Weelden et al., 2003; van Weelden et al., 2005). Proline degradation into glutamate yields one reduced $FADH_2$ and one NADH. Upon further conversion into succinate an additional NADH and one ATP are gained. However, upon glucose-independent growth, succinate is further metabolised via pyruvate into alanine by alanine aminotransferase or cytosolic aspartate aminotransferase (Marciano et al., 2008; Spitznagel et al., 2009). Besides alanine, glutamate and acetate are excreted increasing the energy yield per proline consumed (Coustou et al., 2008). Recently, it was found that proline fuels gluconeogenesis in absence of glucose (Allmann et al., 2013).

1.5 Energy generation in procyclic form *T. brucei*

In procyclic forms (PCF) energy is produced in form of ATP in the cytosol and the mitochondrion. Glycosomal ATP does not contribute to the cellular ATP pool. The glycosomes are presumably surrounded by a semi-permeable single membrane, which impairs ATP/ADP exchange with the cytosol, but allows the transport of glycolytic intermediates (Gualdron-López et al., 2012; Visser and Opperdoes, 1980). In the cytosol, phosphoglycerate kinase isoform B (PGKB) and pyruvate kinase (PYK) generate ATP in the course of glycolysis (Coustou et al., 2003; Deramchia et al., 2014). Production of ATP in the mitochondrion is essential for PCF survival (Millerioux et al., 2012). A key enzyme in mitochondrial substrate level phosphorylation is the succinyl-CoA synthase (SCS). *Tb*SCS phosphorylates ADP and not GDP (Van Hellemond et al., 1998b). SCS is part of both the proline catabolism using reactions of the TCA cycle and the acetate:succinate-CoA transferase (ASCT)/SCS cycle (Bochud-Allemann and Schneider, 2002; Van Hellemond et al., 1998b). ASCT/SCS cycle utilizes acetyl-CoA and succinate as substrates for ATP production. Three major carbon sources have been reported to replenish the acetyl-CoA pool, glucose, threonine and proline. Pyruvate dehydrogenase converts pyruvate into acetyl-CoA. Pyruvate is produced in the course of glycolysis or from proline involving the malic enzyme. Threonine-derived acetyl-CoA is presumably made in two reactions by means of threonine dehydrogenase and 2-amino-3-ketobutyrate-CoA lyase (AKB-CoA lyase). However, this pathway has not been completely experimentally validated, yet (Berriman et al., 2005; Millerioux et al., 2013).

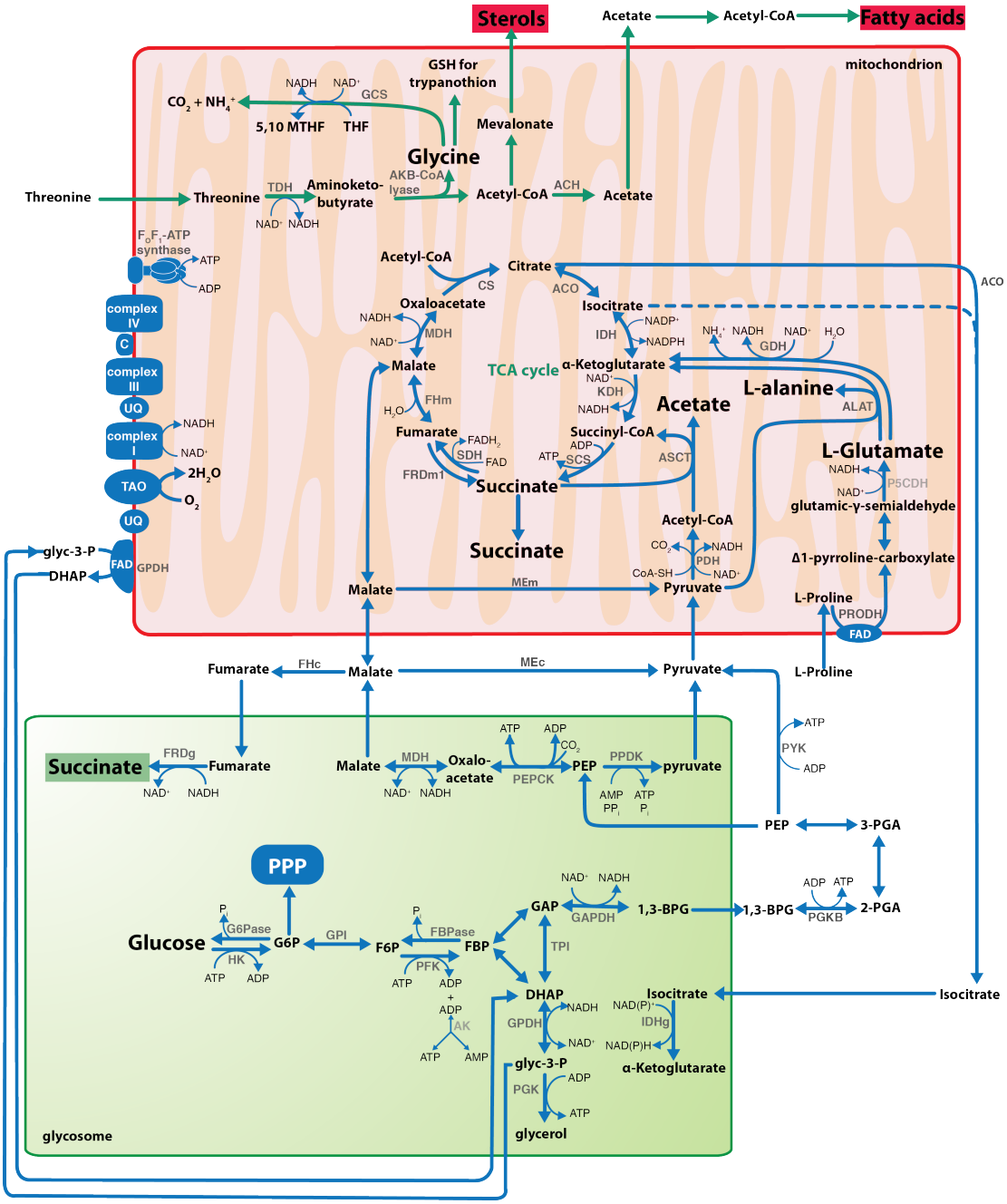

Figure 3 Metabolic Pathways Scheme. Abbreviations: ACH = Acetyl-CoA thioesterase; ACO = aconitase; AK = Adenylate kinase; AKB-CoA lyase = amino-ketobutyrate lyase; ALAT = alanine aminotransferase; ASCT = Acetate:Succinate CoA-transferase; C = cytochrome c; CS = citrate synthase; FBPase = fructose 1,6-bisphosphatase; FH = Fumarase; FRD = Fumarate reductase; G6Pase = glucose-6-phosphatase; GAPDH = glyceraldehyde 3-phosphate dehydrogenase; GCS = glycine cleavage system; GPDH = glycerol-3-phosphate dehydrogenase; GPI = glucose 6-phosphate isomerase; GSH = glutathione; HK = hexokinase; IDHg = glycosomal isocitrate dehydrogenase; IDHm = mitochondrial isocitrate dehydrogenase; KDH = α-ketoglutarate dehydrogenase; MDH = malate dehydrogenase; MEc= cytosolic malic enzyme; MEm = mitochondrial malic enzyme; P5CDH = pyrroline-5-carboxylate dehydrogenase; PEPCK = Phosphoenolpyruvate carboxykinase; PFK = Phosphofructokinase; PGK = Phosphoglyceratge kinase; PPDK = pyruvate phosphate dikinase; PPP = Pentose Phosphate Pathway; PRODH = proline dehydrogenase; PYK = pyruvate kinase; SCS = Succinyl-CoA synthetase; SDH = succinate dehydrogenase; TPI = Triose phosphate isomerase, UQ = ubiquinol;

PCF harbour one large branched mitochondrion with a complete albeit unique respiratory chain (Acestor et al., 2011). Upon glucose withdrawal oxidative phosphorylation besides substrate level phosphorylation is essential for energy generation. However, in glucose rich medium the need for a functional F_0F_1-ATP synthase yielded contradictory results, ranging from being essential to being dispensable (Lamour et al., 2005; Zikova et al., 2009).

In trypanosomes the first six or seven enzymes of glycolysis are compartmentalized in peroxisome-like organelle called glycosomes (Opperdoes and Borst, 1977). As hexokinase and phosphofructokinase are not allosterically regulated, the compartmentation is necessary to prevent accumulation of glycolytic intermediates. Here, especially sugar phosphates would accumulate, which is accompanied by depletion of the cellular ATP pool (Haanstra et al., 2008; Nwagwu and Opperdoes, 1982; Thevelein and Hohmann, 1995). In the course of glycolysis one molecule NADH is produced and two molecules ATP are consumed. As neither NADH nor ATP can leave the glycosome, a tightly balanced production and consumption of these small molecules is essential (Visser and Opperdoes, 1980). There are two possibilities for re-oxidation of NADH in the glycosome. First, the glycerol-3-phosphate (Gly-3-P)/ dihydroxyacetone phosphate (DHAP) shuttle is used by both BSF and PCF. Here, Gly-3-P produced by the NAD-dependent Glyc-3-P dehydrogenase (NAD-GPDH) is exported while DHAP is imported into the glycosome. In the mitochondrion FAD-dependent NAD-GPDH re-oxidizes Glyc-3-P into DHAP and transfers electrons to the ubiquinone pool (Guerra et al., 2006). Second, in PCFs, NAD^+/NADH ratio is mainly balanced by means of the glycosomal succinate shunt oxidizing two molecules of NADH upon complete conversion of PEP into succinate (Besteiro et al., 2002; Ebikeme et al., 2010). ATP is recovered from ADP and AMP by means of PEP carboxykinase and pyruvate phosphate dikinase (PPDK), respectively (Bringaud et al., 2006).

1.6 The Krebs cycle in *T. brucei*- Current status

The function of the canonical tricarboxylic acid (TCA) cycle described in textbooks is to complete oxidation of glucose and glycerol derived acetyl-CoA into CO_2. Intermediates leave the TCA cycle to feed biosynthetic pathways and gluconeogenesis. Anaplerotic substrates generated in the course of amino acid degradation and fatty acid oxidation refuel the Krebs cycle. Homologues of all enzymes of the TCA cycle are encoded in the *T. brucei* genome. No or only low activities of TCA cycle enzymes were detected in bloodstream forms (BSFs). However, in procyclic forms (PCFs) enzymatic activities for all TCA cycle enzymes have been described (Durieux et al., 1991). Trypanosomes do not

oxidize glucose in the TCA cycle for energy generation. In fact, aconitase activity is not essential for BSFs and PCFs survival under culture conditions (van Weelden et al., 2003). However, aconitase expression and activity is developmentally regulated increasing during BSF to PCF differentiation (Durieux et al., 1991; Saas et al., 2000). Isotopologue profiling with different carbon sources revealed that the main metabolic flux does not use all TCA cycle reactions. Malate derived from glucose or glycerol can enter the mitochondrion to produce succinate via fumarase (FH) and fumarate reductase (FRDm1) (Coustou et al., 2005; van Weelden et al., 2005). In absence of glucose, proline enters the TCA cycle in form of α-ketoglutarate and can exit it as malate, which is converted into acetate and alanine. Alanine and glutamate are the major end products of proline degradation. However, in presence of glucose, proline is partially oxidized into glutamate and succinate, which are excreted as end products (Coustou et al., 2008). Yet, there are no data supporting a proline or glucose catabolism that involves malate dehydrogenase (MDHm), citrate synthase (CS), (ACO) and isocitrate dehydrogenase (IDHm). However, these enzymes are expressed and active in PCFs (Aranda et al., 2006; Durieux et al., 1991). The TCA cycle is a central hub providing precursors for biosynthetic pathways besides energy generation. Acetyl-CoA is the building block for *de novo* lipid biosynthesis. In higher eukaryotes citrate/malate shuttle confers citrate transport from the mitochondrial matrix to the cytosol. Cytosolic ATP-dependent citrate lyase (ACL) converts citrate into oxaloacetate and lipogenic acetyl-CoA (Hatzivassiliou et al., 2005; Inoue et al., 1966). Interestingly, *T. brucei* potential ACL homologue is not involved in *de novo* lipid biosynthesis (Riviere et al., 2009). Instead of citrate, PCF and BSF trypanosomes transport acetate across the inner mitochondrial membrane. In the cytosol acetate is activated via acetyl-CoA synthase (AceCS) for lipogenesis and cholesterogenesis. (Millerioux et al., 2013).

1.7 Comparing the metabolism of trypanosomes with cancer cells

It is common for proliferating cells to consume more nutrients than quiescent ones. Besides increased generation of energy, dividing cells have a higher demand for reduction equivalents in form of NADPH and building blocks for *de novo* biosynthesis (DeBerardinis et al., 2008). Cancer cells adapt their metabolism to ensure proliferation in the tumor microenvironment where oxygen and nutrients can get scarce as an increased glucose consumption leads to its deprivation and insufficient vascularisation does one more thing (Birsoy et al., 2014; Hirayama et al., 2009). The interplay of

restrictions in nourishment on one hand and the great demand for energy and building blocks on the other hand are challenges that cancer cells share with trypanosomes. The fashion in which trypanosomes and transformed cells redistribute the metabolic network to overcome these obstacles can be almost considered as convergent evolution. Trypanosomes cultured under glucose-rich conditions convert glucose mainly into the partially oxidized end products like pyruvate in BSFs as well as acetate and succinate in PCFs (Bringaud et al., 2006). The glucose "fermentation" in BSF is comparable to the Warburg effect, a cancer associated phenotype for which an increase in glucose consumption in combination with aerobic glycolysis and lactate production is characteristic (Cori and Cori, 1925; Ferreira, 2010; Warburg, 1925). The Warburg effect was found to be linked to hypoxia and the associated signalling cascade involving hypoxia inducible factor (HIF) and the van-Hippel Lindau (VHL) tumor suppressor gene (Semenza, 2010). Upon activation of the HIF pathway, enzymes of glycolysis and lactate production are upregulated whereas pyruvate dehydrogenase (PDH) is inactivated by PDH kinase 1 blocking the entry to the TCA cycle (Kim et al., 2006). Just like in BSF trypanosomes, in cancer cells having the Warburg phenotype glucose-derived pyruvate is diverted away from the TCA cycle (van Weelden et al., 2003; Vander Heiden et al., 2009).

Generally, anaplerosis of TCA cycle intermediates is important to maintain supply of biosynthetic precursors and prevent their depletion by cataplerosis (DeBerardinis et al., 2007). Amino acid catabolism as well as pyruvate carboxylase mediated conversion of glucose into oxaloacetate (OAA) provides anaplerotic substrates for the TCA cycle (Owen et al., 2002). Glucose deprivation is common in certain tumor microenvironments as well as in the tsetse fly (Cairns et al., 2011; Vickerman, 1985). Upon glucose withdrawal insect stage trypanosomes as well as tumor cells rewire their metabolism to the utilisation of non-carbohydrate anaplerotic substrates all above proline and glutamine, respectively (Daye and Wellen, 2012; Evans and Brown, 1972; Le et al., 2012). Proline catabolism and glutaminolysis converge on the same pathway supplying the TCA cycle with α-ketoglutarate (αKG) via glutamate (GLU). The degradation of glutamine was recently brought into focus while investigating in the aberrant metabolism of transformed cells under hypoxia, aglycemia or defective mitochondria (Ahn and Metallo, 2015). It was found that glutaminolysis is bifurcated at αKG. One branch, the oxidative glutaminolysis, uses the canonical oxidative direction of the TCA cycle. Here, malate exits the TCA cycle and is converted via pyruvate into acetyl-CoA and lactate or, alternatively, OAA is produced to maintain progression of the TCA cycle (DeBerardinis et al., 2007; Le et al., 2012). The other branch, the reductive

carboxylation glutaminolysis (RCG), acts in the opposite direction requiring an NADP-dependent isocitrate dehydrogenase and the aconitase operating in reverse producing citrate. As a result of aerobic glycolysis shunting pyruvate away from the TCA cycle, citrate depletion promotes RCG independently from oxidative phosphorylation (Mullen et al., 2012; Smolková and Ježek, 2012; Wise et al., 2011). Interestingly, in cells with the Warburg phenotype RCG can be inhibited by supplementation of external citrate or acetate (Gameiro et al., 2013). Citrate generated in the course of glutaminolysis is exported into the cytosol to yield lipogenic acetyl-CoA (Metallo et al., 2011). It has been found in various human cultured cell lines, that both NADP(H)-dependent isocitrate dehydrogenase (IDH) in the cytosol (IDH1) and the mitochondrion (IDH2) are able to catalyse the reverse carboxylation reaction (Filipp et al., 2012; Leonardi et al., 2012).

Besides energy generation, glucose provides precursors for biosynthesis of nucleotides, non-essential amino acids and folate mediated one-carbon metabolism (Locasale, 2013; Vincent et al. 2015). In absence of glucose, biosynthetic building blocks are made by gluconeogenesis from non-carbohydrate carbon sources. Gluconeogenesis is ubiquitously found in all kingdoms although with some modifications. In human it is restricted to the liver, kidney and presumably to the intestine (Nuttall et al., 2008). Substrates of gluconeogenesis are lactate, glycerol, glucogenic amino acids (Berg et al., 2012; Kaleta et al., 2011).

Phosphoenol pyruvate (PEP) is considered to be the starting substrate of gluconeogenese. In the context of glycolysis pyruvate kinase (PYK) catalyses the conversion of PEP into pyruvate in an irreversible manner. In human cells PYK activity is bypassed in order to produce PEP from pyruvate. Here, the first enzyme in this pathway, pyruvate carboxylase (PEPC), generates OAA from pyruvate. As trypanosomes lack a PEPC homologue, OAA is produced from malate by MDH (Berriman et al., 2005). The second step, the reversible conversion of OAA into PEP is mediated by PEP carboxykinase (PEPCK). PEPCK is a key enzyme for gluconeogenesis and found in both human and trypanosomes. In cancer cells, PEPCK was identified to be crucial for glucose-independent growth in a glutamine-rich environment (Montal et al., 2015; Vincent et al.). Trypanosomal PEPCK is known to be involved in succinic fermentation pathway to maintain ADP/ATP balance in the glycosome (Besteiro et al., 2002). In contrast to human cells, *T. brucei* express a pyruvate phosphate dikinase (PPDK) which catalyses a reversible reaction similar to PYK converting AMP into ATP upon pyruvate production. PPDK plays a crucial role in maintaining glycosomal ADP/ATP balance during glycolysis (Cosenza et al., 2000; Deramchia et al., 2014). The exact roles of PPDK and PEPCK in gluconeogenesis remain to be elucidated.

1.8 Reduction equivalents and redox homeostasis

The pyridine nucleotides NADH and NADPH play distinct roles in metabolism. Besides $FADH_2$, NAD(H) is a central mediator of energy metabolism fuelling the respiratory chain with electrons. NADPH provides reducing power for biosynthetic reactions and maintaining the cellular redox balance. Redox homeostasis is important for survival of cells. Most of the cellular $NAD(P)^+$ pool is bound to proteins. The cytosol provides a highly oxidizing environment with free NAD^+/NADH ratios of about 700 in contrast to ratios between 3 and 10 in the mitochondrion (Stubbs et al., 1972). NADP(H) exists predominantly in its reduced form with cytosolic $NADP^+$/NADPH ratios of 0.014 in rat liver cells and 0.045 in yeast (Berg et al., 2012; Zhang et al., 2015). Mammalian mitochondria as well as bacteria have an enzyme called nicotinamide nucleotide transhydrogenase (NNT). NNT catalyses the hydride ion transfer between NAD(H) and NADP(H) driven by the proton motive force. The reaction principle is similar to that of ATPases. The proton gradient at the inner mitochondrial membrane favours the formation of NADPH (Hatefi and Yamaguchi, 1996). Trypanosomes lack a NNT candidate gene consequently coenzyme balance has to be maintained by other pathways (Berriman et al., 2005).

The major causes for oxidative stress are reactive oxygen species (ROS) that can cause lipid peroxidation, DNA damage and oxidation of cysteinyl sulfhydryl residues of proteins. Thiol-based detoxification mechanisms defending oxidative stress have evolved in different organisms; all depend on NADPH as electron donor (Holmgren et al., 2005). An increase in the NADP(H) pool size mediated by NAD kinase (NADK) was found to act protective against ROS (Gray et al., 2012; Magni et al., 2006; McGuinness and Butler, 1985). In trypanosomes the GSH reductase system is replaced by an unique redox metabolism based on trypanothione $T(SH)_2$ as central antioxidant. The $T(SH)_2$ (N^1, N^8 bis(glutathionyl)spermidine) consists of one spermidine moiety linking two GSH molecules that form an intra-molecular disulfide bond upon oxidation. Trypanothione reductase regenerates $T(SH)_2$ by oxidating one NADPH equivalent (Fairlamb et al., 1985). The trypanosomal thiol metabolism also comprises a thioredoxine-like protein, called tryparedoxine (TXN) as well as mono- and dithiol glutaredoxins (Grx) (Ceylan et al., 2010; Krauth-Siegel and Comini, 2008). Trypanosomes express four superoxide dismutase isoforms, but no catalase (Berriman et al., 2005; Wilkinson et al., 2006). Hydrogen peroxides are reduced by trypanothione/tryparedoxine peroxidases (2-cys peroxiredoxines), a cysteine homologue to the GSH peroxidases and an ascorbate-dependent hemoperoxidase (Schlecker et al., 2005). The main source for endogenously produced ROS is the electron transport chain, which is important for insect stage

trypanosomes upon glucose withdrawal (Lamour et al., 2005). Trypanosomes encounter oxidative stress as a result of immune response in the mammalian host as well as in the proventriculus of the tsetse fly vector (Brunet, 2001; Hao et al., 2003). High NADPH levels are maintained by malic enzyme isoforms in the mitochondrion and the cytosol as well as by the pentose phosphate pathway in glycosomes and cytosol (Allmann et al., 2013). Alternative possible sources for NADPH are isocitrate dehydrogenases (IDH) catalysing the oxidative decarboxylation of isocitrate. In nonmalignant human cells IDH2 is a NADPH supplier for maintaining redox homeostasis in the mitochondrion. NADP(H) dependent IDH enzymatic activity depends on reduced cysteine residues (Fatania et al., 1993; Smyth and Colman, 1991). Oxidative stress causes an increase in GSSG/GSH ratio leading to a glutathionylation of proteins. Though glutathionylation of Cys269 protects IDH1 and IDH2 from oxidative damage it inactivates the enzyme (Kil and Park, 2005; Shin et al., 2009).

1.9 Isocitrate dehydrogenase

In evolution, the first isocitrate dehydrogenase (IDH) ancestors used NAD^+ as co-substrate and 3.5 billion years later $NADP^+$-dependent IDHs evolved (Zhu et al., 2005). IDH can be classified into different subfamilies depending on the oligomeric state and coenzyme dependency. The monomeric IDH occurs exclusively in bacteria and with 10 % sequence similarity to other IDH subfamilies it is assumed to have evolved independently (Imabayashi et al., 2006). Subfamily I attributed IDHs are homo-dimers, NAD^+ or $NADP^+$ dependent and are found in bacteria and archaea. Subfamily II (type II) consists of $NADP^+$-dependent homo-dimers mainly found in eukaryotes and a few in eubacteria. Subfamily III comprises eukaryotic mitochondrial NAD^+-dependent hetero-oligomeric as well as eubacterial NAD^+ or $NADP^+$ dependent homo-tetrameric IDHs. Due to the sequence homology of >30 % subfamily I and III are combined to form type I IDH (Zhu et al., 2005). Monomeric and type II IDHs are found to use $NADP^+$ as a cofactor. However, NAD^+ dependency was recently described for monomeric (*Ca*IDH, *Cc*IDH) and type II (*Mi*IDH, *Ol*IDH) IDH in bacteria and algae, respectively (Wang et al., 2015).

2 Materials and methods

2.1 Materials

2.1.1 Antibiotic stock solutions

Ampicillin (100 mg/ml in H_2O)	Boehringer, Mannheim
Blasticidin (10 mg/ml in H_2O)	Merck, Darmstadt
Hygromycin (10 mg/ml in H_2O)	Calbiochem, Darmstadt
Neomycin, G418 (10 mg/ml in H_2O)	Sigma, Steinheim
Phleomycin (10 mg/ml in H_2O)	Cayla, Toulouse, France
Puromycin (10 mg/ml in H_2O)	Sigma, Steinheim
Tetracycline (10 mg/ml in EtOH)	Sigma, Steinheim

2.1.2 Antibodies

Primary antibodies

name	source	type	origin	dilution
Immunofluorescence and flow cytometric analyses				
αBARP	rabbit	polyclonal	kind gift of Roditi, Bern (Urwyler et al., 2007)	1:400
αEP	mouse	monoclonal	TBRP1/247, BIOZOL	1:500
αcalflagin	mouse	polyclonal	kind gift (Tyler et al., 2009)	1:1,000
Western blot analysis				
αACO	rabbit	polyclonal	recombinant full length protein expressed in *E.coli* (Pineda) (Stefan Allmann)	1:3,000
αCS	rabbit	polyclonal		1:1,000
αIDHg	rabbit	polyclonal		1:2,000
αIDHm	rabbit	polyclonal		1:2,000
αENO	rabbit	polyclonal	kind gift of Michels, Brussels (Hannaert et al., 2003a)	1:10,000
αLipDH	rabbit	polyclonal	kind gift from Krauth-Siegel, Heidelberg (Roldán et al. 2011)	1:2,000
αPFR	mouse	monoclonal	kind gift from Gull, Oxford (Woods et al., 1989)	1:3,000
αTY (BB2)	mouse	monoclonal		1:4,000

Secondary antibodies

IRDye® 800CW goat anti-mouse (H+L)	LI-COR, Bad Homburg
IRDye® 680CW goat anti-rabbit (H+L)	LI-COR, Bad Homburg
Alexa Fluor® 488 goat anti-mouse (H+L)	ThermoFisher Scientific, Darmstadt

2.1.3 Bacteria cell lines

E. coli SURE — *e14-(McrA-) Δ(mcrCB-hsdSMR-mrr) 171 endA1 supE44 thi-1 gyrA96 relA1 lac recB recJ sbcC umuC::Tn5 (Kan^r) uvrC [F´ proAB lacI^q ZΔM15 Tn10 (Tet^r)]* (Stratagene, Amsterdam)

E. coli XL10-Gold — *endA1 glnV44 recA1 thi-1 gyrA96 relA1 lac Hte Δ(mcrA)183 Δ(mcrCBhsdSMR-mrr)173 tetR F'[proAB lacIqZΔM15 Tn10(Tet^r Amy CmR)]* (Stratagene, Amsterdam)

2.1.4 Procyclic form cell lines

Nomenclature of genotypes according to guidelines published in 1998 (Clayton et al., 1998). pLew100v5-RBP6^{Ti} and pHD1146-CS-TY^{Ti} constructs were transfected on the background of WT and null mutants. All mutants used in this project are listed in the table.

Trypanosoma brucei brucei wild type strains

EATRO1125-T7T — received from Bringaud (Bordeaux, France) (Bringaud et al., 2000)

AnTat 1.1 — Antwerp Trypanozoon antigen type 1.1, Clone of EATRO1125 E. Pays (Brussels, Belgium) and P. Ovarath (Tübingen, Germany) (Geigy et al., 1975)

name	AnTat 1.1 1313
made by	(Alibu et al., 2005)
genotype	*TETR BLE*
clone/pool	clone
constructs	pHD1313
selection marker	G418, 10 µg/ml; phleomycin 2.5 µg/ml; hygromycin 25 µg/ml

name	AnTat 1.1 1313 ΔACO
made by	S. Allmann
genotype	*TETR BLE Δaco::NEO/Δaco::HYG*
clone/pool	clone
constructs	pBSK-NEO, pBSK-HYG, pHD1313
selection marker	G418, 10 µg/ml; phleomycin 2.5 µg/ml; hygromycin 25 µg/ml

name	AnTat 1.1 1313 ΔCS
made by	S. Allmann
genotype	*TETR BLE Δcs::NEO/Δcs::HYG*
clone/pool	clone
constructs	pHD1313, pBSK-NEO, pBSK-HYG
selection marker	G418, 10 µg/ml; phleomycin 2.5 µg/ml; hygromycin 25 µg/ml

name	AnTat 1.1 1313 ΔACO/ΔCS
made by	S. Allmann
genotype	*TETR BLE Δaco::NEO/Δaco::HYG Δcs::PAC/Δcs::BLAS*
clone/pool	clone
constructs	pHD1313, pBSK-NEO, pBSK-HYG, pBSK-PAC, pBSK-BLAS
selection marker	G418, 10 µg/ml; phleomycin 2.5 µg/ml; hygromycin 25 µg/ml blasticidin 5 µg/ml; puromycin 1 µg/ml

name	AnTat 1.1 1313 ΔIDHg
made by	S. Allmann
genotype	*TETR BLE Δidhg::NEO/Δidhg::HYG*
clone/pool	clone
constructs	pHD1313, pBSK-NEO, pBSK-HYG
selection marker	G418 10 µg/ml; phleomycin 2.5 µg/ml; hygromycin 25 µg/ml

name	AnTat 1.1 1313 ΔIDHm
made by	S. Allmann
genotype	*TETR BLE Δidhm::NEO/Δidhm::HYG*
clone/pool	clone
constructs	pHD1313, pBSK-NEO, pBSK-HYG
selection marker	G418 10 µg/ml; phleomycin 2.5 µg/ml; hygromycin 25 µg/ml

name	AnTat 1.1 1313 ΔN10ACO
made by	N. Ziebart
genotype	*TETR BLE Δaco::NEO/TY::ΔN10ACO::PAC*
clone/pool	clone
constructs	pHD 1313, p3077-PAC, pBSK-NEO
selection marker	G418 10 µg/ml; phleomycin 2.5 µg/ml; puromycin 1 µg/ml

name	AnTat 1.1 1313 *Tb*CS-TY^{Ti}
made by	N. Ziebart
genotype	*TETR::BLE TbCS::TY^{Ti}::PAC*
clone/pool	clone
constructs	pHD1313, pHD1146
selection marker	phleomycin 2.5 µg/ml; puromycin 1 µg/ml

name	AnTat 1.1 1313 ΔACO *Tb*CS-TY^{Ti}
made by	N. Ziebart
genotype	*TETR::BLE Δaco::NEO/Δaco::HYG TbCS::TY^{Ti}::PAC*
clone/pool	clone
constructs	pHD1313, pHD1146-PAC, pBSK-NEO, pBSK-HYG
selection marker	G418 10 µg/ml; hygromycin 25 µg/ml; phleomycin 2.5 µg/ml; puromycin 1 µg/ml

name	AnTat 1.1 1313 ΔIDHg *Tb*CS-TY^{Ti}
made by	N. Ziebart
genotype	*TETR::BLE Δidhg::NEO/Δidhg::HYG TbCS::TY^{Ti}::PAC*
clone/pool	clone
constructs	pHD1313, pHD1146, pBSK
selection marker	G418 10 µg/ml; hygromycin 25 µg/ml; phleomycin 2.5 µg/ml; puromycin 1 µg/ml

name	AnTat 1.1 1313 ΔIDHm *Tb*CS-TY^{Ti}
made by	N. Ziebart
genotype	*TETR::BLE Δidhm::NEO/Δidhm::HYG TbCS::TY^{Ti}::PAC*
clone/pool	clone
constructs	pHD1313, pHD1146-PAC, pBSK-NEO, pBSK-HYG
selection marker	G418 10 µg/ml; hygromycin 25 µg/ml; phleomycin 2.5 µg/ml; puromycin 1 µg/ml

name	AnTat 1.1 1313 ΔN10ACO *Tb*CS-TY^{Ti}
made by	N. Ziebart
genotype	*TETR BLE Δaco::NEO/TY::ΔN10ACO::PAC TbCS::TY^{Ti}::HYG*
clone/pool	clone
constructs	pHD1313, pBSK-NEO, p3077-PAC, pHD1146-HYG
selection marker	G418 10 µg/ml; phleomycin 2.5 µg/ml; puromycin 1 µg/ml; hygromycin 25 µg/ml

name	EATRO 1125-T7T
made by	(Bringaud et al., 2000)
genotype	*TETR::HYG T7RNAP::NEO*
constructs	pHD328, pLew114
selection marker	G418 10 µg/ml; hygromycin 25 µg/ml

name	EATRO 1125-T7T ΔCS
made by	N. Ziebart
genotype	*TETR::HYG T7RNAP::NEO Δcs::BLAS/Δcs::PAC*
clone/pool	clone
constructs	pHD328, pLew114, pBSK-BLAS, pBSK-PAC
selection marker	G418 10 µg/ml; puromycin 1 µg/ml; hygromycin 25 µg/ml; blasticidin 10 µg/ml

name	EATRO 1125-T7T ΔIDHg
made by	S. Allmann
genotype	*TETR::HYG T7RNAP::NEO Δidhg::BLAS/Δidhg::PAC*
clone/pool	clone
constructs	pHD328, pLew114, pBSK-BLAS, pBSK-PAC
selection marker	G418 10 µg/ml; puromycin 1 µg/ml; hygromycin 25 µg/ml; blasticidin 10 µg/ml

name	EATRO 1125-T7T ΔIDHm
made by	N. Ziebart
genotype	*TETR::HYG T7RNAP::NEO Δidhm::BLAS/Δidhm::PAC*
clone/pool	clone
constructs	pHD328, pLew114, pBSK-BLAS, pBSK-PAC
selection marker	G418 10 µg/ml; puromycin 1 µg/ml; hygromycin 25 µg/ml; blasticidin 10 µg/ml

name	EATRO 1125-T7T ΔCS
made by	N.Ziebart
genotype	*TETR::HYG T7RNAP::NEO Δcs::BLAS/Δcs::PAC*
clone/pool	clone
constructs	pHD328, pLew114, pBSK-BLAS, pBSK-PAC
selection marker	G418 10 µg/ml; puromycin 1 µg/ml; hygromycin 25 µg/ml; blasticidin 10 µg/ml

name	EATRO 1125-T7T ΔFBPase
made by	kind gift of Bringaud (Bordeaux, France)
genotype	*TETR::HYG T7RNAP::NEO Δfbpase::BLAS/Δfbpase::PAC*
clone/pool	clone
constructs	pHD328, pLew114, pBSK-BLAS, pBSK-PAC
selection marker	G418 10 µg/ml; puromycin 1 µg/ml; hygromycin 25 µg/ml; blasticidin 10 µg/ml

name	EATRO 1125-T7T RBP6^{Ti}
made by	N. Ziebart
genotype	*TETR::HYG T7RNAP::NEO TbRBP6^{Ti}::BLE*
clone/pool	pool
constructs	pHD328, pLew114, pLew100v5-BLE
selection marker	G418 10 µg/ml; hygromycin 25 µg/ml; phleomycin 5 µg/ml

name	EATRO 1125-T7T ΔCS RBP6^{Ti}
made by	N. Ziebart
genotype	*TETR::HYG T7RNAP::NEO Δcs::BLAS/Δcs::PAC TbRBP6^{Ti}::BLE*
clone/pool	pool
constructs	pHD328, pLew114, pBSK-BLAS, pBSK-PAC, pLew100v5-BLE
selection marker	G418 10 µg/ml; puromycin 1 µg/ml; hygromycin 25 µg/ml; blasticidin 10 µg/ml; phleomycin 5 µg/ml

name	EATRO 1125-T7T ΔIDHg RBP6 ^{Ti}
made by	S. Allmann
genotype	*TETR::HYG T7RNAP::NEO Δidhg::BLAS/Δidhg::PAC TbRBP6^{Ti}::BLE*
clone/pool	pool
constructs	pHD328, pLew114, pBSK-BLAS, pBSK-PAC, pLew100v5-BLE
selection marker	G418 10 µg/ml; puromycin 1 µg/ml; hygromycin 25 µg/ml; blasticidin 10 µg/ml; phleomycin 5 µg/ml

name	EATRO 1125-T7T ΔIDHm RBP6 ^{Ti}
made by	N. Ziebart
genotype	*TETR::HYG T7RNAP::NEO Δidhm::BLAS/Δidhm::PAC TbRBP6^{Ti}::BLE*
clone/pool	pool
constructs	pHD328, pLew114, pBSK-BLAS, pBSK-PAC, pLew100v5-BLE
selection marker	G418 10 µg/ml; puromycin 1 µg/ml; hygromycin 25 µg/ml; blasticidin 10 µg/ml; phleomycin 5 µg/ml

name	EATRO 1125-T7T ΔFBPase RBP6 ^{Ti}
made by	N. Ziebart
genotype	*TETR::HYG T7RNAP::NEO Δfbpase::BLAS/Δfbpase::PAC TbRBP6^{Ti}::BLE*
clone/pool	pool
constructs	pHD328, pLew114, pBSK-BLAS, pBSK-PAC, pLew100v5-BLE
selection marker	G418 10 µg/ml; puromycin 1 µg/ml; hygromycin 25 µg/ml; blasticidin 10 µg/ml; phleomycin 5 µg/ml

2.1.5 Chemicals

Acids and Bases	Roth, Karlsruhe; Applichem, Darmstadt
Agarose	Biozym, Hessisch Oldendorf
Amino acids	AppliChem, Darmstadt Sigma-Aldrich, München
Bradford –solution	Applichem, Darmstadt
BSA	Carl Roth, Karlsruhe
CASYton	OMNI Life Science, Bremen
Complete EDTA-free protease inhibitor	Roche, Mannheim
DAPI (4,6 Diamidino-2-phenylindole)	Sigma, Taufkirchen
dNTPs (10 mM)	Roche, Mannheim
Ethidium bromide	Roth, Karlsruhe
Fetal Calf Serum	PAA, GE Healthcare Life Sciences, München
Immersion Oil 518N	Thermo Scientific, Darmstadt
Media supplements	AppliChem, Darmstadt; Thermo Scientific, Darmstadt; Sigma-Aldrich, München
Organic solvents	Roth, Karlsruhe; AppliChem, Darmstadt; Merck Millipore, Darmstadt
PhosSTOP	Roche, Mannheim
[U-^{13}C] proline	Cambridge Isotope, Andover, USA
Rotiphorese® Gel 30 (37.5:1)	Carl Roth, Karlsruhe
SDM79-CG4P2TA powder	GE Healthcare Life Sciences, München
Size standards (DNA Protein)	NEB, Frankfurt

Standard and fine chemicals	AppliChem, Darmstadt; Merck Millipore Darmstadt; Roth, Karlsruhe
Streptomycin-Penicillin 100x	Sigma-Aldrich, Darmstadt
[1,2-^{13}C2] threonine	Sigma-Aldrich, Darmstadt
Vectashield Mounting Medium H1000	BIOZOL, Eching
XerumFree™	TNCBIO, Eindhoven (Netherlands)

2.1.6 Computer software

4Peaks	© 2006 Mek&Tosj.com
Adobe Acrobat X Pro 10.1.16	© 1987-2012 Adobe systems Inc.
Adobe Illustrator CS5 15.0.2	© 1987-2010 Adobe systems Inc.
Adobe Photoshop CS5 12.0.4	© 1987-2010 Adobe systems Inc.
Analyst® Software v1.5.2	SCIEX, Foster City (CA)
BLAST basic local alignment tool	blast.ncbi.nlm.nih.gov/Blast.cgi
CLC Main Workbench 6.7	© 2013 CLC bio, a QIAGEN® company
EndNote X7	© 1988-2015 Thomson Reuters
Fiji for Mac OS X open-source platform	
FlowJo 8.8.7	© 1996-2009 Tree Star
Gene Construction Kit 3.5	© 1999-2008 Textco BioSoftware
ImageStudioLite 3.1.4	© 2012 LI-CORE Inc.
LabSolution Software	SHIMADZU, Duisburg
Microsoft Excel 14.2.4	© 2010 Microsoft Corporation
Microsoft PowerPoint 14.2.4	© 2010 Microsoft Corporation
Microsoft Word 14.2.4	© 2010 Microsoft Corporation
OligoAnalyzer® Tool	eu.idtdna.com/calc/analyzer
Progenesis® QI for proteomics	© 2016 Nonlinear Dynamics, WATERS
TriTryp database	tritrypdb.org/tritrypdb/

2.1.7 Consumables and Supplies

1 kb DNA ladder	NEB Frankfurt
8-strips (0.2 ml)	VWR International, Darmstadt
BTX cuvette, 2 mm gap	VWR International, Darmstadt
Cell culture flasks	Greiner Bio-One, Frickenhausen
Coverslips (square, 17 mm)	Roth, Karlsruhe
CytoOne Filter cap T-225	StarLab, Hamburg

Falcon® conical centrifuge tube 15 ml	Fisher Scientific, Schwerte
Immobilon FL PVDF membrane	CLN, Freising
Microscope slide	VWR International, Darmstadt
Petri dishes	Greiner Bio-One, Frickenhausen
Polypropylen tubes	Greiner Bio-One, Frickenhausen
Polystyrol 5 ml round bottom tube Falcon	Fisher Scientific, Schwerte
Reaction tubes	Sarstedt, Nürnberg
Sterile filter Ø 0.22 µm	Merck Millipore, Darmstadt
TipOne Filter Tips 10-1000 µl	StarLab, Hamburg
UV-STAR microplate 96-well	Greiner Bio-One, Frickenhausen
Whatman blotting paper 1MM	Macherey & Nagel, Düren

2.1.8 Enzymes

Calf intestine alkaline phosphatase	NEB, Frankfurt
Phusion® High-fidelity polymerase	NEB, Frankfurt
Restriction endonucleases	NEB, Frankfurt
T4 DNA Ligase	PROMEGA, Mannheim

2.1.9 Equipment

Bioruptor® UCD-200, Diagenode		Thermo Scientific, Darmstadt
BTX™-Harvard Apparatus ECM™ 630		Fisher Scientific, Schwerte
CASY TT-2IA-1562 CASY TT-2IA-1562		OMNI Life Science, Bremen
Centrifuge	ROTANTA 460R	Hettich Lab Technology, Tuttlingen
	Eppendorf™ 5417R	Fisher Scientific, Schwerte
Dionex™ ICS-5000+ Reagent-Free™ HPIC™		Thermo Scientific, Darmstadt
Dionex™ ICS-5000+ EG Eluent generator		Thermo Scientific, Darmstadt
DU® 640 Spectrophotometer		Beckmann Coulter, Krefeld
Eppendorf™ Thermomixer 5436		Fisher Scientific, Schwerte
FACSCalibur™ Dual Laser Flow Cytometer		Becton Dickinson, Heidelberg
GCMS-GP2010 Plus		SHIMADZU, Duisburg
Geldoc 2000		Bio-Rad, München
GFL 1083 shaking water bath		GFL, Burgwedel
Herasafe™ KS Class II, biological safety cabinet		Thermo Scientific, Darmstadt
Incubator Thermo Heracell 240		Thermo Scientific, Darmstadt
InoLab Oxi 730 pH meter		WTW, Weilheim

IonPac AG11 guard column	Thermo Scientific, Darmstadt
IonPac AS11 anion exchange column	Thermo Scientific, Darmstadt
Geldoc 2000	BIO-RAD, München
Microscopes Axiovert 25	Carl Zeiss, Jena
Axioimager M1	Carl Zeiss, Jena
DeltaVision Elite	GE Healthcare Life Sciences, München
Mini-PROTEAN® 3 Multi-Casting Chamber	BIO-RAD, München
Mini-PROTEAN® Tetra Vertical Electrophoresis Cell	BIO-RAD, München
Nanodrop1000	Thermo Scientific, Darmstadt
Pipetboy acu 2	INTEGRA, Biebertal
PIPETMAN® Classic™ P2, P10, P200, P1000	Gilson, Middleton (USA)
PowerPac™ HC Power Supply	BIO-RAD, München
Odissey® IR Imaging System	LI-COR, Bad Homburg
Q Exactive™ Hybrid Quadropole-Orbitrap™ Mass Spectrometer	Thermo Scientific, Darmstadt
Quartz cuvettes 2 ml	firstvial, Hang Zhou
SCIEX 4000 QTRAP® system	SCIEX, Foster City (CA)
TECAN Infinite M200 Pro	TECAN group, Männedorf, Schweiz
Trans-Blot® Turbo™ Transfer System	BIO-RAD, München
UltiMate 3000 RSLCnano-UHPLC system	Thermo Scientific, Darmstadt
Ultra Clear UV Plus system	EVOQUA Water Technologies GmbH
Veriti® Thermal PCR Cycler	Thermo Scientific, Darmstadt
Vortex-Genie® 2	VWR, Darmstadt

2.1.10 Kits

NucleoSpin Extract II	Macherey & Nagel, Düren
NucleoSpin Plasmid	Macherey & Nagel, Düren
NucleoSpin Tissue	Macherey & Nagel, Düren
Wizard® SV Gel and PCR Clean-Up system	PROMEGA, Mannheim

2.1.11 Media and buffers

Media were prepared with ddH_2O and sterile filtered (pore size Ø 0.22 µm)

SDM79	SDM79 basic medium (Brun and Schonenberger, 1979) modified by G. Cross (SDM79 JRH57453) SDM79-CG4P2TA powder; 7.5 mg/ml hemin; 10 % FCS
Freezing medium	SDM79, 20 % FCS, 20 % glycerol
LB medium	1 g Bacto- tryptone; 5 g yeast extract; 10 g NaCl; pH 7
LB agar plates	LB medium with 16 g/l agar
Cytomix	10 mM K_2HPO_4/KH_2PO_4 pH 7.6; 25 mM HEPES; 2 mM EGTA; 120 mM KCl; 150 µM $CaCl_2$; 5 mM $MgCl_2$; 0.5 % (w/v) glucose; 1 mM hypoxanthine; 100 µg/ml BSA, sterile filtered
DNA loading dye (6x)	0.4 % orange G, 15 % (w/V) Ficoll 400
Extraction solutions	
GC-MS (TUM, Garching)	100 % MeOH
IC-MS (INSA, Toulouse)	ACN:MeOH:H_2O = 2:2:1(V:V:V)
Laemmli running buffer	25 mM TRIZMA® pH 8.8, 0.1 % (w/V) SDS; 0.192 glycine
Laemmli sample buffer	187.5 mM Tris-HCl, pH 6.8; 37 % glycerol; 12 % SDS; 0.93 % DTT, 6 ‰ Bromphenolblue
Proteome (Bordeaux)	4.5 M urea; 0.2 % SDS, Complete EDTA-free inhibitor
PBS	12 mM Na_2HPO_4; 1.8 mM KH_2PO_4; 137 mM NaCl; 2.7 mM KCl, pH 7.4
PBS/T	1 ×PBS, 0.2 % Tween
Quenching solution	0.9 % NaCl in H_2O: glycerol = 2:3 (V/V)
4 % PFA	PFA is dissolved in PBS under alkaline conditions at 56 °C and pH is adjusted to ~7.4; 2 ml aliquots are stored at -20 °C
TAE	40 mM Tris-HCl, pH 8; 40 mM NaAcetate; 1 mM EDTA
Resolving gel buffer	1.5 mM TRIZMA® pH 8.8; 0.4 % SDS
Resolving gel 10 %	30 % Rotiphorese® Gel 30; 25 % resolving gel buffer; 41.6 % H_2O; 0.066 % TEMED, 0.3 g/l APS
Stacking gel buffer	0.5 mM Tris-HCl pH 6.8; 0.4 % (w/v) SDS
Stacking gel	13 % Rotiphorese® Gel 30; 25 % stacking gel buffer; 62 % H_2O; 0.1% TEMED, 0.5 g/l % APS
STE buffer	25 mM Tris-HCl, pH 7.2; 1 mM EDTA; 10% sucrose
Anode buffer	300 mM TRIZMA® pH 10.4; 20 % (V/V) MeOH
Cathode buffer	25 mM Tris-HCl pH 7.6; 20 % (V/V) MeOH, 40 mM ε-amino- Caproic acid

2.1.12 Plasmids

The pBSK-based constructs used for generation of null mutants were cloned and designed by Allmann (PhD thesis 2014) and Panzer (Diploma thesis 2007). The pLew100v5-RBP6 construct was cloned and designed by Stefan Allmann (PhD thesis 2007). pHD1146-HYG (a pHD 678-derived plasmid lacking the T7 promoter (Estévez et al., 2001)) was a gift from the Clayton lab.

Plasmid name	Original plasmid	Application	Restriction enzymes	PCR primer and template for insert
p3077-ΔN10ACO	p3077	N-terminal in situ replacement of MTS by TY1 tag	HindIII	5' TY Δ10NACO-HindIII 3' TY ΔN10ACO blunt AnTat1.1 1313 gDNA
pHD1146-PAC	pHD1146-HYG	Exchange of resistance cassette from HYG to PAC	BsrGI, Partial digest SnaBI	5' PURO SnaBI 3' PURO BsrGI pTsaRib(puro)VASP
pHD1146-HYG-CS-TY	pHD1146-HYG	Tet inducible over-expression of TbCS-TY HYG marker	pLew100v5_CS-TY	5' CS-OE ApaI 3'CS-OE BamHI
pHD1146-PAC-CS-TY	pHD1146-PAC	Tet inducible over-expression of TbCS-TY PAC marker	pLew100v5_CS-TY	5' CS-OE ApaI 3'CS-OE BamHI

2.1.13 Primers

All primers were designed using Primer-BLAST and the IDT OligoAnalyzer software. Primers were synthesized by Sigma-Aldrich, München.

Name	Sequence	Application
5' TY Δ10NACO-HindIII	CACACaagcttCCGCCACCATGTCCTTGCCGTCAAACAACCCATTTCTAAAA	In situ replacement of MTS by TY1-tag template: pLew20ΔN10ACO
3' TY ΔN10ACO blunt	CTGTCCCAACATGCCCGCTTCCGCCTCAAT	
5' CS-OE ApaI	TTCGgggcccTAACATGTGCATGCGTGCTCGTTAC	CS-TY OE in pHD1146; Template: pLew100v5_CS-TY (Allmann, PhD thesis)
3'CS-OE BamHI	ATGCggatccTCAGTCAAGTGGGTCCTGGTTAGTATGGACTTCCGCTATGTTGTACTT	
5' PURO SnaBI	GTAAGGTCTCGTTGCTGCCATA	Exchange resistance cassette in pHD1146 from HYG to PAC
3' PURO BsrGI	ccccTGTACAACTATTTCAATCATGTC	

2.2 Methods

2.2.1 Trypanosome Cell Culture

2.2.1.1 Cultivation of procyclic trypanosomes

The procyclic form of *Trypanosoma brucei brucei* EATRO1125-T7T and AnTat 1.1 1313 was cultured at 27°C in SDM79 supplemented with 10 % FCS (Brun and Schonenberger, 1981). Glucose-depleted SDM79 (-Gluc) was supplemented with 50 mM N-acetyl D-glucosamine (GlcNAc) instead of 10 mM glucose, which is a non-metabolized glucose analogue inhibiting glucose import (Allmann et al., 2013; Azema et al., 2004). SDM79 (+glycerol) medium contains 20 mM glycerol and 50 mM GlcNAc but no glucose. SDM79 (+glycerol/+glucose) was supplemented with 20 mM glycerol and 10 mM glucose. Cells were grown at exponential phase at a cell density of 1E6 to 2E7 cells/ml.

2.2.1.2 Freezing and thawing cells

For one stabilate 5E7 cells were harvested at 900 ×g, 4 °C for 10 min. The pellet was resuspended in 1 ml freezing medium (SDM79, 20 % FCS, 20 % glycerol), transferred to cryo tubes and stored at -80 °C or -150 °C for long term storage. Stabilates were thawed in a 27 °C waterbath and washed with 5 ml SMD79 medium. Cell pellets were resuspended in 5 ml SDM79 and checked for viability and density by means of microscopy and CASY counter.

2.2.2 Generation of transgenic *Trypanosoma brucei* cell lines

2.2.2.1 Transfection of procyclic form Trypanosomes

Plasmids amplified in *E. coli* were purified using the NucleoSpin plasmid kit (Macherey & Nagel). In order to transfect pure and sterile DNA, the plasmids were precipitated after linearization with restriction enzymes. Here, 1/10 volume of 3 M sodium acetate pH 7 and 1 volume 100 % isopropanol was applied to the digested plasmid and vortexed. After pelleting the plasmid DNA at 14,000 ×g and 4 °C, the DNA pellet was washed once with 70 % EtOH and the dried plasmid pellet was resuspended to a concentration of 1 µg/µl in sterile H_2O. 2E7 procyclic form cells growing at exponential phase were washed once with 1.5 ml cytomix (10 min, 4 °C, 900 xg) and resuspended in 400 µl cytomix containing 10 µg linearized plasmid DNA. Cells were transfected using the BTX™-Harvard Apparatus ECM™ 630 at 1.5 kV, 175 Ω and 25 µF. Transfected cells were transferred into 8 ml SDM79 supplemented with 20 % FCS. In order to get single

clones, an 1:2 end-point dilution was performed in 96-well format. Selection markers were applied 20 h post transfection. Clones and pools were selected in SDM79 20 % FCS supplemented with the corresponding selection markers using concentrations as followed: hygromycin B (25 µg/mL), neomycin (10 µg/mL), blasticidin (10 µg/mL), phleomycin (5 µg/mL for EATRO 1125-T7T; 2.5 µg/ml for AnTat) and puromycin (1 µg/mL) (Riviere et al., 2004).

2.2.2.2 TY-tagged cytosolic aconitase

AnTat 1.1 1313 ΔN10ACO- One aconitase (ACO) allele was replaced with a neomycin resistance cassette using pBSK-Δaco-NEO linearized with EcoRI and SacI. For the second allele, the nucleotides encoding the ten most N-terminal amino acids were replaced *in situ* by a 4 TY1-tag by means of a construct based on p3077 (a pN-PTP derivative (Kelly et al., 2007) (kind gift of Kramer (Würzburg) and Carrington (Cambridge)). The p3077-TY-ΔN10ACO construct was linearised with EcoRI prior transfection.

2.2.2.3 Protein overexpression in procyclic form trypanosomes

2.2.2.3.1 RNA binding protein 6

The EATRO 1125-T7T based cell lines WT and null mutants of aconitase, citrate synthase, fructose 1,6-bisphosphatase (kind gift of Bringaud, Bordeaux), glycosomal and mitochondrial isocitrate dehydrogenase were transfected with pLew100v5-RBP6 (Allmann PhD thesis 2014) and selected in pools. The vector pLew100v5 contains two tetracycline operators and two T7 terminators making it less leaky (Wirtz et al., 1999). Cells were induced with 10 µg/ml tetracycline and analysed every two days.

2.2.2.3.2 Citrate synthase

Citrate synthase (Tb927.10.13430) was expressed in a tetracycline inducible manner in AnTat 1.1 1313 WT and null mutants of aconitase (ACO), glycosomal and mitochondrial isocitrate dehydrogenase (IDHg and IDHm, respectively) and a cell line expressing ACO only in the cytosol (ΔN10ACO). WT and ΔACO, ΔIDHg, ΔIDHm cell lines were transfected with pHD1146_CS-TY_HYG and ΔN10ACO was transfected with pHD1146_CS-TY_PAC. Clones were selected by 1:2 end point dilutions. The HYG resistance cassette of pHD 1146 (kind gift of Clayton (Heidelberg)) was exchanged into PAC (pHD 1146-PAC). pHD 1146 and pHD1146-PAC contained the full open reading frame of *Tb*CS and a 4TY1 tag and was linearized with NotI. For equal CS expression levels different tetracycline

concentrations were applied to the cell lines (WT: 1 µg/ml; ΔACO: 0.1 µg/ml; ΔN10ACO: 0.01 µg/ml; ΔIDHg: 1 µg/ml; ΔIDHm: 0.006 µg/ml).

2.2.2.3.3 Gene knock outs

In order to generate homozygous knock outs in EATRO 1125-T7T of citrate synthase or mitochondrial isocitrate dehydrogenase (Tb927.8.3690), one allele was replaced by a puromycin (PAC) and the other allele by a blasticidin (BLAS) resistance cassette via homologous recombination. Procyclic EATRO 1125-T7T cells were transfected with pBSK-derived DNA fragments containing the resistance marker gene flanked by the gene of interest untranslated region (UTR) sequences (pBSK constructs generated by Allmann and Panzer). The clonal cell lines with the genotype *TETR::HYG T7RNAP::NEO Δgoi::BLAS/Δgoi::PAC* is called EATRO 1125-T7T ΔGOI.

2.2.3 DNA methods

2.2.3.1 Polymerase chain reaction (PCR)

For each PCR reaction 5 µl purified gDNA or 20 ng plasmid were applied as template. The standard reaction volume for control PCR and insert PCR for cloning was 20 µl and 50 µl, respectively. The extension time of Phusion® High-fidelity DNA polymerase was 30 sec/1000 bp. Annealing temperatures of primers depend on the GC-content and were calculated by subtracting 5 °C from the melting temperature supplied with the data sheet by Sigma-Aldrich.

GC buffer	4.0 µl
H_2O	7.8 µl
dNTPs (10 mM)	0.4 µl
Fwd_primer (10 µM)	1.0 µl
Rev_primer (10 µM)	1.0 µl
gDNA	5.0 µl
DMSO	0.6 µl
Phusion	0.2 µl
total	20.0 µl

	Temperature	Time	
Initial denaturation	98 °C	10 min	
Denaturation	98 °C	30 sec	25-30 cycles
Annealing	X °C	30 sec	
Elongation	72 °C	X sec	
Final elongation	72 °C	5 min	
Storage	12 °C	∞	

2.2.3.2 Restriction digest and ligation of DNA fragments

Plasmids and PCR amplicons were digested with restriction endonucleases using the conditions recommended by NEB. Ligation of plasmids and inserts was performed in 20 µl for 2 h at room temperature or at 16 °C over night. Here, 50 ng plasmid were ligated with a 5-fold excess of insert molecules.

2.2.3.3 DNA quantification and DNA sequencing

DNA concentrations and DNA purities were determined using the NanoDrop 1000. DNA was sequenced at the sequencing service of the LMU Biology I department using the "cycle, clean and run" protocol and the BigDye 3.1 sequencing chemistry. 150 ng of plasmid DNA was mixed with 10 mM Tris-Cl, pH 8.5 and 3.2 pmol primer in a total volume of 7 µl.

2.2.3.4 Analytical and preparative agarose gelelectrophoresis

DNA samples were mixed with 6x DNA loading dye and separated by length of the DNA fragments. 1 % agarose gels containing 1 µg/ml ethidium bromide were ran in TAE running buffer at 10 V/cm^2 until the orange G migration front entered the buffer reservoir. 6 µl of 1 kb DNA ladder (NEB) was applied as size standard. Images of agarose gels were taken with the Geldoc 2000 (BIO-RAD). Plasmids and PCR amplicons digested with restriction enzymes for cloning were purified by gel extraction using the NucleoSpin Extract II kit (Macherey & Nagel).

2.2.3.5 $CaCl_2$ transformation of bacteria

50 µl $CaCl_2$ chemically competent XL-10 gold or SURE *E. coli* cells (Stratagene) were thawed on ice for 15 min and mixed with 5-10 ng plasmid or alternatively with 10 µl of the ligation mixture. After incubating on ice for 20-30 min, cells were heat-shocked for 30 sec at 42 °C and chilled for 2 min on ice. 900 µl LB medium without antibiotics was added prior 20 min incubation at 37 °C, while shaking at 8,000 rpm. Cells were 10-fold enriched, spread on LB-agar plates containing 100 µg/ml ampicillin as selection marker and incubated over night at 37 °C.

2.2.3.6 DNA isolation

For transfection of trypanosomes with DNA constructs, plasmid DNA was extracted from *E. coli* using the NucleoSpin Plasmid kit (Macherey & Nagel). In order to check *E. coli* clones for successful transformation of plasmids, the "Easypreps" protocol was used to isolate plasmids from 2 ml over night culture (Berghammer and Auer, 1993).

2.2.4 Protein methods

2.2.4.1 Preparation of whole cell lysates

1E7 procyclic trypanosomes were harvested at 900 ×g for 10 min at 4 °C and washed once with 1 ×PBS. The cell pellets were resuspended in 50 µl 1 ×Laemmli sample buffer and boiled for 5 min at 95 °C. 10 µl containing 2E6 cells were applied in one pocket of 10 % polyacrylamide gels.

2.2.4.2 SDS-Polyacrylamide gelelectrophoresis

Proteins were separated according to their molecular weight by means of discontinuous polyacrylamide gelelectrophoresis (PAGE) (Laemmli, 1970). Up to 10 one dimensional 10 % SDS-PAGE gels were casted using Mini-PROTEAN® 3 Multi-Casting Chambers (BIO-RAD) at the same time as described by Gallagher (Gallagher, 2006). Protein samples were resolved at 20 mA/gel in Mini-PROTEAN® Tetra Vertical Electrophoresis Cell (BIO-RAD) using Laemmli running buffer.

2.2.4.3 Western blot analysis

Proteins resolved in polyacrylamide gels were transferred on PVDF membranes using the semi-dry Western blot method (Kyhse-Andersen, 1984). PVDF membranes were activated for 2 min in 100 % methanol prior washing with ddH_2O. A sandwich was stacked starting with two Whatman® papers soaked with anode buffer, one PVDF membrane, the polyacrylamide gel and one Whatman® paper soaked in cathode buffer. Proteins were transferred for 1 h using BIO-RAD Trans blotter. The amperage induced was calculated as followed: $I\ [mA] = length_{blot} \times width_{blot} \times 0.8$. Membranes were blocked with 5 % (w/V) dry milk powder in 1× PBS for 1 h at RT or at 4 °C over night. Primary antibodies were applied for 1 h in 1 % (w/V) dry milk in 1× PBS/T. After washing the membranes four times for 5 min with PBS/T, species specific secondary antibodies conjugated to IRDye680 or IRDye800 were applied for 1 h in 1 % (w/V) dry milk in PBS/T supplemented with 0.02 % SDS in the dark. Blots were washed four times for 5 min with PBS/T and once with ddH_2O in the dark. Dried blots were scanned with LI-COR Odissey Infrared imaging system and the LI-COR unicorn software was used to determine fluorescence signal intensity for absolute protein quantification.

2.2.4.4 Digitonin fractionation

Digitonin titration was performed as described (Blattner et al., 1992). Digitonin concentrations were chosen proportional to the protein concentration. A 1 % digitonin stock solution was freshly prepared and heated for 5 min at 95 °C until digitonin is completely dissolved. Nine digitonin working dilutions in the range of 0 to 1 $mg_{digitonin}/mg_{protein}$ were prepared in STE buffer. All steps of the cell fractionation were performed on ice and with centrifuges and buffers pre-cooled to 4 °C. For each digitonin fraction 1.4 $\times 10^8$ cells were harvested at 900 ×g for 10 min. According to determinations of the cellular total protein content conducted by Allmann (personal communication), 1.4E8 cells are equivalent to 560 µg of protein. Cell pellets were washed thrice in STE buffer and resuspended in 200 µl digitonin containing STE solution and incubated for 5 min at 25 °C. Samples were centrifuged at 10,000 ×g for 5 min and the supernatants were transferred into fresh 1.5 ml reaction tubes and mixed with 40 µl 6× Laemmli buffer. The pellets were washed thrice in 1x PBS and resuspended in 240 µl 1× Laemmli buffer. For subcellular localisation 5-20 µl were applied to 10 % SDS-PAGE gels. Here, enolase and lipoamide dehydrogenase served as marke proteins for cytosolic and mitochondrial localisation, respectively.

2.2.5 Isocitrate dehydrogenase enzymatic assays

AnTat 1.1 1313 WT and the null mutants of glycosomal and mitochondrial isocitrate dehydrogenase (ΔIDHg and ΔIDHm, respectively) were analysed for NAD^+ and $NADP^+$-dependent activities. 4E8 cells were harvested at 900 ×g for 10 min at 4 °C and washed once with chilled 1 ×PBS. The cell pellets were shock-frozen in liquid nitrogen and stored until further use at -80 °C. Cell pellets were lysed in lysis buffer (50 mM Tris-Cl pH 7 or pH 8, 0.5 mM $MnCl_2$, 1 ×cOmplete EDTA-free protease inhibitor (Roche)) and sonicated for 5 min with the Bioruptor UCD-200 (Diagenode) at 320 W, 20 kHz for 15 sec pulse and 30 sec pause in ice water. After determination of protein concentration in the lysates by means of Bradford assay following the protocol provided with the Bradford assay solution by Applichem (Bradford, 1976) and a BSA calibration curve, citrate was added to a final concentration of 1 mM to stabilize the IDH enzyme (Overath et al., 1986). Initially, IDH activity assays were performed in 1 ml in quartz cuvettes using 100 µl lysate and changes in absorption were measured at 340 nm using the DU® 640 spectrophotometer (Beckman Coulter). Background activities were determined at RT for 3 min every 10 sec in 50 mM Tris-Cl pH7, 1 mM citrate, 0.5 mM $MnCl_2$, 10 mM in presence of one cosubstrate and the enzymatic reaction was measured for another

3 min after addition of isocitrate to a final concentration of 5 mM. Later IDH enzymatic activities were determined in UV transparent 96-well plates using the TECAN Infinite M200 Pro. Reactions were performed in 200 µl containing 10 µl whole cell lysate with increased cosubstrate concentrations of 12 mM NAD^+ and 4 mM $NADP^+$ at 27 °C. Background activity was determined in presence of cosubstrates for 3 min and enzyme activity was determined for another 3 min after injection of isocitrate to a final concentration of 5 mM. Concentrations of produced NAD(P)H were calculated by means of the Beer-Lambert law using an the extinction NAD(P)H coefficient at 340 nm ε_{340} 6.22 $mM^{-1}cm^{-1}$ and a path length of 1 cm for cuvettes and 0.5555 cm for 96-well plates. Background activity was subtracted prior calculating the enzymatic activity $(n[\text{nmol}] \times (t\,[\text{min}] \times m_{protein}[\text{mg}])^{-1}$.

2.2.6 Flow cytometry analysis of stage-specific surface marker

BARP detection required addition of 5 mM bathophenanthroline disulphonic acid (BPS) into the culture medium for >8 h prior harvesting (Urwyler et al., 2007). 2E7 cells were harvested and fixed over night with 2 % paraformaldehyde in 1× PBS at 4 °C, washed thrice with 1× PBS and resuspended in 500 µl 1× PBS. Cells were probed with polyclonal rabbit α-BARP (1:400) (Urwyler et al., 2007) (kindly provided by Isabel Roditi) and monoclonal mouse- α-procyclin EP (TBRP1/247, 1:500) in 1 % BSA. For calflagin detection 3× 10^7 cells were permeabilised with 0.2 % NP-40 for 5 min prior incubation with polyclonal mouse α-calflagin (1:1,000) (Tyler et al., 2009) in 1 % BSA. Alexa Fluor® 488-conjugated goat raised species-specific antibodies were used as secondary antibodies. Samples were analysed with the FACSCalibur™ cell analyser (Becton Dickinson) and data were evaluated with the FlowJo 8.8.6 software.

2.2.7 Immunofluorescence analyses of stage-specific markers

For immunofluorescence analyses, 5E7 cells were harvested and fixed in 400 µl 2 % paraformaldehyde in 1× PBS over night at 4 °C. Samples probed for BARP expression were treated with 5 mM BPS in the culture medium >8 h prior harvesting (Urwyler et al., 2007). Fixed cells were washed three times with 1× PBS at 900 ×g, 4 °C for 10 min and stored in 600 µl 1× PBS at 4 °C until further use. About 50-150 µl of the fixed cell suspension was applied and settled for 10-15 min on silanised coverslips. After washing three times with 1× PBS, cells were probed with primary and secondary antibodies as described for flow cytometry. Images were acquired with the GE DeltaVision Elite microscope using 100-fold magnification using DIC as well as the DAPI and the

FITC/AF488 channel. Immunofluorescence signals were deconvolved with the SoftWoRx software. The Fiji is Just ImageJ software was used for Z-stacks, brightness/contrast adjustments, channel merging and application of pseudocolors to the channels.

2.2.8 Fluorescence microscopy analyses of fly life cycle stages

Differentiation kinetics were determined in a time frame of ten days. Parasite smears were prepared every two days after induction of RBP6 overexpression, whereof day 0 corresponds to uninduced cells. About 1E7 cells were einriched in a volume of 30-50 µl and 10 µl were applied on one end of a microscope slide and spread with another slide and air-dried. Smears were fixed with methanol over night at -20 °C, dried and rehydrated for 15 min in 1× PBS at room temperature. Nuclei and kinetoplasts were stained with 0.1 µg/ml DAPI in 1× PBS for 5 min at room temperature and washed twice with 1× PBS and once with ddH_2O. The dried slides were mounted with VECTASHIELD™ antifade medium and sealed with nail polish. Images of DIC and DAPI were taken with the Zeiss AxioImager M1 using 63-fold magnification. Life-cycle stages were determined by means of cell morphological features. Here, size, shape and the relative position of the kinetoplast to the nucleus were taken into account (ROTUREAU and VAN DEN ABBEELE, 2013). A cell is considered as epimastigote form (EMF), if the kinetoplast has a juxtanuclear position or a localisation at the anterior end of the nucleus. Metacyclic forms (MFs) are smallest in size and the kinetoplast is located in close proximity to the plasma membrane at the rounded posterior tip of the cell. Procyclic forms (PCFs) are bigger than MFs and the kinetoplast is in between the posterior tip of the cell and the nucleus. For each time point >100 cells were characterised in biological triplicates.

2.2.9 Protocol optimization for quantitative determination of citrate

In trypanosomes citrate is a metabolite with low abundance. In order to determine absolute citrate concentrations in *T. brucei* reliably, we evaluated different methods together with the Portais lab (Toulouse) using ion chromatography/mass spectrometry (IC/MS). The "filter method" is suitable for ^{13}C stable isotope labelling (Allmann et al., 2013), but for determining ^{12}C absolute citrate levels in 2E7 cells the citrate background was too high. The same problem was faced when determining citrate with the method used for untargeted metabolomics (Vincent et al., 2012) using 3.3E7 cells per sample. The modified protocol based on the "differential method" published for *E. coli* failed as compared to extracellular citrate levels intracellular citrate concentrations were negligibly low (Taymaz-Nikerel et al., 2009). Together with the Portais lab (Toulouse)

we chose a protocol based on the one published by Villas-Bôas (Villas-Bôas and Bruheim, 2007) using 4E8 cells to be best for rapid quenching of metabolism and with minimized background. Here, trypanosomal metabolism was quenched as described previously including some modifications (Villas-Bôas and Bruheim, 2007) and extracted in MeOH:ACN:H_2O (V:V:V = 2:2:1) for 2 h at -20 °C.

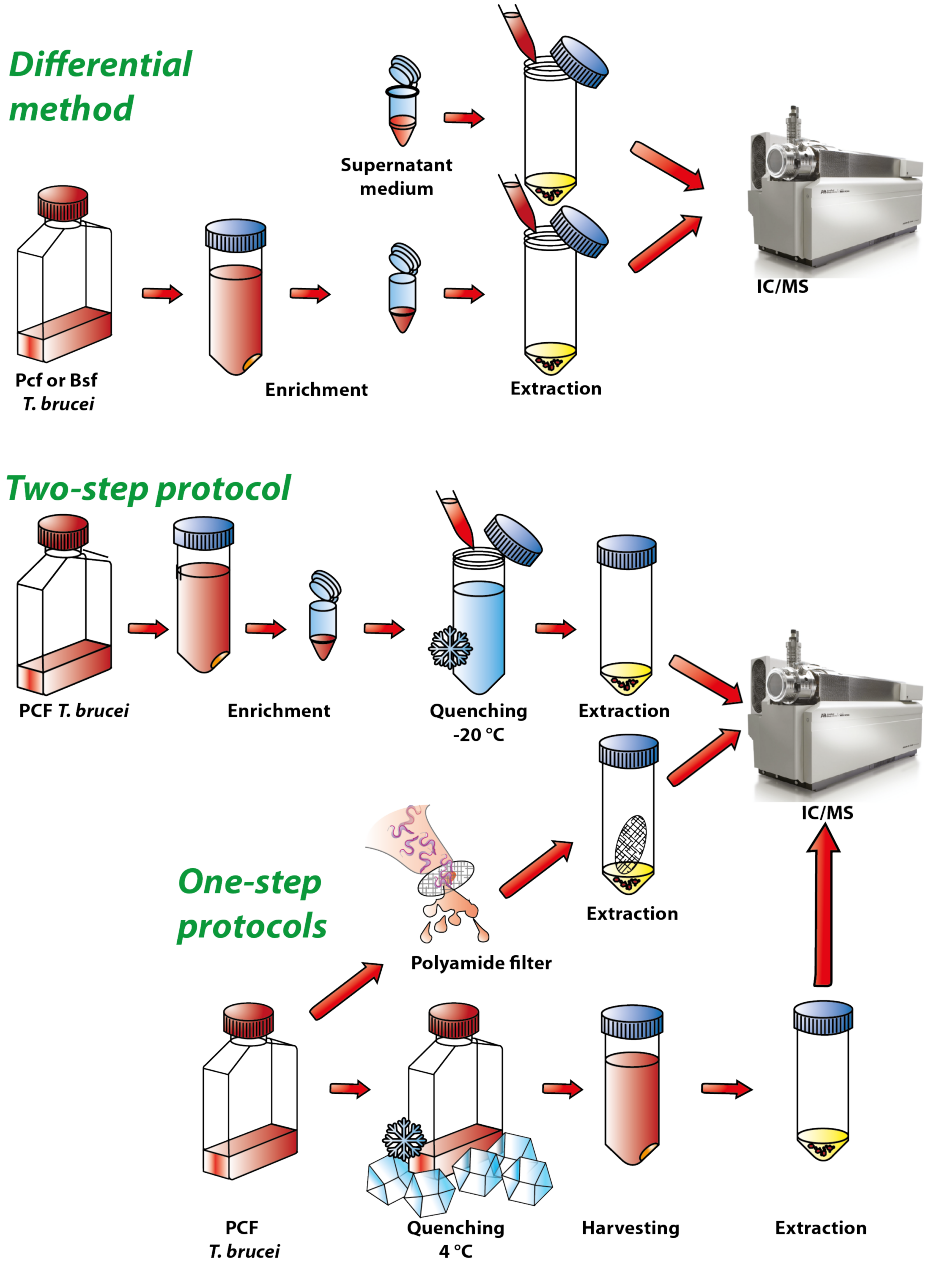

Figure 4 Schematic overview of the different quenching methods evaluated for citrate determination. In the differential method citrate concentration was determined for cells in 500 µl medium (endometabolome and exometabolome) as well as in 500 µl supernatant medium (exometabolome). The difference after subtracting the exometabolome from the endometabolome/exometabolome represents the intracellular citrate concentrations (Taymaz-Nikerel et al., 2009). The one-step protocols using polyamide filters or quenching in an ethanol-water bath at 4°C was performed as described in (Allmann et al., 2013) and (Vincent et al., 2012), respectively. The two-step protocol using 4E8 cells was chosen as favoured method as it combines a rapid quenching step at -20 °C with a washing step at -20 °C, modified from Villas-Bôas (Villas-Bôas and Bruheim, 2007).

2.2.10 GC/MS for determination of absolute citrate concentration

Here, we used the method optimized together with the Portais lab (Toulouse), but with an alternative extraction method suitable for GC/MS. AnTat 1.1 1313 WT and null mutants of aconitase (ACO), citrate synthase (CS), glycosomal and mitochondrial isocitrate dehydrogenase (IDHg and IDHm, respectively), a double null mutant of ACO and CS as well as a cell line expressing a cytosolic ACO, but no mitochondrial ACO (ΔN10ACO) were cultured for 10 d in absence and presence of glucose and 4E8 procyclic form cells were harvested at a cell density of 8E6-1.5E7 cells/ml at 900 ×g, 27 °C for 10 min. The cell pellet was resuspended in a final volume of 500 µl supernatant and completely injected into 4.5 ml quenching solution 0.9 % NaCl in glycerol:H_2O (3:2) kept at -20 °C in 30 % ethanol slurry. The samples were centrifuged at 10,000 ×g at -20 °C for 10 min (Heraeus, Kendro Biofuge Stratos) and the supernatant was aspirated quantitatively. The pellets were resuspended in 1 ml methanol and sonicated for 3 min (Bioruptor UCD-200, 320 W, 20 kHz, 30 sec pulse - 30 sec pause) in ice water. The following steps were performed by the Eisenreich lab (TUM, Garching). Deuterated citric acid (Citric acid-2,2,4,4-d_4; Sigma-Aldrich) was added as internal standard to a final concentration of 500 nM. Lysates were centrifuged at 5,000 ×g at 7 ° for 1 h and a 0.5 ml aliquot of the supernatant was evaporated at RT under nitrogen supply. The resulting residues were lyophilized at 1.0 mbar over night, solved in 100 µl dry acetonitril and derivatized with 100 µl *N*-(*tert*-butyldimethylsilyl)-*N*-methyltrifluoracetamide containing 1% *N*-*tert*-butyldimethylsilylchloride at 70 °C for 40 min. The resulting TBDMS derivatives were used for gas chromatography-mass spectrometry (GC/MS).

GC/MS was performed on a GC-QP 2010 plus (Shimadzu,Duisburg, Germany) equipped with a fused silica capillary column (equityTM-5; 30m by 0.25mm, 0.25-µm film thickness (Supelco, Bellafonte, PA).The mass detector worked in electron ionization (EI) mode at 70 eV. 2 µl of the solution were injected in split mode (1:5) at an injector and interface temperature of 260°C. The column was held at 220 °C for 2 min and then developed with a temperature gradient of 3 °C/min to a final temperature of 280 °C. Each sample was analyzed in scan and SIM mode at least two times. Data were collected with LabSolution software (Shimadzu, Duisburg, Germany). The retention time for TBDMS-citrate and TBDMS-citrate-d_4 was 14.23 min and 14.18 min, respectively. For quantification the characteristic m/z values 591 and 595 for TBDMS-citrate and TBDMS-citrate-d_4 (each corresponding to M-57) measured in SIM mode were used. For each cell line three independent biological replicates cultured at different time points were taken at different time points each consisting of three technical replicates.

2.2.11 Stable isotope labelling using [U-^{13}C] proline

Procyclic AnTat 1.1 1313 WT and the null mutants of aconitase (ΔACO), citrate synthase (ΔCS), glycosomal isocitrate dehydrogenase (IDHg), mitochondrial isocitrate dehydrogenase (ΔIDHm) and the double null mutant ΔACO/ΔCS were grown for ten days under glucose depleted culture conditions in presence of 50 mM N-acetyl D-glucosamine. For each time course 1E9 cells were washed twice with 1× PBS at 900 ×g and 27 °C for 10 min. Cell pellets were resuspended in 5 ml labeling solution MS-grade 1× PBS with 2 mM [U-^{13}C5] proline to a cell density of 2E8 cells/ml and incubated at 27 °C and 5 % CO_2 atmosphere. Four time points were analysed 0 min, 15 min, 30 min and 120 min. Endometabolome and exometabolome were analysed by injecting 500 µl of labeling solution containing 1E8 cells into 4.5 ml extraction solution (ACN:MeOH:H_2O (V:V:V = 2:2:1)) and cooled down to -20 °C. Metabolites were extracted for 1-5 h at -20 °C and stored at -80 °C. For analysis of the exometabolome, 550 µl of labeling solution containing 1.1E8 cells were cleared at 10,000 ×g and 4 °C for 30 sec and 500 µl of the supernatant were snap frozen in liquid nitrogen and stored at -80 °C.

The following steps were performed by the Portais lab (INSA Toulouse). Samples were evaporated under vacuum in a SC110A SpeedVac Plus (Thermo Fisher Scientific, Sunnyvale, CA) for 6 h and then stored at -80°C for further use. Dried samples were resolubilized in 250 µl Milli-Q (Merck-Millipore Darmstadt) purified water and analyzed by ion chromatography coupled with a triple quadrupole mass spectrometer (ion chromatography–coupled tandem mass spectrometry). Liquid anion exchange chromatography was performed with the Thermo Scientific Dionex ICS-5000$^+$ Reagent-Free HPIC system (Thermo Fisher Scientific) equipped with an eluent generator system (ICS-5000+ EG, Dionex) for automatic base generation (KOH). Analytes were separated within 45 min, using a linear KOH gradient elution applied to an IonPac AS11 column (250 × 2 mm, Dionex) equipped with an AG11 precolumn (50 × 2 mm, Dionex) at a flow rate of 0.35 ml/min. The gradient was as follows: equilibration with 0.5 mM KOH, 1.1 min; KOH ramp from 0.5 to 4.1 mM, 1–9.5 min; constant concentration 5.1 min; isocratic ramp to 9.65 mM in 9.4 min; isocratic ramp to 60 mM in 8 min; isocratic ramp to 90 mM in 0.1 min; constant concentration 6.9 min; drop to 0.5 mM in 0.1 min; and equilibration at 0.5 mM KOH for 1.9 min. The column and autosampler temperatures were thermostated at 29°C and 4°C, respectively. The injected sample volume was 15 µl. Analytes were determined in triplicates from separately cultured trypanosomes in biological triplicates. Tandem mass spectrometry analyses was performed in the negative mode with a 4000QTRAP hybrid triple quadrupole/linear ion trap mass spectrometer (ABSciex, Foster City, CA) equipped with a Turbo V source (AB Sciex/MDS

Sciex, Toronto, ON, Canada) for electrospray ionization. The multiple reaction monitoring (MRM) approach was used for detection of carbon isotopologue distributions (CIDs) with a mass resolution of 0.5 amu at half peak height. Fragmentation was done by collision-activated dissociation using nitrogen as the collision gas at medium pressure. The nebulizer gas pressure was 50 psi, the desolvation gas pressure was 60 psi, the temperature was 650 °C, and the capillary voltage was 3.3 kV. Instrument control, data acquisition, and data analysis were performed with Analyst version 1.5.2 software.

Following organic acids were determined: citrate, isocitrate, succinate, fumarate, malate, *cis*-aconitate, α-ketoglutarate, 2-hydroxyglutarate and the phosphorylated compounds: glucose 6-phosphate (G6P), fructose 6-phosphate (F6P), mannose 6-phosphate (M6P), fructose 1,6-bisphosphate (FBP), 6-phosphogluconolactone (6PG), ribulose 5-phosphate (R5P), phosphoenolpyruvate (PEP), 2- or 3- phosphoglycerate (2PG/3PG), sedoheptulose 7-phsophate (Sed7P). The daughter ions of phosphate groups (PO_3^-, m/z = 79, or $H_2PO_4^-$, m/z = 97) for phosphorylated metabolites, and fragments with loss of a carboxylic group ($[M-H-^{12}CO_2]^-$ or $[M-H-^{13}CO_2]^-$) for organic acids. Carbon isotopologue distributions (CIDs) were calculated from isotopic clusters after correction for naturally occurring isotopes of elements other than carbon using IsoCor (Millard et al., 2012) and considering the natural isotopic abundances (Rosman, 1998).

Metabolite Name	Number of transitions
Fumarate	8
Succinate	8
Malate	8
alpha-KetoGlutarate (alpha-KG)	10
Phosphoénolpyruvate (PEP)	4
Cis-Aconitate	12
2/3-Phosphoglycerate (2/3PG)	4
Citrate/iso-Citrate	24
2-HydroxyGlutarate (2-OHGlu)	12
Ribose-5P/Ribulose-5P/Xylulose-5P	6
Glucose-6P	7
Fructose-6P	7
Mannose-6P	7
6-PhosphoGluconate (6-PG)	7
Sedoheptulose-7P (Sed7P)	8
Fructose-1,6-DP (FBP)	7
1,3-DiPG	4
Gly3P	4
Total	147

2.2.12 Quantitative proteome analysis

2.2.12.1 Sample preparation for proteomic analysis

Cells were cultured for 10 d in four different SDM79 variants. SDM79 lacking both glucose and glycerol supplemented with 50 mM N-acetyl D-glucosamine (GlcNAc) (-gluc/-glyc) or containing both 10 mM glucose and 20 mM glycerol but no GlcNAc (+gluc/+glyc). SDM79 supplemented with 50 mM GlcNAc and 20 mM glycerol (-gluc/+glyc) or only 10 mM glucose was added (+gluc/-glyc). After ten days in the different culture conditions 1.5E8 cells/sample cells were harvested. The cell pellets were washed once with SDM79 without FCS, resuspended in 400 µl 4.5 M urea, 0.2 % SDS and Roche cOmplete EDTA-free protease inhibitor and sonicated (Bioruptor UCD-200, 320 W, 20 kHz, two cycles 15 sec pulse - 30 sec pause). Trichloroacetic acid was added to a final concentration of 15 % V/V, mixed and incubated over night at 4 °C. The samples were washed twice with acetone and the pellet was air-dried in a laminar flow hood. The pellet was resuspended in 7 M urea, 2 M thiourea and 4 % CHAPS and incubated over night at RT. Samples were sonicated as described before and the supernatant was cleared for 15 min at 20,000 ×g and 4 °C. Protein yields were quantified with Bradford assay and SDS-PAGE.

2.2.12.2 Sample preparation for proteomic analysis

(performed by Dupuy (cgfb PROTÉOME, Université de Bordeaux))

Samples were loaded on a 10% acrylamide SDS-PAGE gel. Migration was stopped when samples were entered the resolving gel and proteins were visualized by Colloidal Blue staining. Each SDS-PAGE band was cut into 1 mm × 1 mm gel pieces. Gel pieces were destained in 25 mM ammonium bicarbonate (NH_4HCO_3), 50% Acetonitrile (ACN) and shrunk in ACN for 10 min. After ACN removal, gel pieces were dried at room temperature. Proteins were first reduced in 10 mM dithiothreitol, 100 mM NH_4HCO_3 for 30 min at 56°C then alkylated in 100 mM iodoacetamide, 100 mM NH_4HCO_3 for 30 min at room temperature and shrunken in ACN for 10 min. After ACN removal, gel pieces were rehydrated with 100 mM NH_4HCO_3 for 10 min at room temperature. Before protein digestion, gel pieces were shrunken in ACN for 10 min and dried at room temperature. Proteins were digested by incubating each gel slice with 10 ng/µL of trypsin (T6567, Sigma-Aldrich) in 40 mM NH_4HCO_3, 10% ACN, rehydrated at 4°C for 10 min, and finally incubated overnight at 37°C. The resulting peptides were extracted from the gel by three steps: a first incubation in 40 mM NH_4HCO_3, 10% ACN for 15 min at room temperature and two incubations in 47.5 % ACN, 5% formic acid for 15 min at

room temperature. The three collected extractions were pooled with the initial digestion supernatant, dried in a SpeedVac, and resuspended with 25 µL of 0.1% formic acid before nanoLC-MS/MS analysis.

2.2.12.3 nanoLC-MS/MS analysis

(performed by Dupuy (cgfb PROTÉOME, Université de Bordeaux))

Online nanoLC-MS/MS analyses were performed using an Ultimate 3000 RSLC Nano-UPHLC system (Thermo Scientific, USA) coupled to a nanospray Q-Exactive hybrid quadruplole-Orbitrap mass spectrometer (Thermo Scientific, USA). Ten microliters of each peptide extract were loaded on a 300 µm ID x 5 mm PepMap C_{18} precolumn (Thermo Scientific, USA) at a flow rate of 20 µL/min. After 5 min desalting, peptides were online separated on a 75 µm ID x 25 cm C_{18} Acclaim PepMap® RSLC column (Thermo Scientific, USA) with a 4-40% linear gradient of solvent B (0.1% formic acid in 80% ACN) in 108 min. The separation flow rate was set at 300 nL/min. The mass spectrometer operated in positive ion mode at a 1.8 kV needle voltage. Data were acquired using Xcalibur 2.2 software in a data-dependent mode. MS scans (m/z 300-2000) were recorded at a resolution of R = 70000 (@ m/z 200) and an AGC target of 1E6 ions collected within 100 ms. Dynamic exclusion was set to 30 s and top 15 ions were selected from fragmentation in HCD mode. MS/MS scans with a target value of 1E5 ions were collected with a maximum fill time of 120 ms and a resolution of R = 35000. Additionally, only +2 and +3 charged ions were selected for fragmentation. Others settings were as follows: no sheath and no auxiliary gas flow, heated capillary temperature, 200°C; normalized HCD collision energy of 25% and an isolation width of 3 m/z.

2.2.12.4 Database search and results processing

(performed by Dupuy (cgfb PROTÉOME, Université de Bordeaux))

Mascot and Sequest algorithms through Proteome Discoverer 1.4 Software (Thermo Fisher Scientific Inc.) were used for protein identification in batch mode by searching against a *Trypanosoma brucei* TREU927 database (9 976 entries, release 9.0) from http://tritrypdb.org/ website. Two missed enzyme cleavages were allowed. Mass tolerances in MS and MS/MS were set to 10 ppm and 0.02 Da. Oxidation of methionine, acetylation of lysine and deamidation of asparagine and glutamine were searched as variable modifications. Carbamidomethylation on cysteine was searched as fixed modification. Peptide validation was performed using Percolator algorithm [(1)] and only

"high confidence" peptides were retained corresponding to a 1% False Positive Rate at peptide level.

2.2.12.5 Label-Free Quantitative Data Analysis

(performed by Dupuy (cgfb PROTÉOME, Université de Bordeaux))

Raw LC-MS/MS data were imported in Progenesis LC-MS QI (Nonlinear Dynamics Ltd, Newcastle, U.K) for feature detection, alignment, and quantification. All sample features were aligned according to retention times by manually inserting up to two hundred landmarks followed by automatic alignment to maximally overlay all the two-dimensional (m/z and retention time) feature maps. Singly charged ions and ions with higher charge states than six were excluded from analysis. All remaining features were used to calculate a normalization factor for each sample that corrects for experimental variation. Peptide identifications (with $p<0.01$, see above) were imported into Progenesis. For quantification, all unique peptides of an identified protein were included and the total cumulative abundance was calculated by summing the abundances of all peptides allocated to the respective protein. No minimal thresholds were set for the method of peak picking or selection of data to use for quantification. For each biological replicate, the mean normalized intensities and standard deviation were calculated and ratio was deducted. Noticeably, only non-conflicting features and unique peptides were considered for calculation at protein level. Quantitative data were considered for proteins quantified by a minimum of 2 peptides. As an indication of the confidence of that protein's presence, the sum of the peptide scores (confidence score) is calculated for each protein from the search algorithm. This score includes unique peptides as well as switched off peptides, the later decreasing the confidence score.

3 Results

3.1 Citrate metabolism is not essential for growth of procyclic forms in absence of glucose

The enzymes of citrate metabolism aconitase (ACO), citrate synthase (CS), glycosomal and mitochondrial isocitrate dehydrogenase (IDHg and IDHm, respectively) are not essential for bloodstream forms (BSFs) and procyclic forms (PCFs) grown in glucose-rich cultures (Panzer, Diploma thesis 2007; Allmann PhD thesis 2014). As glucose gets scarce after the tsetse fly feeds on mammals and is only shortly available for PCFs colonizing the midgut (Vickerman, 1985), we analysed growth of null mutants of citrate metabolism in glucose-depleted cultures. First we defined glucose-depleted PCF culture conditions. PCFs can consume glucose in culture and even prefer glucose over proline (Lamour et al., 2005). The commonly used standard culture medium SDM79 contains around 10.5 mM glucose (Brun and Schonenberger, 1979). Here, 10 mM glucose is added and ~0.5 mM glucose is due to supplementation with 10 % fetal calf serum (FCS). Lamour and co-workers developed a derivative of SDM79 medium, named SDM80. SDM80 has a reduced glucose content of 0.15 mM, as it was supplemented with 9 % dialysed FCS and 1 % normal FCS instead of 10 % normal FCS (Lamour et al., 2005). However, dialysis also removes nutrients from FCS other than glucose introducing unknown aberrations into the culture system. Replacing FCS by the fully defined, animal-component free culture supplement XerumFree™ (TNCbio) was not successful, despite a period of gradual adaptation of the culture to the FCS alternative. N-acetyl D-glucosamine (GlcNAc), presumably derived from chitin degradation of the pupae, binds to hexose transporters of PCFs and BSFs and inhibits the uptake of glucose (Azema et al., 2004; Ebikeme et al., 2008). Based on these information we created a glucose deficient medium (SDM79 –gluc). Here, we modified standard SDM79 containing 10 % FCS by replacing 10 mM glucose with 50 mM GlcNAc to block uptake of FCS-derived glucose.

Table 1 Population doubling time (PDT) of AnTat 1.1 1313 procyclic WT and mutant cell lines. AnTat 1.1 1313 wild type (WT) and null mutants of aconitase (ΔACO), citrate synthase (ΔCS), cytosolic ACO ΔN10ACO (Δaco/TY::ΔN10ACO), glycosomal and mitochondrial isocitrate dehydrogenase (ΔIDHg and ΔIDHm, respectively) as well as the double null mutant ΔACO/ΔCS were grown in SDM79 medium in presence of 10 mM glucose (+gluc) and in absence of glucose with supplementation of 50 mM GlcNAc (-gluc).

	WT	ΔN10ACO	ΔACO	ΔCS	ΔACO/ΔCS	ΔIDHg	ΔIDHm
+gluc	12h	12h	12h	12h	13h	13h	15h
-gluc	16h	20h	17h	17h	17h	17h	20h

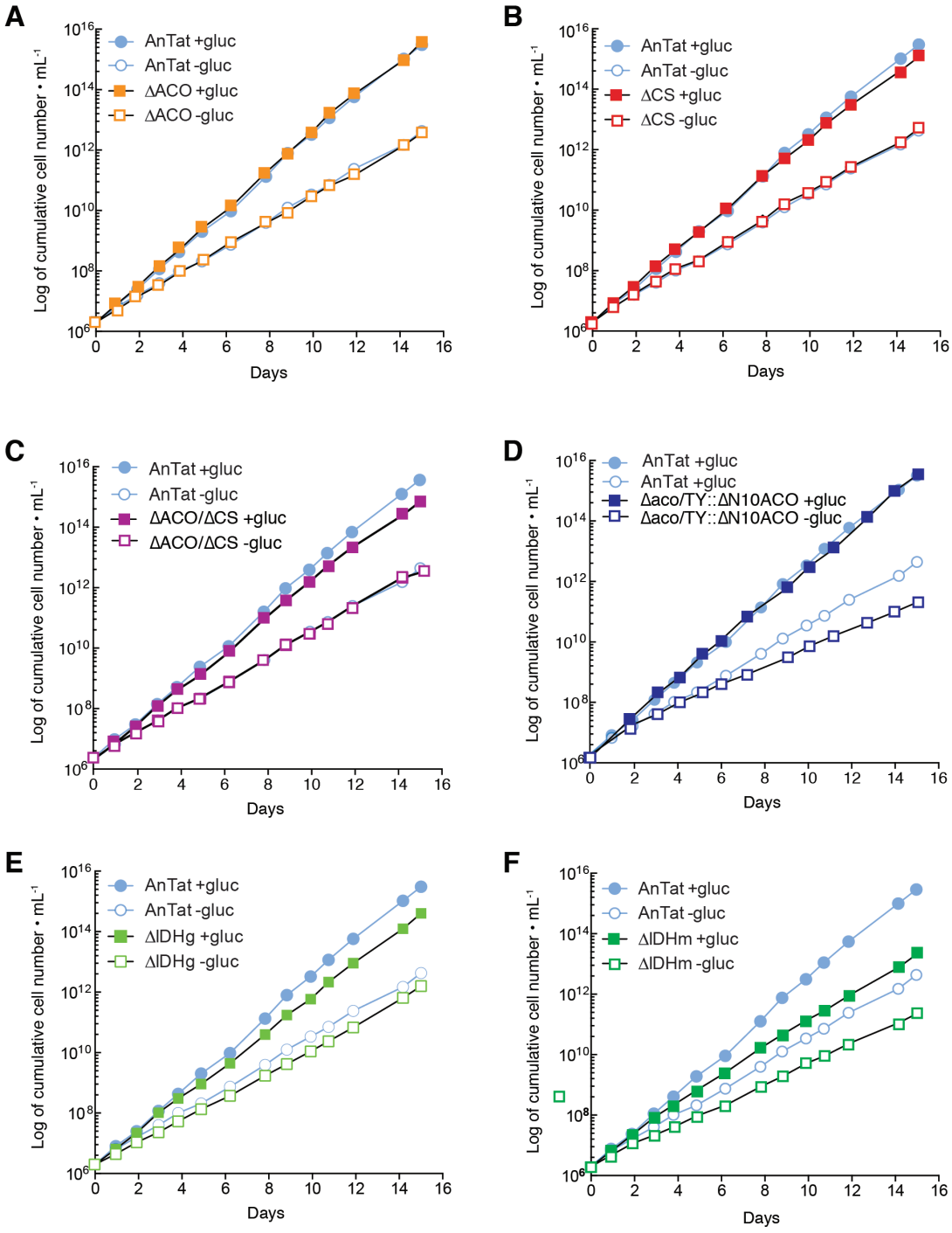

Figure 5 Procyclic WT cells and metabolic mutants do not depend on glucose to maintain growth
Procyclic form AnTat 1.1 1313 WT and null mutant cell lines were grown in SDM79 medium in presence of 10 mM glucose (+gluc, filled squares and circles) and in absence of glucose with supplementation of 50 mM N-acetyl-glucosamine (-gluc, empty squares and circles). Cells were cultured at exponential growth phase with cell densities ranging from 1E6 to 2E7 cells/ml. [A] to [F] Semi-logarithmic graphs of cumulative cell number. Light blue curves correspond to WT growth as reference in each panel.

Wild type (WT) and null mutants of ACO, CS, IDHg, and the double knockout mutant ΔACO/ΔCS are viable in absence of glucose and have a population doubling time of 12 h to 13 h, which is increased to 16 h to 17 h upon glucose withdrawal (Fig. 5 [A]-[E]). Null mutants were verified using Western blot analysis (Fig. 6 [C]). The ΔIDHm null mutant exhibits the biggest growth phenotype, as the PDT is 15 h and 20 h in presence and absence of glucose, respectively. In comparison to WT cells, the cell line with ACO expression restricted to the cytosol Δaco/TY::ΔN10ACO (ΔN10ACO) shows a growth phenotype in absence of glucose with a PDT of 20 h.

3.2 Glucose and glycerol specifically regulate enzyme expression in (iso-)citrate metabolism

After the tsetse fly bite, nutrients are absorbed by the gut epithelium and released by digestive enzymes from the blood meal. We here propose that glucose is depleted early after the blood meal and glycerol is released by lipases from degradation of red blood cell membranes and is transiently available. Later on, proline is considered the main carbon source, as it can fully replace glucose as carbon and energy source in procyclic form (PCF) *T. brucei* cultures (Lamour et al., 2005). Even though aconitase (ACO), citrate synthase (CS), glycosomal and mitochondrial isocitrate dehydrogenase (IDHg and IDHm, respectively) are not essential for growth in glucose- and glycerol- depleted medium, quantitative Western blot (WB) analyses revealed that expression of ACO, CS and IDHg is upregulated upon glucose and glycerol withdrawal in two different *T. b. brucei* strains, EATRO 1125-T7T and AnTat 1.1. However, neither glucose nor glycerol regulates IDHm expression (Fig. 6 [A], [B]). Previously, Lamour and co-workers showed that glucose regulates a key enzyme of proline metabolism, proline dehydrogenase (Lamour et al., 2005). A proteomic approach was applied to get a systematic expression profile of glucose and glycerol regulated proteins. Here, ACO, CS and IDHg were among the top of the metabolic hits having a glucose- and glycerol-dependent regulation of expression. An increase was observed in ACO protein levels of 1.3- and 2-fold, IDHg protein levels of 4- and 2-fold and CS protein levels of 2- and 4-fold in WB and proteome analyses, respectively. No significant regulation was observed for IDHm (Fig. 6 [B]). CS expression levels vary among the different cell lines. In contrast to EATRO 1125-T7T, CS is not detectable in AnTat 1.1 in presence of glucose by means of WB. The difference in CS expression in the two trypanosomal lines may be introduced by a higher number of passages resulting in an adaptation of the field isolates to cell culture conditions. Similar to AnTat 1.1 WT, null mutants of ACO, CS, IDHg and IDHm differentially express ACO, CS, IDHg but not IDHm in presence and absence of glucose (Fig. 6 [C], [D]).

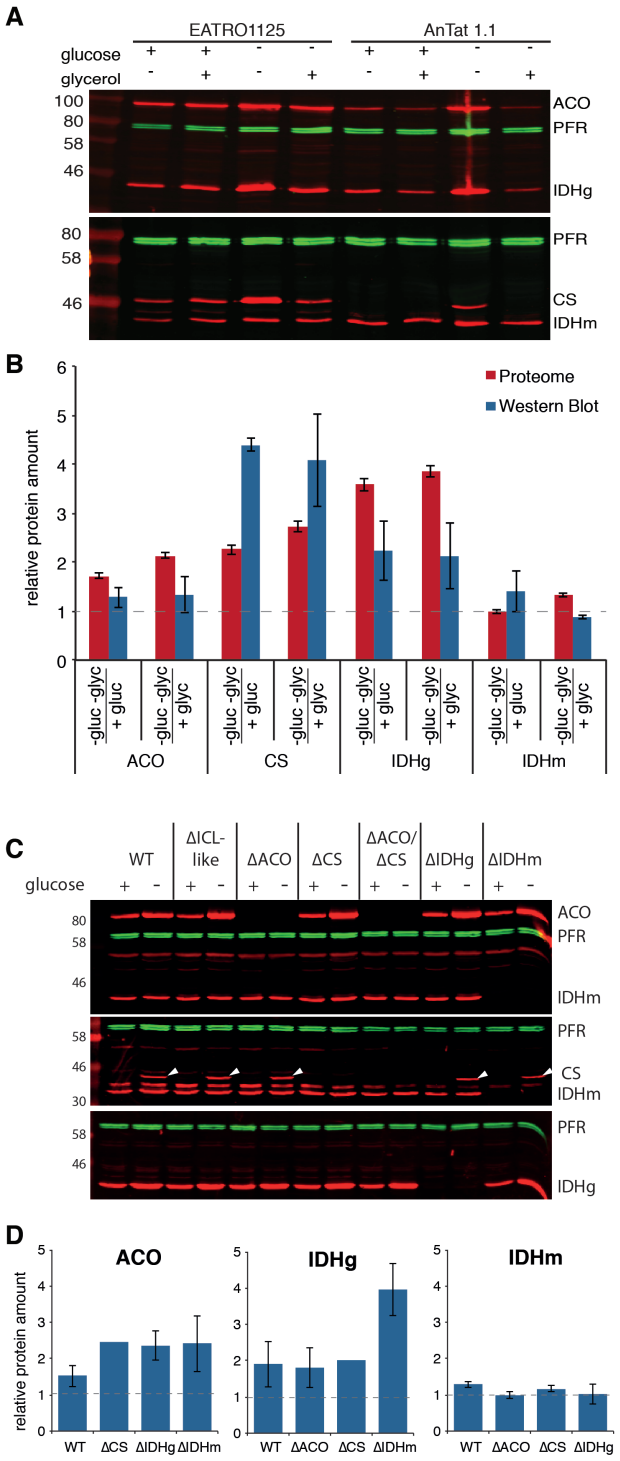

Figure 6 Glucose and glycerol regulate protein expression levels. All cell lines were grown for more than 10 days in SDM79 under different nutritional conditions. [A] and [C] For Western blot (WB) analysis, cell lysates were probed with polyclonal antisera raised in rabbit against aconitase (ACO), citrate synthase (CS), glycosomal and mitochondrial isocitrate dehydrogenase (IDHg and IDHm, respectively). Mouse mAb α paraflagellar rod (PFR) protein served as loading control. [A] WB analysis of EATRO 1125-T7T wild type (WT) and AnTat 1.1 1313 (WT). Cells were cultured in absence and presence of both glycerol and glucose or with one of each carbon source for 10 days. [B] Comparison of data gained by WB and proteome analysis using EATRO 1125-T7T WT cell line. Expression ratios of glucose- and glycerol-depleted to glucose- or glycerol-rich conditions are plotted to evaluate glucose and glycerol regulated protein expression. The quotient of WB samples was calculated after normalisation against PFR. [C] WB analysis of AnTat 1.1 1313 WT and ΔACO, ΔACL, ΔCS, ΔACO/ΔCS, ΔICL-like, ΔIDHg and ΔIDHm mutant cell lines cultured in presence and absence of glucose. [D] Expression ratios of glucose- and glycerol-depleted to glucose-rich conditions. Quotient of WB signals after normalisation against PFR. Error bars, SEM of biological replicates (n = 3), [D] ΔCS ratios probed with αACO or αIDHg correspond to n = 2 (no error bars), ICL-like = isocitrate lyase-like.

3.3 Isocitrate dehydrogenase enzymatic activity

Different isocitrate dehydrogenase (IDH) isoforms have been described in all kingdoms varying in their co-substrate specificity and oligomeric state (Imabayashi et al., 2006). Here, we determined coenzyme specificity for glycosomal and mitochondrial IDH in cleared procyclic form cell lysates. The correct subcellular localisation was verified for IDHg and IDHm by means of digitonin fractionation and Western blot analysis (Stefan Allman PhD thesis, 2014). IDH activity was analysed for IDHg in the ΔIDHm mutant and for IDHm in the ΔIDHg mutant. Glucose regulation of enzymatic activities were determined in lysates of cells grown for more than ten days in absence and presence of glucose. In the first experiments, IDH enzyme assays were performed in a reaction volume of 2 ml with 0.5 mM $NADP^+$ and 0.5 mM NAD^+ (Fig. 7 [A]), as described by Overath et al. (Overath et al., 1986) and pH 7 with main focus on glycosomal IDH (IDHg). The glycosomal pH varies between pH 7.4 and pH 6.8 in presence and absence of glucose, respectively (Lin et al., 2013). Our cooperation partner Inaoka (The University of Tokyo) found that IDHg has dual coenzyme specificity for both $NADP^+$ and NAD^+. Here, enzyme kinetics were determined using recombinant IDHg protein. Recombinantly expressed IDHg has a K_m of 3.466 mM using NAD^+ and a K_m of 0.731 mM using $NADP^+$ as co-substrate (unpublished data, Wang and Inaoka, Tokyo). Based on these K_m values, we repeated the IDH assays in cell lysates with increased co-substrate concentration in a reaction volume of 200 µl in 96-well plates. The IDH activity was measured using 4 mM $NADP^+$ and 12 mM NAD^+ instead of 0.5 mM in order to work with a reaction speed close to V_{max} and validate IDHg $NADP^+$- and NAD^+-specific activities measured for recombinant IDHg protein in cell lysates (Fig. 7 [B], [C]). In the optimised experimental setup, glucose depletion increases NAD^+- and $NADP^+$ specific IDHg activity 3.8- and 3.4- fold, respectively (Fig. 7 [B]). A pH shift by one unit from 7 to 8 does not have a significant impact on IDHg enzymatic activity. The pH in the mitochondrial matrix is around 8 (Alberts et al., 2008). In order to determine the IDHm enzymatic activity at physiological pH, enzyme assays were also performed at pH8 (Fig. 7 [C]). We found that IDHm is strictly limited to $NADP^+$ as co-substrate. In absence of glucose IDHm activity is doubled. The K_m value is not known, as IDHm has not been recombinantly expressed.

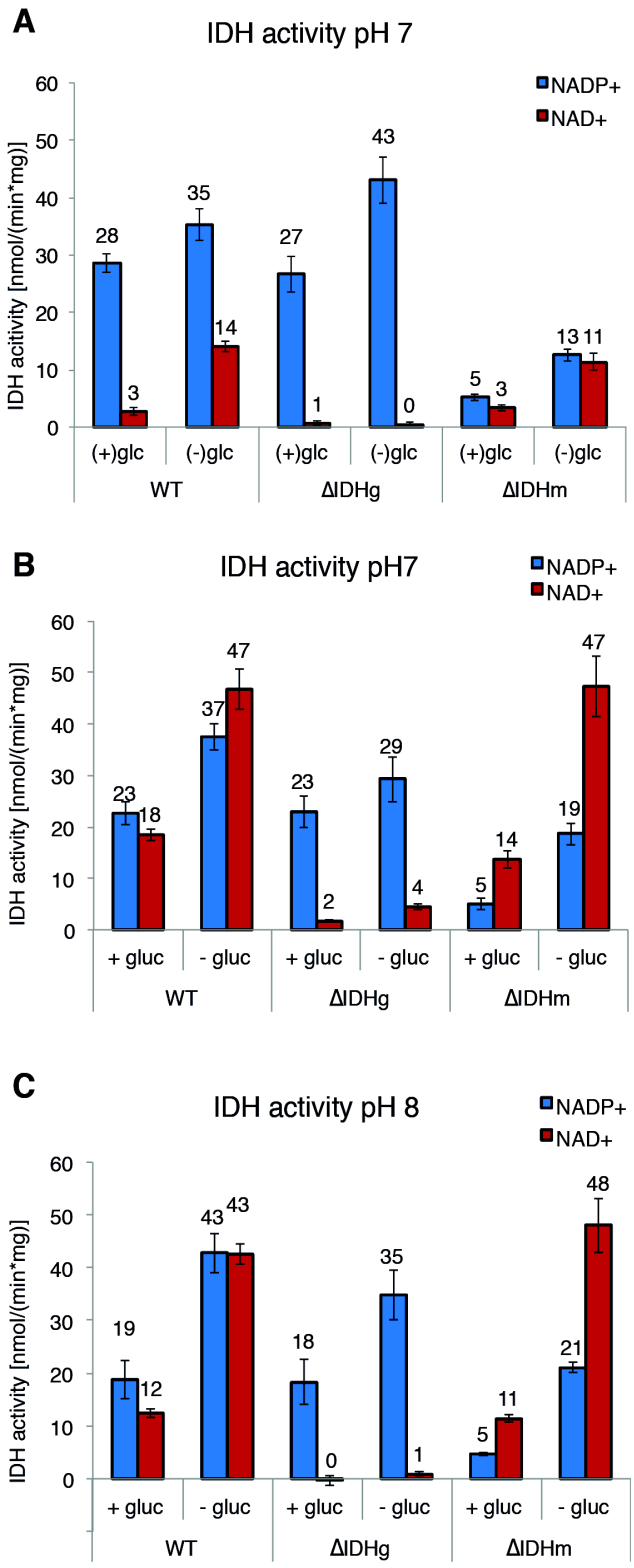

Figure 7 Glucose regulates isocitrate dehydrogenase enzymatic activities. Procyclic AnTat1.1 1313 WT and ΔIDHg and ΔIDHm null mutants were grown in SMD79 medium in absence and presence of glucose for 10 d. NAD(P)H production by the IDH reactions was measured photometrically at 340nm with cleared cell lysates. [A] Enzymatic activities were determined in a reaction volume 2 ml in quartz cuvettes using 0.5 mM $NADP^+$ or 0.5 mM NAD^+ [B] and [C] Enzymatic activities were determined in 200 µl in 96-well plates at pH 7 and pH 8, respectively. Assays were performed with 4 mM $NADP^+$ or 12 mM NAD^+. Error bars represent the SEM of biological triplicates (n = 3).

3.4 Glycosomal IDH is the major sink for isocitrate

Glycosomes are peroxisome-like organelles with a peculiar role in trypanosomal metabolism. The first six to seven enzymes of glycolysis are located to the glycosomes (Visser and Opperdoes, 1980). The role of an isocitrate dehydrogenase isoform (IDHg) in the glycosome is not known. As we found that IDHg is catalytically active, we aimed to provide evidence of an active flux through IDHg and the identification of the isocitrate supplying enzymes. In order to address this question, we determined absolute citrate concentrations in AnTat 1.1 wild type (WT) and null mutants of IDHg as well as null mutants of the mitochondrial citrate metabolism by means of gas chromatography/ mass spectrometry (GC/MS) (Fig. 8 [B] and [C]).

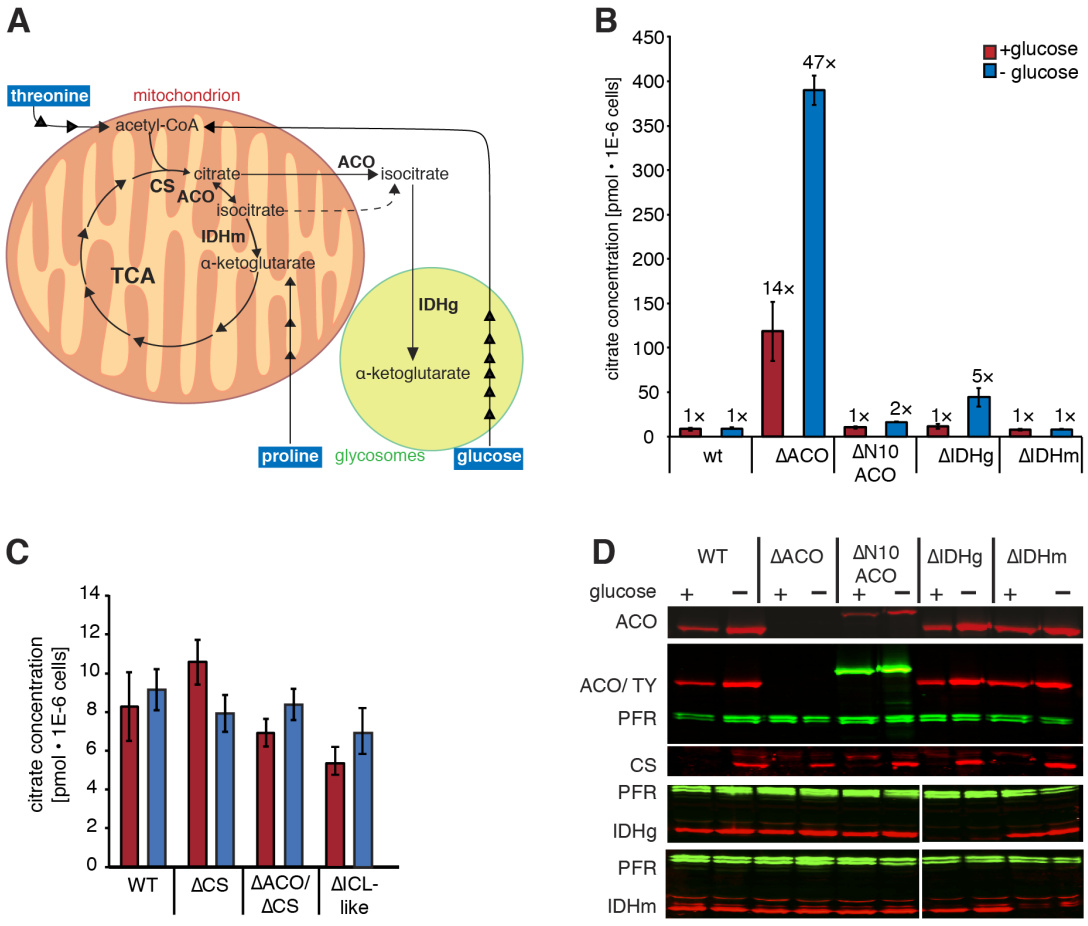

Figure 8 Glycosomal IDHg is the major sink for isocitrate. [A] Illustration shows major anaplerotic reactions feeding the TCA cycle in *T. brucei*. Dashed arrows mark putative fluxes. [B] Procyclic AnTat 1.1 WT and homozygous null mutants of ΔACO, ΔIDHg and ΔIDHm as well as the mutant expressing ACO only in the cytosol (ΔN10ACO) were cultured for 10 d in presence and absence of glucose. Citrate concentrations were determined by GC/MS. [C] citrate concentrations of ΔCS, ΔACO/ΔCS and ICL-like protein. [D] Control Western blot (WB) analysis of WT and null mutants cultured for 10 d in glucose-rich (+) and glucose-depleted (-) medium. Vertical white line in the IDHg and IDHm blot indicate the excision of two lanes from this blot. Samples used for ACO/CS and IDHg/IDHm WB derived from different biological replicates. ACO, aconitase; CS, citrate synthase; ICL-like, isocitrate lyase like protein; IDHg, glycosomal isocitrate dehydrogenase; IDHm, mitochondrial isocitrate dehydrogenase; PFR, paraflagellar rod protein; TCA, tricarboxylic acid.; WB, Western blot; WT, wild type.

Using citrate measurements in WT as reference, deletion of aconitase (ACO) increases citrate concentrations 14-fold in presence of glucose and 40-fold in absence of glucose. In absence of ACO, citrate produced by citrate synthase (CS) cannot drain off and accumulates. CS is upregulated upon growth in glucose-depleted medium (Fig. 6 [A]). We assume that an increase in CS protein levels elevates the metabolic flux along with the amount of citrate produced. *T. brucei* expresses one ACO gene, whose product has a dual subcellular localisation to the cytosol and mitochondrion (Saas et al., 2000). A truncated ACO mutant lacking the mitochondrial targeting sequence (Δaco/TY::ΔN10ACO, termed ΔN10ACO) has a cytosolic localisation (Appendix Fig. A 1). In comparison to WT, citrate levels measured in ΔN10ACO mutant were not increased in presence of glucose and doubled in absence of glucose rescuing the strong ΔACO phenotype. The inner mitochondrial membrane is impermeable for metabolites. A prerequisite for the rescue of the citrate accumulation phenotype of ΔACO by ΔN10ACO is the existence of a citrate transport mechanism across the inner mitochondrial membrane. The results provide indirect evidences for the presence of a mitochondrial citrate transporter. Independently from glucose availability, the deletion of IDHm does not affect citrate levels, as IDHg activity compensates the missing IDHm activity. However, deletion of IDHg results in a five-fold accumulation of citrate in absence of glucose. In glucose-rich culture conditions, CS protein levels are low and only a small amount of citrate is produced that may drain off via IDHm. However, IDHm cannot compensate a deletion of IDHg in absence of glucose. Here, IDHm activity is not sufficient to convert the high citrate amounts produced by increased CS protein levels and an accumulation of citrate is observed. Conclusively, the main flux of citrate produced in the TCA cycle is directed to IDHg and not IDHm.

The double null mutant ΔACO/ΔCS cannot produce citrate. Therefore, citrate concentrations measured in ΔACO/ΔCS mutant are considered as background introduced during sampling or measuring. Citrate levels in WT, the null mutants ΔCS and isocitrate lyase-like protein (ΔICL-like) are below background (Fig. 8 [C]). Therefore the method is not sufficient to accurately detect a glucose effect on citrate levels in WT, ΔCS and ΔIDHm.

We assume that the increased citrate levels in absence of glucose in the ΔACO and ΔIDHg mutant are related to the elevated CS expression levels. Inducible overexpression of citrate synthase fused to a C-terminal TY1-tag validated that increased citrate production correlates with increased CS protein levels. Cell lines inducible for CS-TY expression with tetracycline were generated: AnTat 1.1 CS-TY^{Ti} (WT CS-TY^{Ti}) as well as ΔACO CS-TY^{Ti}, ΔN10ACO CS-TY^{Ti}, ΔIDHm CS-TY^{Ti} and ΔIDHg CS-TY^{Ti}. Digitonin

fractionation proved the correct subcellular localisation of CS-TY to the mitochondrion (Appendix Fig. A 1). Tetracycline concentrations were adapted for equal CS expression levels in the different cell lines. CS-TY was overexpressed for two days in glucose-rich medium and the citrate content was analysed by GC/MS. Compared to AnTat 1.1 WT cultures, citrate concentrations are tripled in AnTat 1.1 overexpressing CS-TY (WT CS$^+$). In comparison to WT CS$^+$, CS overexpression on the background of ΔACO and ΔIDHg increases citrate levels 14- and 6-fold, respectively, whereas citrate concentrations in the ΔIDHm CS$^+$ mutant are not elevated (Fig. 9 [A]). Overexpression of CS in WT, the ΔIDHg and the ΔIDHm mutant is tolerated, but slightly delays growth. However, overexpression of CS in ACO deficient cells is lethal after six days (Fig. 9 [B]). Even though expression a cytosolic ACO (ΔN10ACO) alone decreases citrate levels upon upregulation of the endogenous CS in absence of glucose, ΔN10ACO CS$^+$ has a severe growth phenotype in culture for ten days after CS induction (Fig. 9 [B]) and heavily accumulates citrate after two days (Fig. 9 [A]). However, after 10 days the ΔN10ACO CS$^+$ culture resumes growth, though CS expression levels are not decreased. Interestingly after ten days, citrate concentrations in the ΔN10ACO CS$^+$ culture are below WT CS$^+$ citrate levels. Here, a complete rescue of the growth defect and the citrate accumulation phenotype has been achieved. As mechanism for the rescue phenotype we postulate an upregulation of a citrate transport mechanism across the mitochondrial inner membrane. Citrate levels in the ΔACO CS$^+$ and the ΔACO mutant grown in glucose-depleted medium are similar around 400 pmol per million cells. In contrast to ΔACO CS$^+$, the ΔACO mutant is perfectly viable and proliferative in absence of glucose. Assuming the adaptation of the ΔN10ACO is due to upregulation of a mitochondrial citrate transporter, accumulation of citrate in the ΔACO CS$^+$ mutant may primarily be intra-mitochondrial. Glucose-dependent regulation of CS takes 5-10 days (Stefan Allmann, personal communication). Consequently, the ΔACO mutant has time to adapt to increasing CS levels, for instance by upregulating the mitochondrial citrate transporter and distribute citrate among the cytosol and the mitochondrion, decreasing mitochondrial citrate concentrations to a non-toxic level. Conclusively, we provide evidence that citrate produced by citrate synthase is transferred from the mitochondrion to the cytosol and converted into isocitrate by cytosolic aconitase (ΔN10ACO). Isocitrate is imported into the glycosome fuelling IDHg.

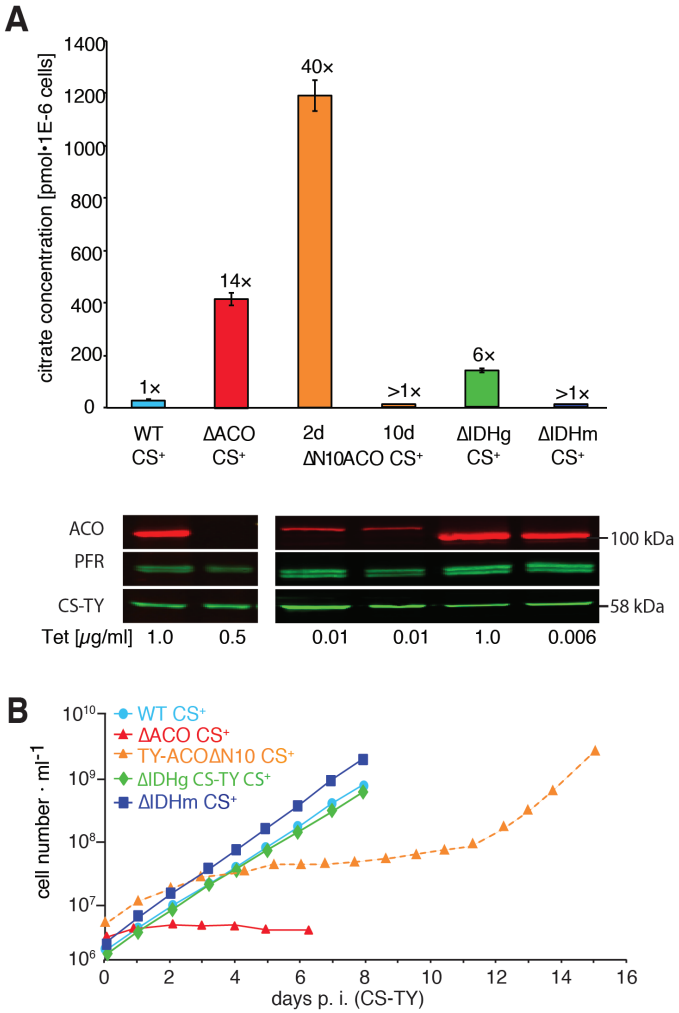

Figure 9 Artificial surplus production of citrate accumulates in metabolic null mutants. [A] *Tb*CS fused to a C-terminal TY1-tag (CS-TY) was inducibly overexpressed in WT AnTat 1.1 as well as in the background of ΔACO, ΔN10ACO, ΔIDHg and ΔIDHm mutant cell lines. Induced CS expression is indicated as CS+. Cells were cultured in presence of glucose and harvested 2 days post induction (p. i.) (and additionally after 10 d p. i. in case of ΔN10ACO). Citrate concentrations were determined by means of GC/MS (SEM of biological triplicates). CS-TY expression levels were adjusted by tetracycline (Tet) titration and validated by Western blot analysis. [B] Growth determination of AnTat mutants after induction of CS-TY overexpression. ACO, aconitase, CS, citrate synthase; IDHg, glycosomal isocitrate dehydrogenase; IDHm, mitochondrial isocitrate dehydrogenase; PFR, paraflagellar rod protein; WT, wild type.

3.5 African trypanosomes use an alternative pathway for citrate production in addition to citrate synthase

Depending on nutrient availability, two major citrate producing enzymatic reactions have been described. In a condensation reaction citrate synthase (CS) produces citrate from oxaloacetate and acetyl-CoA (Berg et al., 2012). A carbon dioxide fixing activity has been described for $NADP^+$ -dependent isocitrate dehydrogenases (IDH) reductively carboxylating α-ketoglutarate (α-KG) to isocitrate (Mullen et al., 2012). Attempts to generate a double null mutant of CS combined with mitochondrial IDH (ΔCS/ΔIDHm) or glycosomal IDH (ΔCS/ΔIDHg) or the double knock out ΔIDHg/ΔIDHm failed. However,

establishment of a double null mutant lacking aconitase (ACO) and CS (ΔACO/ΔCS) was successful. In order to generate a double knockout cell line, we transfected the constructs to delete the two alleles of the gene of interest on the background of a complete knockout of CS, IDHg or IDHm. We got clones resistant to all four selective markers. Integration of the resistance genes in the correct locus was validated by means of PCR (Allmann and Ziebart, data not shown). However, PCR of the gene targeted in the second place revealed that at least one copy is still present in the genome and Western blot analyses confirmed its expression. It has previously been reported, that knockout attempts of essential genes often result in the selection of aneuploidic clones with additional chromosomal copies (Cruz et al., 1993).

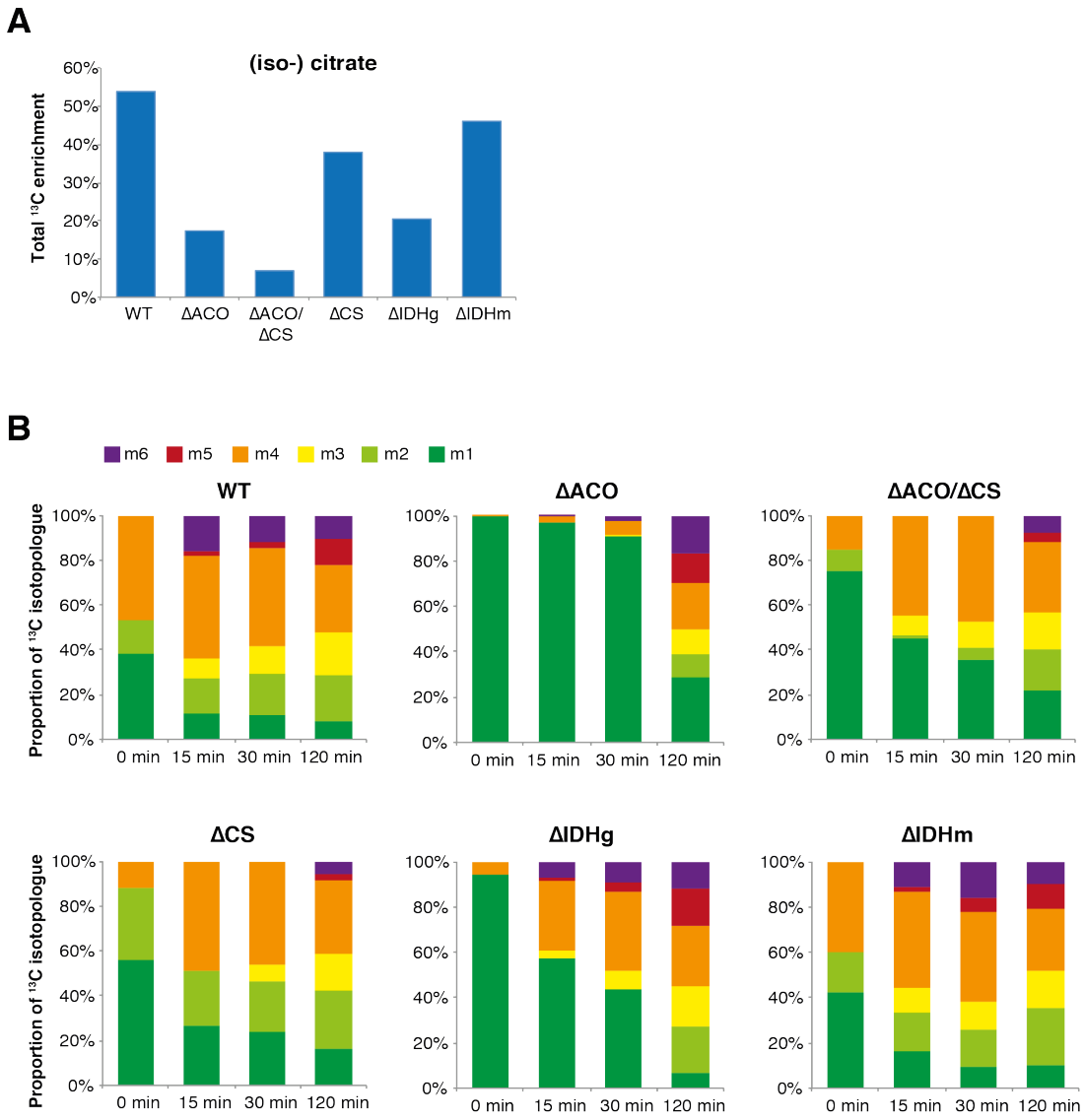

Figure 10 Proportion of ^{13}C enrichment from [U-^{13}C] proline detected in (iso-)citrate. Procyclic AnTat 1.1 WT and null mutants of ΔACO, ΔCS, ΔIDHg, ΔIDHm and the double knockout ΔACO/ΔCS were grown for 10 days in SDM79 in absence of glucose. For ^{13}C stable isotope labelling, the cells were incubated in PBS containing 2 mM [U-^{13}C] proline for 0 min, 15 min, 30 min and 120 min. 1E8 cells in 500 µl labelling solution were analysed by IC-MS/MS. [A] Total enrichment of ^{13}C in citrate (sum of m1, m2, m3, m4, m5 and m6). [B] Proportion of isotopologues relative to total ^{13}C enrichment. ACO, aconitase, CS, citrate synthase, IDHg, glycosomal isocitrate dehydrogenase; IDHm, mitochondrial isocitrate dehydrogenase; WT, wild type.

As the knockout mutants of CS and IDHm, but not the double null mutant ΔCS/ΔIDHm, could be generated, we assumed that CS and IDHm have redundant roles in the citrate production pathway. GC/MS analyses of CS-overexpressing mutants validated a role of CS in citrate production (Fig. 10 [A]). On the other side, in enzymatic assays a $NADP^+$-dependent decarboxylating activity could be detected for *Tb*IDHm (Fig. 7). However, we did not succeed in establishing an enzyme assay to determine the IDH activity for reductive carboxylation reaction in cell lysates (data not shown).

Stable isotope labelling with [U-^{13}C]-proline was applied to investigate, whether *Tb*IDHm has a reductive carboxylation activity. The time course of the ^{13}C enrichment profiles is shown for each mutant and metabolite in the appendix (Fig. A 4). As previously published as evidence for a gluconeogenic flux in trypanosomes, we detected [U-^{13}C] proline derived ^{13}C enrichment in glycolytic intermediates and sugar phosphates of the pentose phosphate pathway (Allmann et al., 2013). The isotopologue profiles of ^{13}C enrichment determined for the intermediates of glycolysis and the pentose phosphate pathway were similar between WT and the tested mutants. Considering the stable isotope labelling data, a deletion of IDHg does not affect the percentage of ^{13}C enrichment in gluconeogenic intermediates. Thus a relation between IDHg and gluconeogenesis could not be established. Marginal differences are present in the isotopologue composition of the tricarboxylic acid (TCA) cycle intermediates fumarate, malate, succinate and α-KG. However, the (iso-)citrate isotopologue profile looks different in each mutant (Fig. A 4).

The presence of the m5 isotopologue of (iso-)citrate would be an indicator for reductive carboxylation of [U-^{13}C] proline-derived α-KG. We expected a decrease in the abundance of m5 (iso-)citrate isotopologue in the ΔIDHm or ΔIDHg null mutant, if one IDH isoform is the source for m5 (iso-)citrate. The proportion of m5 isotopologue relative to total ^{13}C label incorporation into (iso-)citrate is 11 % in WT and ΔIDHm and 16 % in ΔIDHg null mutant after 2 h (Fig. 10 [B]). Based on these data, it is unlikely that one of the IDH isoforms can act in reverse. The m5 (iso-)citrate isotopologue may derive from isotope scrambling or condensation of m1 acetyl-CoA with m4 oxaloacetate.

In the ΔCS null mutant ^{13}C incorporation is detected in ~38 % of all citrate molecules (Fig. 10 [A]). Here, citrate has to be produced by an alternative enzymatic activity, as the cells are deficient in CS and the IDH isoforms are not involved in (iso-)citrate production due to the low abundance of m5 (iso-)citrate. We hypothesize that an isocitrate lyase-like protein could be an alternative supplier for isocitrate from succinate and glyoxylate (Fig. 18). The m6 (iso-)citrate isotopologue can be produced by condensation of proline-derived m4 oxaloacetate and m2 acetyl-CoA catalysed by CS. In the analysed time points

later than 15 min, the m6 proportion of total ^{13}C enrichment is 11-16 % in WT, whereas m6 was not detected in ΔCS at all until 2h and at 2h the m6 proportion was <6 %.

The ΔACO/ΔCS null mutant is incapable of producing citrate as no alternative citrate-producing pathway other than via ACO or CS has been described in any organism. Therefore we assign the detected total ^{13}C enrichment of ~7 % after 2 h in the ΔACO/ΔCS to isocitrate (Fig. 10 [B]). In WT a ^{13}C incorporation is detected in 54 % of the (iso-)citrate molecules after 2 h (Fig. 10 [A]). After 2 h, in the ΔACO and the ΔIDHg null mutant, ^{13}C is detected in 17 % and 20 % of all (iso-)citrate molecules, respectively (Fig. 10 [A]).

3.6 Trypanosomes produce high levels of 2-hydroxyglutarate

Recent publications revealed that the xenometabolite 2-hydroxyglutarate (2-HG) is involved in tumorigenesis (Engqvist et al., 2014). In bacteria D-2-HG is not a xenometabolite, but a building block for butyrate synthesis (Szafrański et al., 2015). We first detected racemic 2-HG by means of absolute metabolite quantification analysis using GC/MS in AnTat1.1 wild type (WT) as well as in the null mutants of aconitase (ΔACO), glycosomal and mitochondrial isocitrated dehydrogenase (ΔIDHg and ΔIDHm, respectively). In presence of glucose, 2-HG concentrations are similar in the WT and the null mutants around 75-95 pmol/10^6cells. Upon glucose depletion, intracellular 2-HG levels are increased. In WT and the ΔIDHg mutant 2-HG concentrations are in the range of 250 pmol/10^6cells and in the ΔACO and the ΔIDHm null mutant around 350 and 450 pmol/10^6cells, respectively. Thus we exclude a role of IDHg and IDHm in 2-HG production. The main source for 2-HG as oncometabolite in tumours is IDH1 or IDH2 harbouring a specific missense mutation (Yan et al., 2009). In human tumours, 2-HG concentrations of up to 25 pmol/$\mu g_{protein}$ were detected (Pusch et al., 2014). In trypanosomes, we determined 2-HG concentrations of 25 pmol/$\mu g_{protein}$ and 60-110 pmol/$\mu g_{protein}$ in presence and absence of glucose, respectively (Fig. 11 [A]), if calculations based on a total trypanosomal protein content of ~4 µg/10^6cells (Stefan Allmann, personal communication).

Glutamate is an intermediate of proline conversion into α-ketoglutarate (α-KG). In absence of glucose glutamate levels are 6-10-fold elevated in WT and ΔIDHg, ΔIDHm and ΔACO mutant providing indirect evidence for an increased flux through the proline degradation pathway.

Several 2-HG producing enzymatic activities have been described (Fig. 19). In order to identify the source for 2-HG we analysed metabolic fluxes by means of stable isotope

labelling using [U-^{13}C] proline. The most abundant 2-HG isotopologue is m5 with more than 90 %. The time course of label incorporation into 2-HG looks similar to α-ketoglutarate (α-KG) (Appendix Fig. A4). The enrichment profiles of 2-HG and α-KG suggest that 2-HG is produced from proline-derived α-KG. There is no significant difference in the time course of ^{13}C label incorporation between WT and null mutants of ACO, CS, IDHg, IDHm and the double null mutant of ACO and CS.

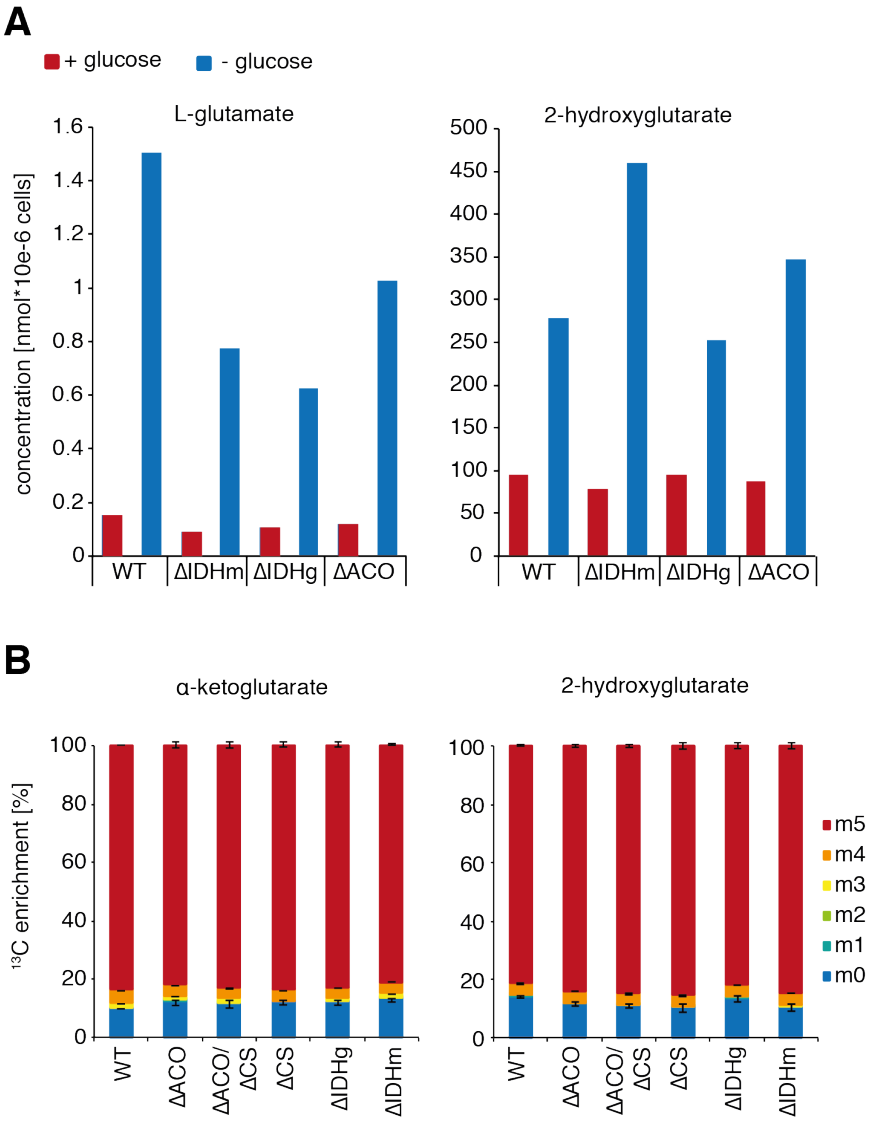

Figure 11 In trypanosomes, 2-hydroxyglutarate is not a xenometabolite. [A] Absolute glutamate and 2-HG concentrations determined in WT and ΔIDHg, ΔIDHm and ΔACO null mutants in presence and absence of glucose. [B] Procyclic AnTat 1.1 WT and ΔACO, ΔACO/ΔCS, ΔCS, ΔIDHg and ΔIDHm null mutant cell lines were cultured for 10 d in absence of glucose prior IC-MS/MS detection of ^{13}C enrichment in α-KG and 2-HG after 2 h of incubation in presence of [U-^{13}C] proline. 2-HG, 2-hydroxy-glutarate, α-KG, α-ketoglutarate; ACO, aconitase; CS, citrate synthase; IDHg, glycosomal iscitrate dehydrogenase; IDHm, mitochondrial isocitrate dehydrogenase; WT, wild type.

3.7 Nutritional signals regulate fly-stage differentiation in culture

RNA binding protein 6 (RBP6) was shown to be a central regulator of fly-stage differentiation. Overexpression of RBP6 in PCFs induces development of epimastigote (EMFs) and metacyclic forms (MFs) in culture (Kolev et al., 2012). We reproduced the RBP6 in culture differentiation system and generated an EATRO 1125-T7T *RBP6*^{Ti} cell line being inducible for RBP6 with tetracycline (Stefan Allmann). In the following, the tetracycline induced cell lines are denoted with RBP6^{+}. The differentiation kinetics show the quantification of PCF, EMF and MF populations scored by means of fluorescence microscopy analyses (Fig. 13 and Fig. 15). Here, the life cycle stage of each cell was determined by means of the stage-specific morphology based on cell size and shape as well as the relative position of the kinetoplast to the nucleus (Fig. 12 [A]-[C]). In PCF trypomastigotes the kinetoplast is at the posterior part of the cell, whereas in EMFs the kinetoplast migrates to the opposite side of the nucleus and is found at the anterior part of the cell or in close proximity to the nucleus. MF trypomastigotes are smaller than EMFs and PCFs with the kinetoplast at the very end of the rounded posterior tip and a flagellum similar in shape to BSFs (ROTUREAU and VAN DEN ABBEELE, 2013). Comparing the differentiation kinetics in this work with the ones published by Kolev and co-workers (Kolev et al., 2012), we observe a more efficient metacyclogenesis. We obtain ~1.25-fold more EMFs after two days. After four days, ~30 % of the cells already have a characteristic MF morphology and after six days MF subpopulation reaches its peak at 55 % (Fig. 13 [A]). In comparison, in the kinetics published by Kolev and co-workers it takes seven to eight days until MF population emerges and the maximum MF population size is ~40 % (Kolev et al., 2012). The difference in the differentiation efficacy could either be a matter of the cell line used, Lister 427 (29:13) versus EATRO 1125-T7T, or the medium, Cunningham's medium (4 mM glucose) (Cunningham, 1977) versus our optimized differentiation protocol using SDM79, where the uptake of FCS-derived glucose is inhibited by 50 mM N-acetylglucosamine (GlcNAc) and glucose and glycerol are excluded (Fig. 13 [A]).

Environmental signals can induce *T. brucei* life cycle stage differentiation. In culture, transformation of bloodstream forms (BSF) to PCFs can be mimicked by exposure to citrate/*cis*-aconitate and by cold shock (Dean et al., 2009; Engstler and Boshart, 2004). We found that metabolic signals influence fly-stage development in culture. The influence of 10 mM glucose on RBP6-driven differentiation was analysed in induced WT *RBP6*^{Ti} cultures (WT RBP6^{+}). We observed that, despite continuous application of tetracycline, RBP6 expression levels are decreasing over time in successfully

differentiating cultures. In presence of 10 mM glucose, RBP6 overexpression is not downregulated over time and growth is maintained, though with a delayed population doubling time compared to uninduced cultures. Glucose in the medium prevents EMF to MF development in WT RBP6+. The EMF population of WT RBP6+ cells cultivated in presence of glucose has twice the size of WT RBP6+ cells grown in absence of glucose, after four days (Fig. 13 [B]). EMFs undergo two asymmetric divisions in the tsetse fly: In the proventriculus and the foregut, long dividing EMFs produce non-proliferative long EMFs and dividing short EMFs. Later in the salivary glands, the second asymmetric division of attached EMFs yields proliferative EMF and non dividing MF daughter cells (ROTUREAU and VAN DEN ABBEELE, 2013). The increased size of the EMF population, along with growth maintenance and inhibition of EMF developmental progression to the MFs, suggests that the EMF population is frozen in either the long proliferative EMF or short EMF stage in glucose-rich medium. Growth could also be maintained by the PCF population, which has almost twice the size in presence of glucose, than in absence of glucose (Analysis of kinetics, growth and WB showing RBP6 expression in presence of

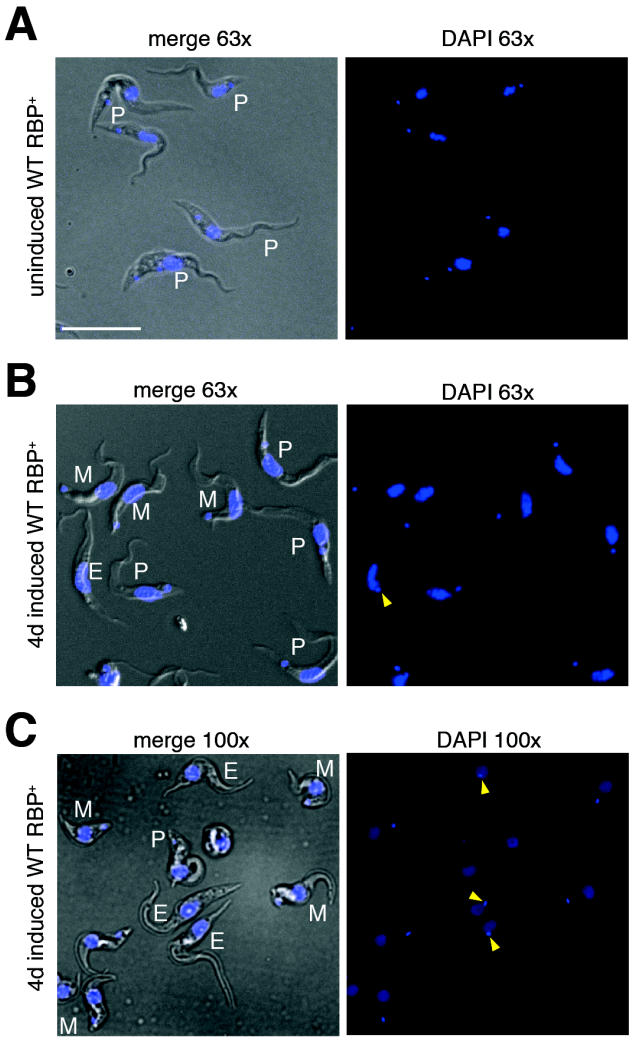

Figure 12 Evaluation of differentiation stage by morphology. Cells were characterised by means of morphological features like size and shape and the relative position of the kinetoplast to the nucleus using DAPI to stain DNA. More detailed descriptions are provided in 2.2.8 [A] uninduced control containing only procyclic forms. [B] and [C] In absence of glucose (-Gluc), a mixed culture establishes containing procyclic, epimastigote and metacyclic forms, 4 days post induction. [A] and [B] Pictures were taken with the Zeiss AxioImager.M1 with 63x magnification. [C] Pictures were taken with high resolution imaging system GE DeltaVision Elite using 100x magnification. Scale bar, 10 µm.

glucose was performed by Stefan Allmann). The impact of 20 mM glycerol in presence of GlcNAc on the RBP6-driven differentiation is more moderate than glucose. Here, after four days about 80 % of the culture corresponds to EMFs. The development of MFs is delayed by two days and the maximal size of the MF population is reduced by ~65 % in comparison to glycerol-depleted conditions. In presence of glycerol, high RBP6 expression levels are maintained over time. The mixed culture maintains growth until day four followed by a nearly stationary phase coinciding with the appearance of MFs (Fig. 13 [C]). Concluding, glycerol and glucose both counteract RBP6-induced metacyclogenesis.

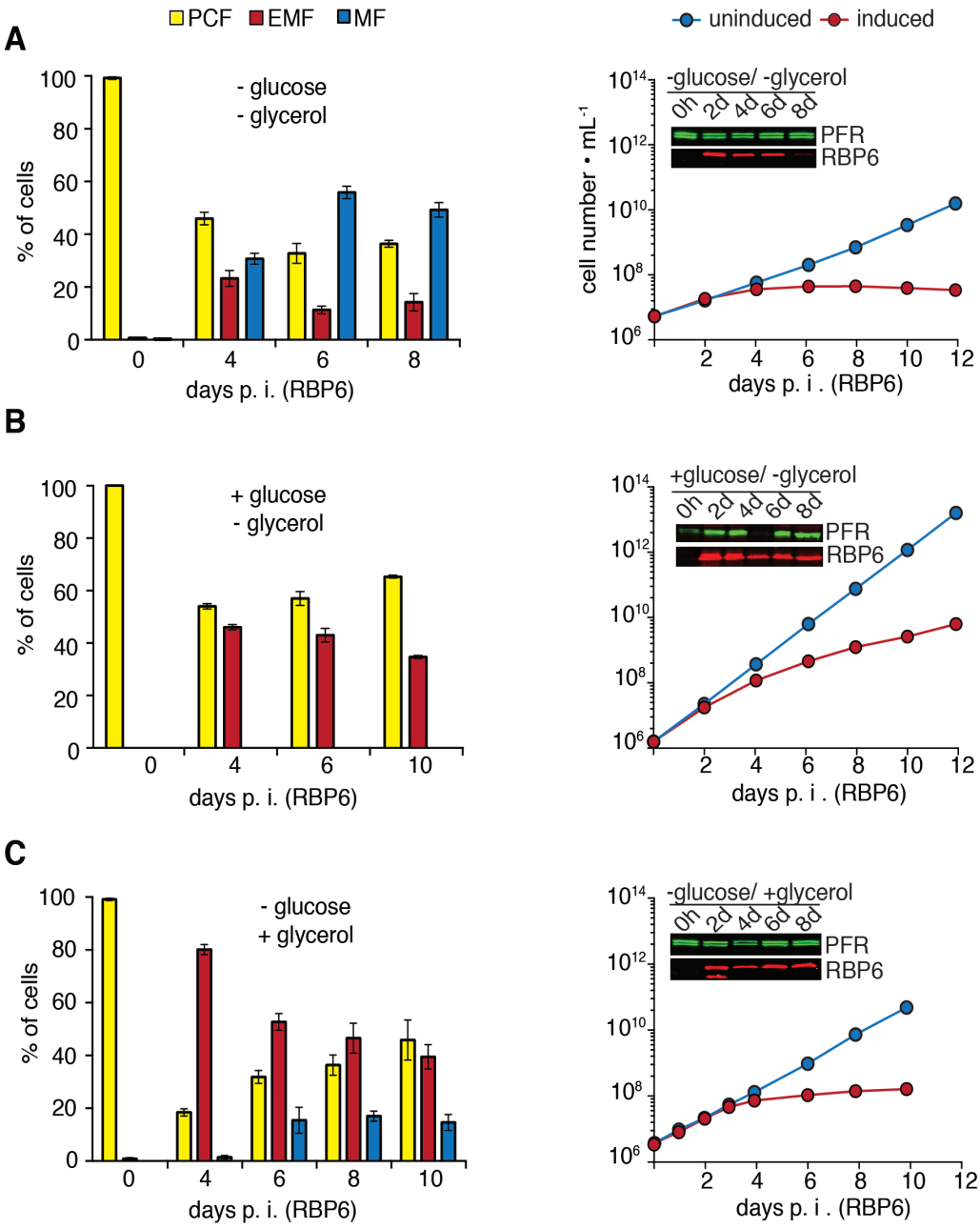

Figure 13 Glycerol and glucose affect RBP6-mediated metacyclogenesis. WT RBP6^{+} cultures were pre-incubated for five days with the nutritional conditions to be tested, prior RBP6 induction. Bar diagrams show differentiation kinetics of cells induced at day 0 for RBP6 overexpression. Subpopulations were determined based on the stage-specific morphological characteristics like shape and size as well as the relative position of the kinetoplast to the nucleus using fluorescence microscopy. Insets in the growth curves show the Western blot analyses of RBP6 expression levels and paraflagellar rod protein (PFR) as loading control from day 0 to day 8 post induction (p. i.). Non-induced WT *RBP6^{Ti}* cultures serve as growth control (blue). [A] Optimized differentiation protocol lacking glycerol and glucose. RBP6-driven differentiation in presence of glucose (data generated by Allmann) [B] or glycerol [C]. For each replicate and time point 100-200 cells were characterised. Error bars represent SEM (n = 3).

3.8 Stage-specific markers are regulated by RBP6 overexpression

Besides changes in morphology, trypanosomal fly-stages also switch their surface coat. Here, the procyclin EP, the brucei alanine-rich protein (BARP) and the metacyclic subset of VSG (M-VSG) are known markers for procyclic form (PCF), epimastigote form (EMF) and metacyclic form (MF) stages, respectively (Graham et al., 1993; Urwyler et al., 2007; Vassella et al., 2001). As the M-VSG isoform expressed in MFs cannot be predicted, we use calflagin a protein localising to lipid rafts in the flagellar membrane as marker for MFs. Calflagin levels in bloodstream forms (BSFs) and MFs are ten-fold enriched compared to PCFs (Emmer et al., 2010). Immunofluorescence analysis (IFA) of WT RBP6^{+} cultures show that two days post induction all cells, PCFs and EMFs, express EP on their surface (data not shown), whereas four days post induction, EP is expressed in PCFs and in most EMFs but not in MFs (Fig. 14 [A] and Appendix Fig. A 5). EP expression has previously been described for salivary gland immature EMFs (Richardson et al., 1986). As predicted from the literature, MFs express high levels of calflagin, whereas a calflagin signal is barely detectable in PCFs and EMFs by IFA four days post induction (Fig. 14 [A]). Interestingly, the population expressing high BARP levels is quite inhomogeneous. We found PCFs and EMFs, which strongly or weakly express BARP, but also EMFs and PCFs that do not express BARP at all (Fig. 14 [B]). In PCFs overexpressing BARP shedding of transgenic BARP by the trypanosomal metalloprotease major surface protease (*Tb*MSP-B) can be prevented by addition of bathophenanthroline disulphonic acid (BPS), an inhibitor of the *Tb*MSP-B (Urwyler et al., 2007). For BARP expression analyses, administration of BPS to the WT RBP6^{+} culture twelve hours prior harvesting did not further improve the endogenous BARP signal of IFA or flow cytometry significantly (data not shown). *Tb*MSP-B expression was reported for PCFs and BSFs (LaCount et al., 2003). It seems only the overexpressed BARP, but not the endogenously expressed BARP, is cleaved by proteolysis. Presumably, *Tb*MSP-B is inactive or absent from the surface in EMFs and therefore BARP expression can be examined without BPS addition.

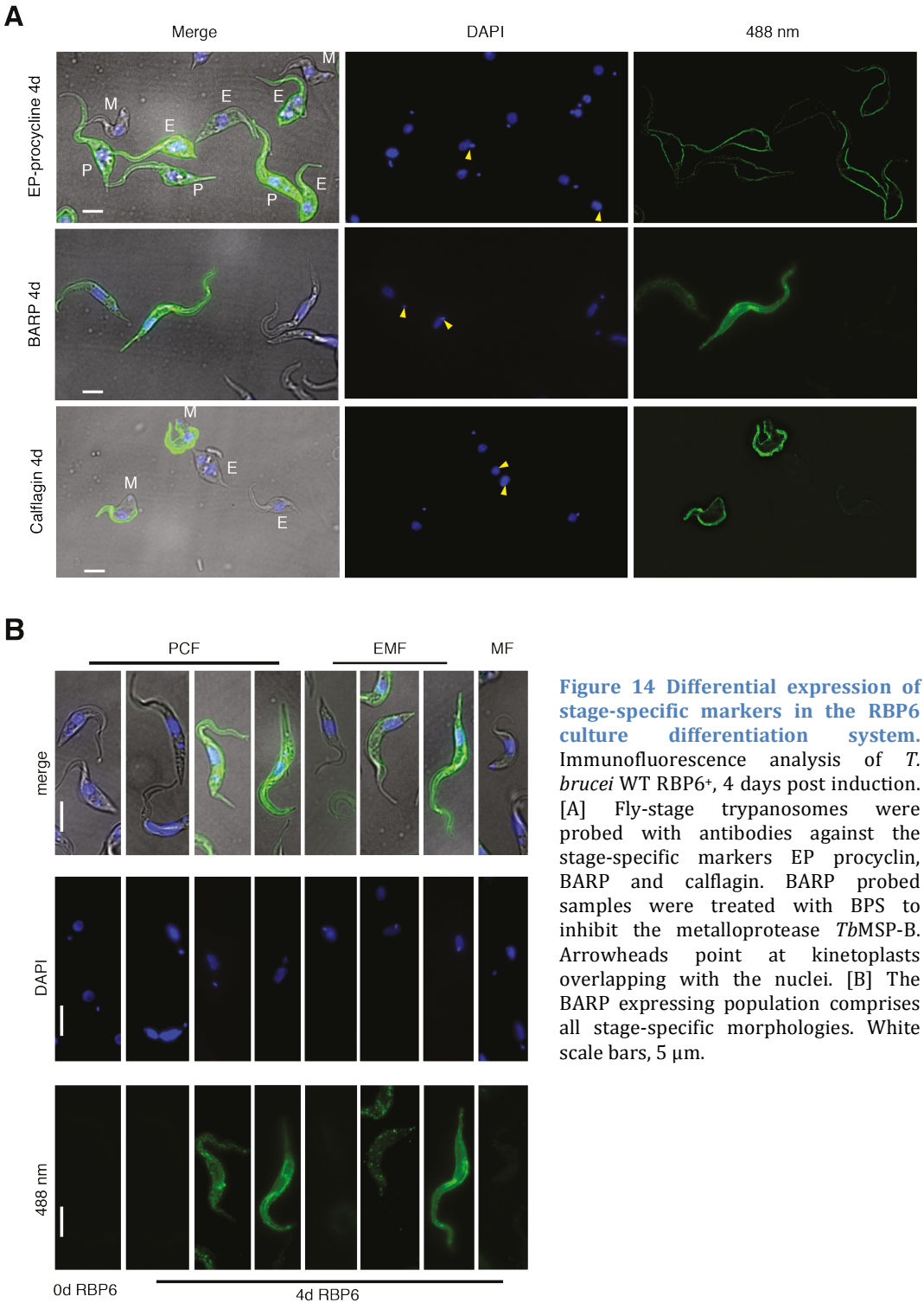

Figure 14 Differential expression of stage-specific markers in the RBP6 culture differentiation system. Immunofluorescence analysis of *T. brucei* WT RBP6+, 4 days post induction. [A] Fly-stage trypanosomes were probed with antibodies against the stage-specific markers EP procyclin, BARP and calflagin. BARP probed samples were treated with BPS to inhibit the metalloprotease *Tb*MSP-B. Arrowheads point at kinetoplasts overlapping with the nuclei. [B] The BARP expressing population comprises all stage-specific morphologies. White scale bars, 5 µm.

3.9 Flow cytometric quantification of stage-specific markers correlates with the fraction of life cycle stages scored by morphology

The immunofluorescence analyses (IFA) of wild type cells overexpressing RBP6 (WT RBP6^{+}) showed a differential expression of the stage-specific markers procyclin EP, brucei alanine-rich protein (BARP) and calflagin in the different life cycle stages after four days of induction. In order to evaluate a bigger sample size, flow cytometry analysis was applied for quantifications of cells high in EP, BARP and calflagin expression (Fig. 15 [A] to [D]). In WT RBP6^{+}, EP expression is maintained in all cells during the first two days post RBP6 induction. After four days the EP positive population is decreased to 45 % similar to the size of the procyclic population. Most cells in the uninduced control at day 0 are negative for BARP expression. Two days post RBP6 induction, the proportion of cells with high BARP protein levels is as large as the size of the EMF population with about 55 % of all cells. However, the amount of cells high in BARP expression is not decreasing to the same extend as the epimastigote population. The bad quantitative correspondence between the proportion of epimastigote forms (EMFs) and cells high in BARP expression after four and six days can be explained by the inhomogeneous composition of the BARP positive population consisting of procyclic forms (PCFs) and EMFs identified by means of IFA (Fig. 14 [B]). Calflagin is detectable at basal levels in PCFs and EMFs using IFA. In metacyclic forms (MFs) calflagin is significantly upregulated. The proportion of cells positive for calflagin is constantly increasing over time and has the same size as the MF subpopulation after four and six days (Fig. 15 [A]). WT RBP6^{+} cells differentially regulate EP, BARP and calflagin over time and a correlation to the population size of PCFs, EMFs and MFs is observed.

3.10 In culture fly-stage development in metabolic null mutants

Even though glucose and glycerol regulate the expression levels of citrate synthase and glycosomal isocitrate dehydrogenase (IDHg), a role of CS, IDHg and mitochondrial isocitrate dehydrogenase (IDHm) for survival in glucose- and glycerol- depleted culture conditions was not identified. Thus we analysed, whether CS, IDHg and IDHm are important for fly-stage development by means of the RBP6-driven differentiation system. One potential role for IDHg in the glycosome can be supply of NADH for gluconeogenesis. The null mutant of fructose 1,6-bisphosphatase (ΔFBPase), a key enzyme of gluconeogenesis, was included into the RBP6 developmental analyses, to investigate, whether gluconeogenesis is important for differentiation.

Until now, the RBP6 system was not applied to investigate fly-stage developmental phenotypes in knockout mutants. In previous *in vivo* experiments, tsetse flies were infected with the ΔIDHg null mutant. Even though, the ΔIDHg mutant established a midgut infection, a colonisation of the salivary glands was blocked (unpublished data, Stefan Allmann and Jan Van Den Abbeele). Taking into account, that the IDHg null mutant has an *in vivo* developmental phenotype, IDHg is a good candidate to approve the suitability of the RBP6 system for null mutant differentiation analyses.

An indicator for successful differentiation of RBP6 overexpressing cells (RBP6$^+$) is a delay in growth in the first four days post induction followed by a stationary phase. Additionally, RBP6 expression levels are decreasing over time, despite a continuous application of tetracycline (Fig. 13 [A]). The growth curves and the RBP6 expression levels in the null mutants ΔCS RBP6$^+$ and ΔIDHm RBP6$^+$ are similar to WT RBP6$^+$ (Fig. 16 [A] and [B], respectively). However, growth and RBP6 overexpression are maintained in the null mutants ΔIDHg RBP6$^+$ and ΔFBPase RBP6$^+$ (Fig. 16 [C] and [D], respectively).

The differentiation kinetics scored by cell morphology analyses look similar for the ΔIDHg RBP6$^+$ and the ΔFBPase RBP6$^+$ mutant. Both establish epimastigote forms (EMFs), but fail to develop metacyclic forms (MFs) (Analysis of kinetics, growth and RBP6 expression in the IDHg null mutant was performed by Stefan Allmann). In the ΔIDHg RBP6$^+$ mutant, about 55 % of the cells are epimastigote after two days. The EMF population size fluctuates around 30-40 % after four to ten days. The EMF population in the ΔFBPase RBP6$^+$ mutant does not vary significantly in size and maintains a proportion of 50 % from two to ten days. Flow cytometric analyses revealed that neither ΔFBPase RBP6$^+$ nor ΔIDHg RBP6$^+$ differentially regulate EP procyclin and calflagin expression levels at all. In comparison to WT RBP6$^+$ cells, the maximal size of the BARP positive population is halved in ΔIDHg RBP6$^+$ and ΔFBPase RBP6$^+$. Only about 30 % and 20 % of the cells express BARP at high levels in ΔIDHg RBP6$^+$ and ΔFBPase RBP6$^+$, respectively. We anticipate that the block is early in EMF development, as the regulation defects are already present in the PCF- and EMF-specific markers EP and BARP, respectively. The developmental phenotype of ΔIDHg RBP6$^+$ is cell autonomous, as it was observed in culture, where environmental factors present in the fly are excluded.

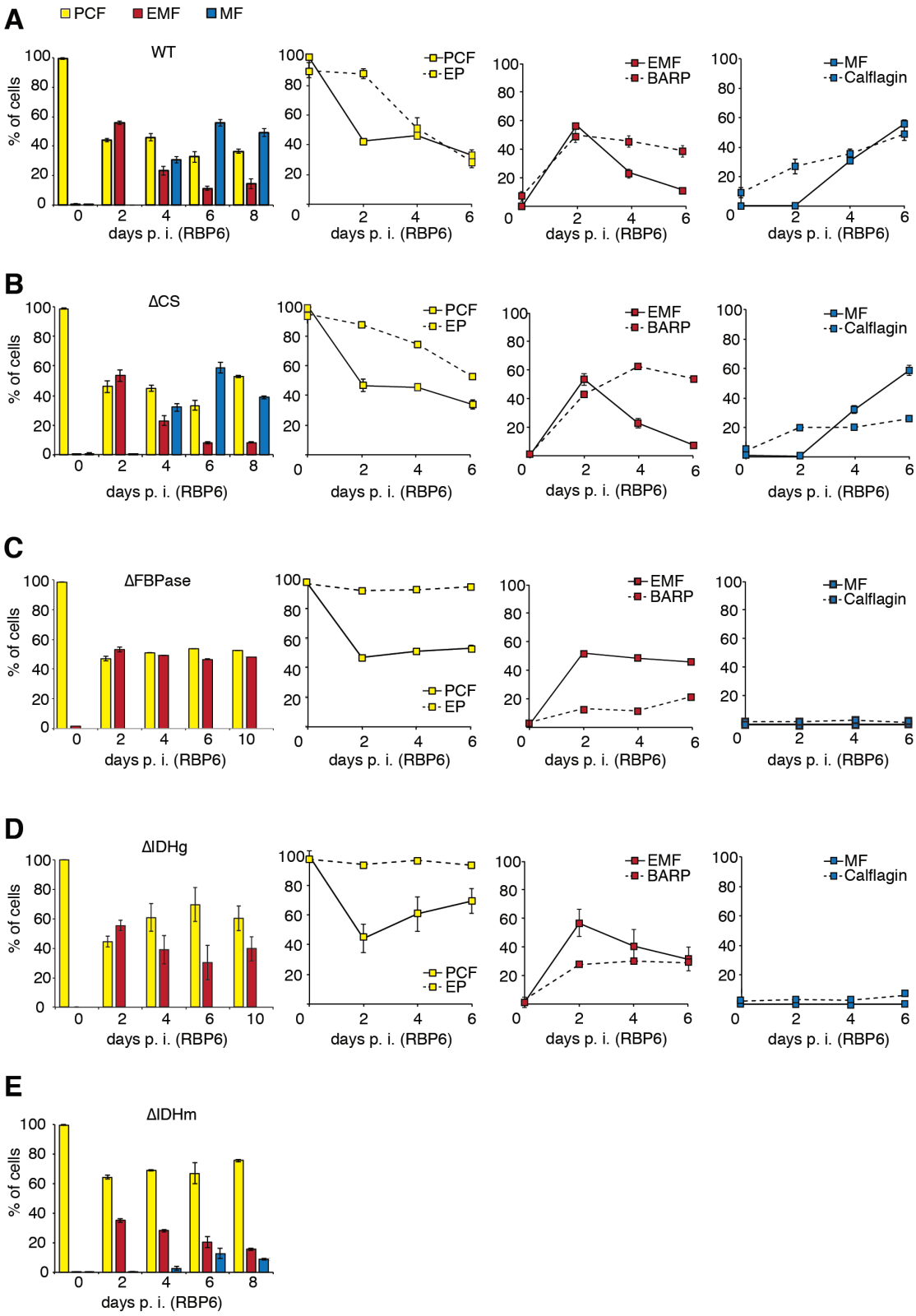

Figure 15 IDHg and FBPase are essential for metacyclogenesis in culture. RBP6-induced differentiation kinetics shown as bar diagrams. Time course experiments comparing the percentage of populations high in fluorescence with the corresponding fly-specific developmental stages determined by morphological analyses is blotted as line charts for wild type (WT) [A] as well as null mutants of citrate synthase (ΔCS) [B], fructose 1,6-bisphosphatase (ΔFBPase) [C], glycosomal and mitochondrial isocitrate dehydrogenase (ΔIDHg [D] and ΔIDHm [E], respectively). Differentiation kinetics were scored as described in 2.2.8. For the flow cytometric analyses of procyclin EP, BARP and calflagin, the cells were gated into two populations with low and high fluorescence signal. EMF, epimastigote form; MF, metacyclic form; PCF, procyclic form; p. i. , post induction, standard bars represent the SEM (n = 3).

We concluded from previous experiments that isocitrate produced in the tricarboxylic acid (TCA) cycle feeds IDHg. Our working hypothesis was that citrate can either be produced by CS or by the IDHm acting in reverse. However, a reductive carboxylation activity of IDHm was not identified in stable isotope labelling experiments (Fig. 10 [B]). Here, we also analysed the impact of a deletion of CS or IDHm on development using the RBP6 system. The ΔCS RBP6$^+$ differentiation kinetics scored by morphology look similar to WT RBP6$^+$. Stage-specific marker analyses by means of flow cytometry showed that there is no perfect quantitative correspondence of the population high in EP expression and the proportion of PCFs at day four and six. Two days post induction about 43 % of the cells upregulate BARP expression, which matches the proportion of cells with characteristic EMF features. In the ΔCS RBP6$^+$ mutant the BARP positive population is further increasing up to 63 % and 55 % on day four and six, respectively; though the proportion of EMFs is decreasing. The population expressing calflagin at high levels in the ΔCS RBP6$^+$ mutant is not increasing over time and fluctuates between 20-26 % after two to six days. Taken together, in the ΔCS RBP6$^+$ mutant only about half of the MFs are calflagin positive at day six. Even though a lack of citrate synthase does not block morphological development, it nevertheless has a delay in marker regulation and is not completely differentiating (Fig. 15 [B]). The mild phenotype associated with a CS deletion in the culture differentiation system suggests redundant pathways producing isocitrate for IDHg and indicates that ΔCS can be almost fully complemented.

A deletion of IDHm decreases differentiation efficiency, but does not completely block EMF and MF development upon RBP6 overexpression. After two days, 35 % less EMFs are observed in the ΔIDHm RBP6$^+$ mutant compared to WT RBP6$^+$ and after four days only 3 % of the cells have a metacyclic morphology. In ΔIDHm RBP6$^+$, the maximal population size of MFs is 13 %, in comparison to 55 % in WT RBP6$^+$ cells. The ΔIDHm-associated phenotype cannot be assigned to a distinct phase in fly-stage development since EMF and MF development is equally affected. Cells with a deletion of IDHm already have a mild growth phenotype in PCF cultures, as the population doubling time is delayed by four hours compared to WT cells (Table 1). The growth phenotype of ΔIDHm may be a problem of cell viability (Fig. 5 [F]) and the unspecific phenotype of ΔIDHm RBP6$^+$ in development suggest a general defect in cell viability making it difficult to conclude on a phenotype of ΔIDHm RBP6$^+$ in development. As the IDHm reaction is not reversible *in vivo* according to metabolic labelling (Fig. 10 [B]), it can be excluded that isocitrate supply to IDHg is limited by the IDHm deletion.

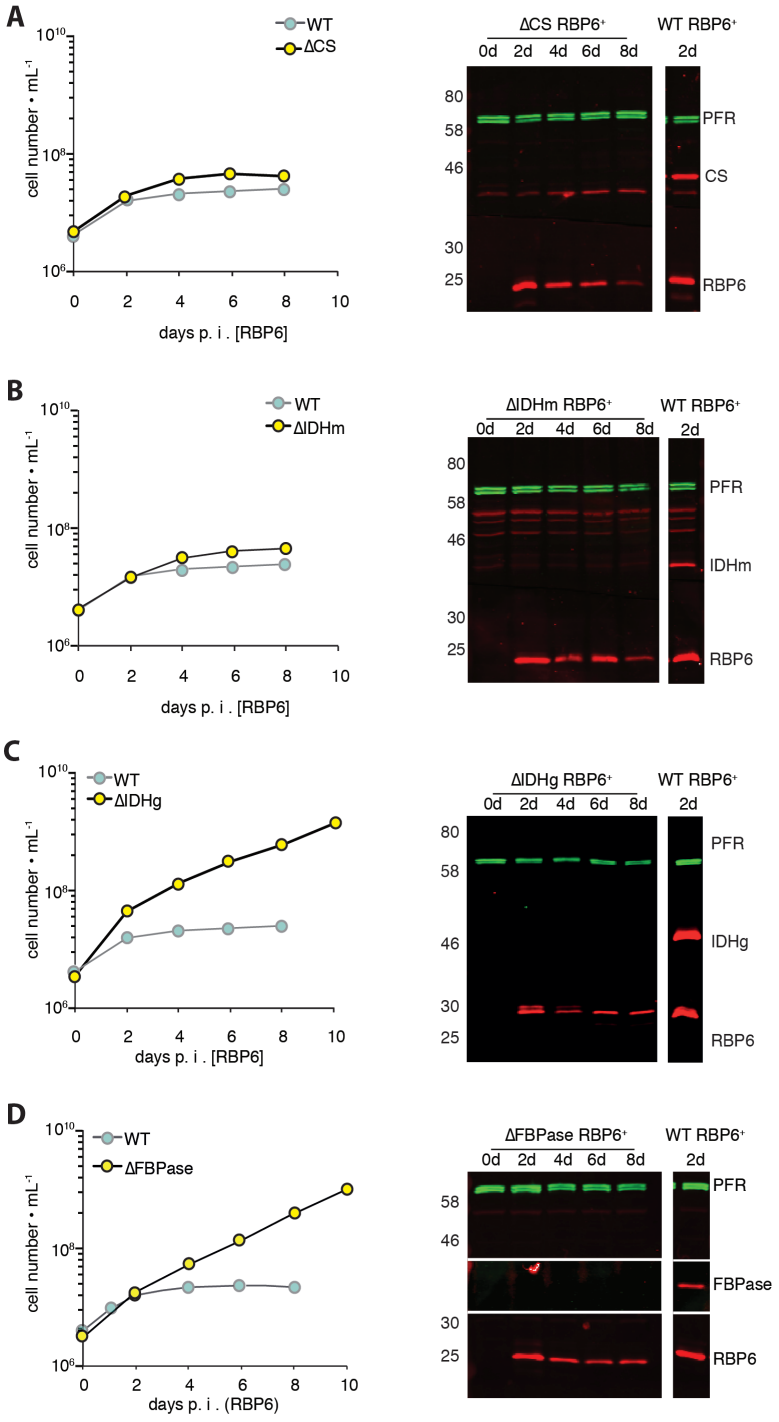

Figure 16 Control of growth and RBP6 expression levels on the background of null mutants. Null mutant cell lines were pre-adapted to SDM79 glucose-depleted conditions prior induction of RBP6 expression on day 0. Semi-logarhitmic blotting of cumulative cell number shown as line chart on the left . WT RBP6+ growth curve is blotted as reference in light blue in each graph. Western blot analysis of induced RBP6 overexpressing cell lines verifies null mutant background of citrate synthase (CS), glycosomal and mitochondrial isocitrate dehydrogenase (IDHg and IDHm, respectively) and fructose 1,6-bisphosphatase (FBPase) as well as RBP6 overexpression levels. Blots were probed with different polyclonal antisera raised in rabbit against recombinant protein of CS, IDHg, IDHm and FBPase. ([C] ΔIDHg growth curve and Western blot analyses were performed by Allmann)

4 Discussion

4.1 Metabolic signals in trypanosomal fly-stage differentiation

Until recently, fly-stage trypanosome culture was restricted to procyclic forms (PCFs). Investigations on later insect-stage trypanosomes necessitated infection and dissection of tsetse flies. Kolev and co-workers reported that overexpression of the RNA-binding protein RBP6 drives fly-stage development in culture upon its overexpression (Kolev et al., 2012). We make use of RBP6 overexpression to identify external metabolic signals and cellular metabolic pathways that influence differentiation efficacy.

In comparison to the differentiation kinetics published by Kolev and co-workers (Kolev et al., 2012), we achieve a faster differentiation kinetic and a higher efficacy by excluding glucose and glycerol from the culture medium. In contrast to the bloodstream form (BSF) into PCF transformation, which depends on external signals citrate/*cis*-aconitate and cold shock (Dean et al., 2009; Engstler and Boshart, 2004), the culture system for fly-stage development is induced by overexpression of RBP6. Even though overexpression of RBP6 is not the physiological way to trigger fly-stage development, the culture differentiation system is still responsive to nutritional signals. Here, glucose and glycerol mitigate the dominant effect of RBP6 and reduce the efficacy of metacyclogenesis. Glycerol allows the development of EMFs and even MFs, albeit the latter with low efficacy, whereas glucose completely blocks the development of EMFs to MFs.

Previously, it has been shown that both glucose and glycerol remodel metabolic fluxes. The presence of either one of the two carbon sources reduces proline consumption and alters the profile of excreted end products (Lamour et al., 2005; van Weelden et al., 2005). Moreover, glucose and glycerol regulate the expression of surface proteins in PCFs. The procyclin GPEET, characteristic for early PCFs, is differentially expressed on the cell surface and present during a specific time upon midgut colonisation. About 24 h post transition from BSFs to PCFs, GPEET is the major surface procyclin and is replaced by EP procyclins upon differentiation into late PCFs, an event coinciding with the migration into the ectoperitrophic space (Vassella et al., 2000). Glucose and glycerol have opposite effects on GPEET expression. On the one hand, GPEET expression is suppressed by an active glycolytic flux in presence of glucose (Morris et al., 2002), which is transiently available after the blood meal (Vickerman, 1985). On the other hand, glycerol promotes and maintains GPEET expression in cultured PCFs (Vassella et al., 2000).

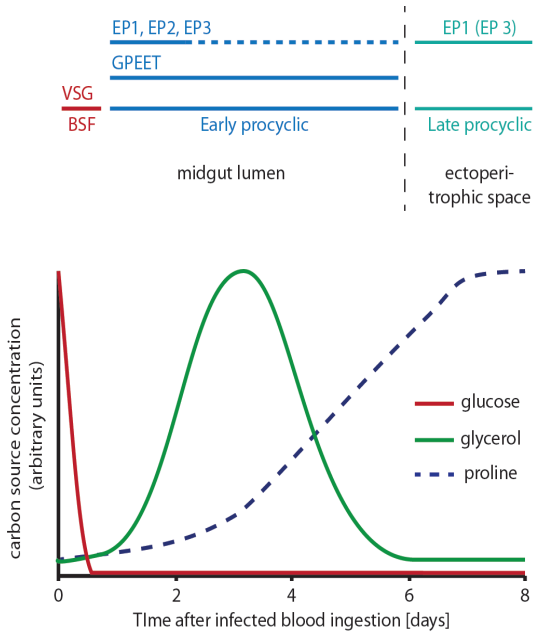

Figure 17 Simplified procyclin expression profile and carbon source availability in the tsetse midgut. In the first 24 h after bloodstream form (BSF) to procyclic form (PCF) transformation, all procyclins are co-expressed and subsequently GPEET is the major surface protein. After 7 days, EP procyclins replace GPEET (Vasella et al. 2000). Anticipated time profile of available carbon sources in the midgut, adapted from InfectERA proposal "TryPaBlock" Boshart, M., Bringaud F., Rotureau, B., Van Den Abbeele, J., Magez, S. with modified time scale.

Glucose and glycerol are not permanently available in the tsetse midgut. We propose a current model in which glucose is depleted shortly after the blood meal and glycerol is the main carbon source for trypanosomes (Fig. 17). Potential sources for glycerol are phospholipids derived from red blood cell membranes and hydrolysed by tsetse fly midgut lipases. Glycerol availability may be the timer for differentiation from early to late PCFs and migration from the midgut lumen to the ectoperitrophic space. Glycerol blocks development of early to late PCFs in culture, as indicated by the maintenance of the expression of the surface marker of early PCFs GPEET. GPEET repression seems to coincide with glycerol depletion and the migration through the peritrophic matrix (Vassella et al., 2000). In accordance to this, glycerol and glucose negatively affect RBP6-driven fly stage differentiation. Thus we provide evidence that the development of fly life cycle stages is under the regulation of the nutritional environment.

Our results reveal the RBP6-driven differentiation system to be a suitable tool to analyse the role of metabolic pathways for differentiation. The null mutant of the glycosomal isocitrate dehydrogenase (ΔIDHg) fails to undergo metacyclogenesis in the RBP6 system. In accordance with these findings, previous experiments with infected tsetse flies showed that cells lacking IDHg colonize the midgut, but fail to infect the salivary glands (Stefan Allmann and Jan Van Den Abbeele, Antwerp).

Trypanosomes adapt to the prevailing conditions in the tsetse fly in various ways. This includes changes in morphology as well as the differential expression of stage-specific markers. High expression of procyclin EP, brucei alanine-rich protein (BARP) and calflagin are characteristic for PCFs, EMFs and MFs, respectively (Rotureau et al., 2012; Urwyler et al., 2007; Vassella et al., 2001). Flow cytometrical analyses of induced WT RBP6^{+} cells showed that populations expressing one of the three stage-specific markers

at a high level correlate with the stage assignments gained by analysis of morphology. Therefore all three markers are suitable to evaluate the differentiation capacity of null mutants in addition to stage determination by morphology. An additional surface marker to check for successful metacyclogenesis is the variable surface glycoprotein (VSG). MFs randomly express one isoform out of a specific subset of variable surface glycoproteins named M-VSGs (Graham and Barry, 1995). VSG expression in induced RBP6$^+$ cultures was proven by electron microscopy and quantitative reverse transcriptase PCR (Kolev et al., 2012). A more accurate quantification of M-VSG expression can be achieved by flow cytometry using the cross-reacting determinant (CRD) specific antibody (Rotureau et al., 2012; Zamze et al., 1988). The CRD epitope is part of the GPI anchor and present in all VSG isoforms.

It seems that the culture-derived metacyclic forms are not readily differentiating into BSFs. WT RBP6$^+$ cultures induced for 6 to 8 days have a subpopulation with a characteristic metacyclic morphology and high calflagin protein levels. However, when transferred into HMI-9 medium, BSF cultures could not be established.

As mentioned before, RBP6-driven *in vitro* differentiation was blocked in the ΔIDHg RBP6$^+$ mutant at the EMF stage and the production of metacyclic forms was completely abolished. Even though differentiation into cells with morphological characteristics of EMFs was successful, the EMF morphology population did not entirely match the size of the BARP positive subpopulation at day two. At any time point most of the cells were EP positive supporting the hypothesis that a lack of IDHg causes a block in early EMF maturation. In accordance with the absence of MFs, the population high in calflagin expression was negligibly low.

As discussed in 4.3, the NAD$^+$-specific IDHg activity could be important for the maintenance of the NAD$^+$/NADH balance allowing gluconeogenic flux in late fly stages. We found that gluconeogenesis is essential for successful metacyclogenesis in culture. Cells lacking fructose 1,6- bisphosphatase (FBPase), a key enzyme in gluconeogenesis, fail to develop MFs and to upregulate calflagin protein levels. Further they do not repress EP expression after RBP6 induction. Interestingly, the phenotype entirely resembles the one found in IDHg deficient cells. The similarity of the developmental phenotype of induced ΔFBPase RBP6$^+$ and ΔIDHg RBP6$^+$ supports the hypothesis that IDHg might play a role in gluconeogenesis during development. However, in PCF cultures a lack of IDHg does not seem to affect gluconeogenesis. The ^{13}C enrichment profile of WT and ΔIDHg are similar for gluconeogenic substrates, if the cells are fed with [U-^{13}C] proline as sole carbon source (described in more detail in 4.2).

Our working hypothesis was that citrate is produced in the tricarboxylic acid (TCA) cycle by citrate synthase (CS) or reductive carboxylation catalysed by the mitochondrial isocitrate dehydrogenase (IDHm) to feed IDHg. However, stable isotope-labelling experiments show that the reverse IDHm reaction does not occur and instead suggest an alternative pathway for (iso-)citrate generation in addition to CS. In the culture differentiation system, the ΔCS RBP6$^+$ mutant resembles the WT RBP6$^+$ differentiation kinetic, based on morphological analyses. However, ΔCS RBP6$^+$ cells do not upregulate calflagin expression in all metacyclic forms. The ΔIDHm RBP6$^+$ mutant has a delayed development and a lower differentiation efficacy than the kinetics described for WT RBP$^+$. A lack of IDHm does not block the development completely at a certain stage, but significantly reduces the efficacy of both EMF and MF development. As IDHm is not involved in the production of citrate, it may contribute to the NADPH supply in the mitochondrion. Further it might act as overflow valve to control mitochondrial isocitrate levels. A double null mutant lacking both IDHg and IDHm could not be established, which can be explained by not tolerable accumulation of isocitrate that could not drain off. Successful differentiation of null mutants in rich culture conditions does not necessarily mean that the mutants succeed in fly midgut and salivary gland colonisation. In culture trypanosomes are not challenged by nutritional bottlenecks, pH and oxidative stress found in tsetse flies (Hao et al., 2003; Liniger et al., 2003; Oberle et al., 2010).

4.2 Analysis of citrate metabolism in procyclic *Trypanosoma brucei*

Previously it has been shown that glucose is not oxidized in the tricarboxylic acid (TCA) cycle (van Weelden et al., 2003). However, citrate synthase (CS), aconitase (ACO) and mitochondrial isocitrate dehydrogenase (IDHm) are expressed. As described in the introduction, the major flux of proline catabolism enters the TCA cycle as α-ketoglutarate (α-KG) and exits it as succinate or malate. Malate is converted via the malic enzyme into the main excretion products alanine and acetate in dependence of glucose availability (Coustou et al., 2008; van Weelden et al., 2005). Glucose-derived malate is converted into succinate by the mitochondrial fumarase (FHm) and fumarate reductase (FRDm) (Coustou et al., 2005). Additionally, citrate is not an intermediate for *de novo* lipogenesis (Millerioux et al., 2013; Riviere et al., 2009). The data published so far leave room for speculations concerning the functions of CS, ACO and IDHm. In BSFs and PCFs the genes encoding for CS, ACO and IDHm are completely dispensable for

growth in rich media (unpublished data Marc Panzer and Stefan Allmann). Additionally, ACO is not essential for BSF to PCF *in vitro* transformation (Saas et al., 2000).

We provide evidences for the existence of a pathway, which is upregulated upon glucose deprivation. Here, citrate produced in the TCA cycle can exit the mitochondrion and enter the cytosol, where the cytoplasmic ACO converts citrate into isocitrate. Isocitrate is imported into the glycosome and fuels the glycosomal isocitrate dehydrogenase (IDHg). In mammalian peroxisomes an α-ketoglutarate/isocitrate transport system has been identified (Visser et al., 2006). The dual localisation of ACO to the cytosol (70 %) and the mitochondrion (30 %) (Saas et al., 2000) could support a split of the flux to fuel IDHm and IDHg at the same time. An enzymatically active ACO lacking the mitochondrial targeting sequence (MTS) to confine expression to the cytosol indirectly substantiates the transport of citrate out of the mitochondrion. In *T. brucei*, a sideroflexin 1 family member has been identified by sequence homology that could facilitate citrate transport across the inner mitochondrial membrane (Colasante et al., 2009). Surprisingly, citrate accumulates in the IDHg null mutant, but not in the IDHm null mutant. Consequently, IDHg and not IDHm is the major sink for isocitrate.

The identification of a connecting pathway between the TCA cycle and IDHg still leaves open questions. All enzymes designated to be involved in this pathway are not essential for BSF and PCF proliferation under standard culture conditions (unpublished data, Marc Panzer und Stefan Allmann). Even though cellular CS, ACO and IDHg protein levels are upregulated in PCFs upon withdrawal of glucose and glycerol, null mutants of CS, ACO, IDHm and IDHg are perfectly viable in absence of glucose and glycerol.

We assigned a key role of the citrate metabolism in insect-stage development. By means of the RBP6-based culture differentiation system (Kolev et al., 2012) the capacities for metacyclogenesis of ΔCS, ΔIDHg and ΔIDHm null mutants were dissected. Here, cells lacking IDHg (ΔIDHg) are stuck in their epimastigote development and fail to produce metacyclic forms in culture. *In vivo* fly experiments confirm the data obtained in culture, as the IDHg null mutant does not establish an infection in the salivary glands (unpublished data, Stefan Allmann und Jan Van Den Abbeele). The ΔCS mutant shows no developmental phenotype in the morphological scoring and the ΔIDHm mutant has only a moderate phenotype. In combination with the fact that $NADP^+$ -dependent IDH homologues are found to be reversible, we analysed whether the flux through CS and IDHm are redundant in terms of producing citrate. However, stable isotope labelling of proline did not confirm this hypothesis. The (iso-)citrate isotopologue M5, which is characteristic for the reductive carboxylation of α-KG by IDH, was not enriched in WT when compared to the IDHm and IDHg null mutants. In the ΔCS cell line, total

enrichment of ^{13}C (iso)citrate isotopologues makes up 73 % of WT. Interestingly, in ΔCS (iso)citrate is not produced by reverse IDH reaction as m4 prevail over m5 isotopologues and the m5 isotopologue proportion is similar to WT. The condensation of m2 acetyl-CoA and m4 OAA both derived from m5 proline yields m6 citrate. In the ΔCS null mutant, m6 citrate is absent until half an hour and present at less than 6 % of total ^{13}C enrichment after 2 h. The m6 proportion of 6 % may be introduced by isotopic scrambling. These findings incite us to speculate about an alternative pathway to produce (iso)citrate independently of acetyl-CoA.

A potential enzyme involved in an alternative (iso)citrate production pathway could be isocitrate lyase (ICL). ICL is normally involved in the glyoxylate cycle found in plants, fungi, archaea and bacteria, but not in placental mammals (Dunn et al., 2009; Kornberg and Krebs, 1957). Together with malate synthase, ICL facilitates the entry of acetate derived from lipolysis into the TCA cycle as an anaplerotic substrate forming the C4-intermediate malate from C2 units. In oil-containing germinating seeds, the glyoxylate cycle and the β-oxidation of fatty acids are colocalised to special organelles called glyoxysomes (LAZAR, 2003). As part of the glyoxylate cycle, ICL catalyses the cleavage of isocitrate into glyoxylate and succinate. The reaction was found to be reversible *in vitro* (Quartararo et al., 2013; Rua et al., 1995). In *Leishmania*, ICL and malate synthase activity along with the detection of acetate-derived glyoxylate has been reported. However, appropriate candidate genes could not be identified by genome analysis (Keegan and Blum, 1993; Opperdoes and Coombs, 2007; Simon et al., 1978). We propose that in *T. brucei* an ICL isoform could act in reverse condensing succinate and glyoxylate to produce isocitrate. Tb927.8.6820 is a potential candidate gene exhibiting ICL features. Initially, due to its homology to ATP-dependent citrate lyases, Tb927.8.6820 was tested for a role in *de novo* lipid biosynthesis, which was not verified (Riviere et al., 2009). A potential source for glyoxylate is glycine. Glycine is excreted as well as incorporated into glutathione (Millerioux et al., 2013) or presumably degraded via the glycine cleavage complex (Berriman et al., 2005). Interestingly, in contrast to *T. cruzi* and *Leishmania spp.*, *T. brucei* lack a serine-hydroxymethyltransferase (SHMT) candidate gene (Gagnon et al., 2006). Several enzymes have been described in different organisms catalysing the conversion of glycine into glyoxylate. Among others, a glycine deaminase has been hypothesized to be potentially involved in the butanol pathway in yeast (Branduardi et al., 2013; Villas-Boas et al., 2005). In *Bacillus subtilis* a glycine oxidase has been characterised encoded by the *yjbR* gene (Nishiya and Imanaka, 1998). An alanine: glyoxylate aminotransferase detoxifies glyoxylate generated by D-amino oxidase from glycine or by hydroxyacid oxidase from glycolate in human liver

peroxisomes (Hoppe, 2010; Pey et al., 2013). In contrast to trypanosomal mitochondrial aspartate aminotransferase (mASAT), trypanosomal cytosolic ASAT was described to be promiscuous for amino acid and keto-acid substrates. However, *Tbc*ASAT does not use glyoxylate as acceptor (Marciano et al., 2008). A useful future experiment to investigate glyoxylate production from threonine involves stable isotope labelling. In *Trypanosoma brucei* threonine is converted into glycine and acetyl-CoA via 2-amino-3-ketobutyrate-CoA (Millerioux et al., 2013). Degradation of [1,2-^{13}C2] L-threonine in this pathway yields [U-^{13}C] glycine and [U-^{12}C] acetyl-CoA. [U-^{13}C] glycine could be converted into [U-^{13}C] glyoxylate, which could together with [U-^{12}C] proline-derived [U-^{12}C] succinate form m2 isocitrate catalysed by a reverse ICL reaction (Fig. 4.1). Consequently, ^{13}C enrichment could be detected in isocitrate and other Krebs cycle intermediates. To ensure sufficient supply of succinate [U-^{12}C] proline needs to be present during the labelling procedure. Flux analysis with [1,2-^{13}C2] L-threonine does not address the question regarding the presence of a malate synthase activity. Malate synthase may condense [U-^{13}C] glyoxylate and [U-^{12}C] acetyl-CoA into m2 malate, which is also formed in the TCA cycle from m2 isocitrate (Fig. 4.1). In case the hypothesis is verified, enzymes of this pathway could be identified by means of sequence homology. With reverse genetic approaches like gene silencing or knock out in combination with metabolic flux analyses, the importance of a modified glyoxylate shunt in producing (iso)citrate can be evaluated.

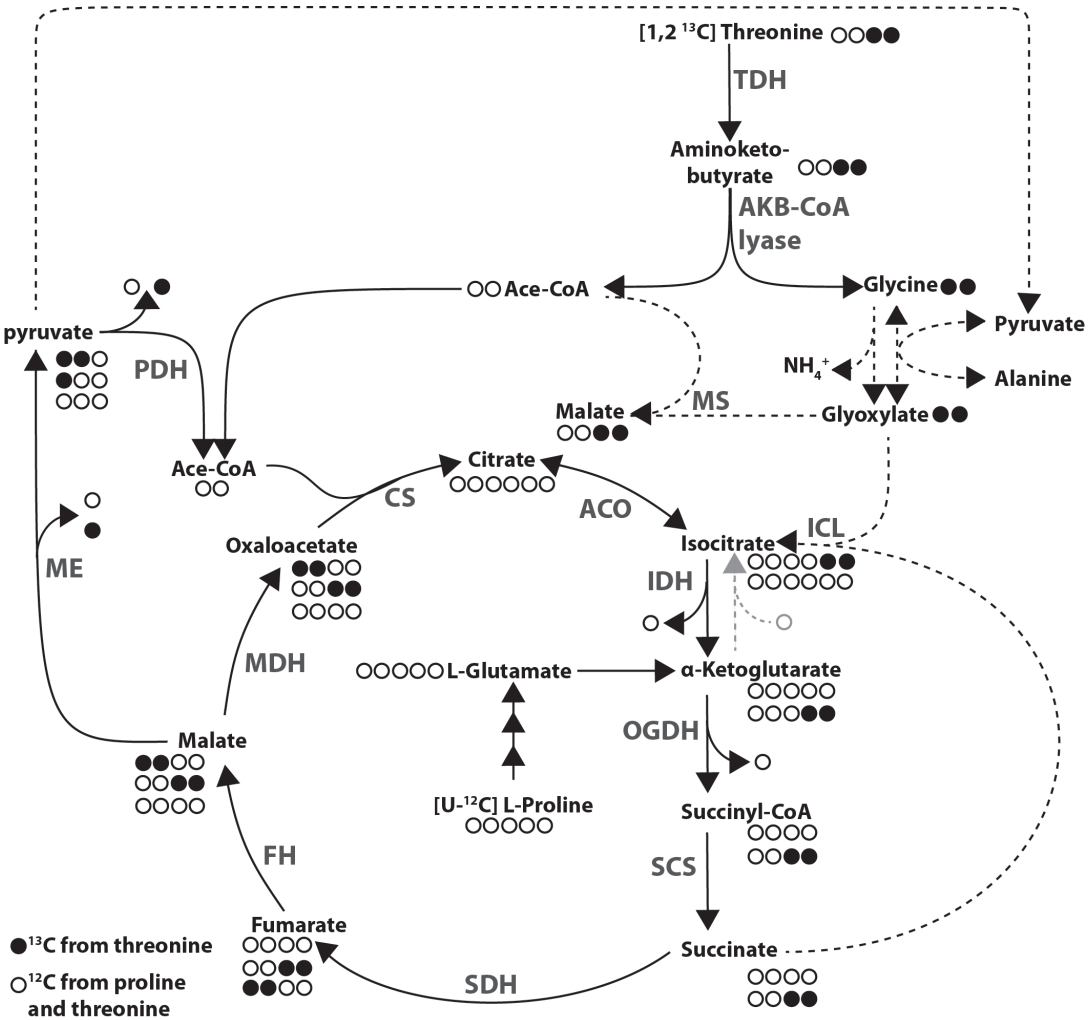

Figure 18 Hypothesis: Alternative pathway for the production of isocitrate. Threonine-derived glyoxylate feeds into the TCA cycle via a reverse isocitrate lyase reaction. The illustration shows proposed (dashed line) and confirmed (continuous line) pathways and the corresponding ^{13}C enrichment from [1,2-^{13}C] threonine in presence of [U-^{12}C] proline. Spheres represent isotopologue profiles starting from the condensation of [U-^{12}C] proline- and [1,2-^{13}C] threonine-derived acetyl-CoA with [U-^{12}C] oxaloacetate by citrate synthase and the condensation of [1,2-^{13}C] threonine-derived glyoxylate with [U-^{12}C] succinate by a reverse ICL reaction. Abbreviations: CS, citrate synthase; ICL, isocitrate lyase; IDH, isocitrate lyase; ME, malic enzyme; MS, malate synthase; PDH, pyruvate dehydrogenase complex

4.3 Glycosomal Isocitrate Dehydrogenase- enzymatic analysis

The need for the glycosomal isocitrate dehydrogenase (IDHg) pathway was defined to the epimastigote (EMFs) and metacyclic forms (MFs). However, whether IDHg has an organelle-specific role in the glycosomes is unknown, yet. We showed that in contrast to the $NADP^+$-dependent mitochondrial isoform (IDHm), the glycosomal IDHg has dual coenzyme specificity for both $NADP^+$ and NAD^+ expanding the number of possible functional roles (unpublished data, Wang, Inaoka and Ziebart). Interestingly, dual coenzyme specificity has already been described for IDH in bacteria (Leyland et al., 1989; Leyland and Kelly, 1991), archaea (Potter, 1993) and fungi (Kim et al., 1996). *Trypanosoma cruzi* IDH has a cytoplasmic localisation and is strictly $NADP^+$ -dependent (Leroux et al., 2011). Therefore we suppose that NADH production by IDHg may have an exclusive role in *T. brucei* glycosomes.

The enzymatic activities of IDHg and IDHm increase more than the actual protein levels. Here, posttranslational modifications (PTMs) may modulate enzymatic activities independent from the expression levels. In many organisms different PTMs regulating IDH enzymatic activities have been described, which can be used as first points of reference in investigating potential *Tb*IDH PTMs. Besides glutathionylation at the active site cysteine residues of $NADP^+$-dependent IDH (Kil and Park, 2005), acetylation at Lys-413 alters IDH2 activity in human cells. Sirtuin 3 mediated deacetylation activates IDH2 (Someya et al., 2010; Yu et al., 2012). The cytosolic IDH1 isoform has a conserved α-helix that self-regulates activity through a conformational change blocking the metal ion binding site (Xu et al., 2004). Bacterial dimeric $NADP^+$ -dependent IDH is regulated by reversible phosphorylation at Ser-113 by the IDH kinase/phosphatase system. Upon aerobic fermentation of acetate, the IDH enzyme pool is partially inactivated to the point, where a balance exists between energy produced in the TCA cycle and biosynthetic precursors generated in the course of the glyoxylate cycle (Cozzone and El-Mansi, 2005).

As IDHg and enzymes involved in isocitrate provision are upregulated in absence of glucose, we raise assumption that there might be a function associated to gluconeogenesis and/or glyceroneogenesis. Gluconeogenesis and glyceroneogenesis share the same pathway to produce dihydroxyacetone phosphate (DHAP) from precursors other than glucose. Gluconeogenesis from proline has been reported in *T. brucei* (Allmann et al., 2013) as well as the production of glycerol from glucose (Creek et al., 2015). In human cells phosphoenolpyruvate carboxykinase (PEPCK) is of significant importance in maintaining and regulating gluconeogenic flux (Stark et al., 2014).

Glycosomes are peroxisome-like organelles harbouring the first six to seven enzymes of glycolysis and are considered to be a closed redox system (Visser and Opperdoes, 1980). IDHg could shift the NADH/NAD^+ balance to a more reducing milieu favouring gluconeogenesis and glyceroneogenesis. In murine hepatocytes an increase in cellular NAD(P)H/$NAD(P)^+$ ratios promotes gluconeogenic flux (Nocito et al., 2015). Enzymes of gluconeogenesis and glyceroneogenesis influence the NADH/NAD^+ ratio in the glycosome. Glycosomal fumarate reductase (FRDg) is unlikely to affect NADH/NAD^+ balance as in absence of glucose only 0.5 % of proline-derived excreted end products account for succinate (Coustou et al., 2008). In our proteomic analysis cytosolic fumarase and FRDg are not significantly regulated upon glucose withdrawal with 0.91- and 1.27- fold, respectively. In a closed system, glycosomal production of glucose from malate is balanced with respect to NAD^+/NADH. For each glucose molecule two NADH are produced by glycosomal malate dehydrogenase (MDHg) and two NADH are consumed by glyceraldehyde 3-phosphate dehydrogenase (GAPDH). So in this simplified situation, an IDHg activity is dispensable. In agreement, the stable isotope labelling experiment with [U-^{13}C] proline using PCFs, a deletion of IDHg did not affect ^{13}C enrichment in gluconeogenic intermediates. It was shown that pyruvate phosphate dikinase (PPDK) is reversible in trypanosomes (Deramchia et al., 2014). In case PPDK and not PEPCK produces PEP for gluconeogenesis, IDHg can provide NADH replacing MDHg as source for NADH. The situation for glyceroneogenesis is however imbalanced and requires another NADH source, whereby IDHg is a good candidate. Here, MDHg produces one NADH, but GAPDH and glycerol-3-phosphate dehydrogenase (NAD-GPDH) each consume one NADH (Deramchia et al., 2014). GPDH has been reported to be involved in glyceroneogenesis occurring in brown adipose tissue and in the liver to maintain lipid homeostasis upon starvation (Kalhan et al., 2008; Reshef et al., 1970). Glycerol 3-phosphate is a precursor for phospholipids and triglycerids (Berg et al., 2012). It has been described for BSFs that the head groups of 8-100 % of the phospholipids are formed by glycolysis-derived glycerol 3-phosphate (Creek et al., 2015). Data from the quantitative proteome show that glucose does not affect NAD-GPDH levels, whereas glycerol 1.8- and 2.2-fold reduces NAD-GPDH and phosphoglycerate kinase (PGK) protein levels, respectively. In absence of glycerol in the medium, glycerol 3-phosphate is produced by NAD-GPDH from glucose in BSFs (Creek et al., 2015) and under glucose depleted conditions glyceroneogenesis can provide glycerol 3-phosphate. In culture, glycerol maintains expression of GPEET, a marker for early PCFs. Availability of glycerol in the midgut may act as timer. Glycerol depletion results in differentiation into late PCFs and migration through the peritrophic matrix

(Vassella et al., 2000). Conclusively, we hypothesize that later insect stages do not have access to glycerol or glucose and depend on glyceroneogenesis for the production of phospholipids and triglycerids. IDHg may contribute NADH for glyceroneogenesis from proline.

In the trypanosomal glycosome, along with the oxidative branch of the pentose phosphate pathway, IDHg could supply NADPH. A peroxisomal localisation of isocitrate dehydrogenase was shown before in mammalian, plants and yeast (Geisbrecht and Gould, 1999; Mhamdi and Noctor, 2015; van Roermund et al., 1998). Generally, NADPH is important for the maintenance of redox balance, oxidative stress defence and biosynthetic pathways. In plants it has been reported that $NADP^+$-dependent IDH is involved in nitro-oxidative stress defence (Leterrier et al., 2012). However, *Arabidopsis* peroxisomal NADP-IDH only plays a minor role in oxidative stress defence (Mhamdi and Noctor, 2015). In human, mitochondrial IDH2 controls redox balance and oxidative stress defence (Jo et al., 2001). *Saccharomyces cerevisiae* expresses three differentially compartmentalised $NADP^+$-dependent IDH isozymes. Yeast peroxisomal IDH3 provides NADPH for β-oxidation of polyunsaturated fatty acids (Henke et al., 1998; van Roermund et al., 1998). The existence of a lipid degradation pathway in cultured PCFs is possible but not supported by recent experiments (Allmann et al., 2014). In mammalian hepatocytes peroxisomal NADPH production by IDH1 was shown to be associated to sterol and lipid biosynthesis. Moreover, IDH1 expression levels are regulated by sterol regulatory element binding proteins 1a and 2 (Shechter et al., 2003). In trypanosomes, biosynthesis of ether-linked lipids from dihydroxyacetone phosphate (DHAP) is another NADPH sink in glycosomes (Michels et al., 2006). Etherlipids can stabilize membranes, prevent acidic/basic hydrolysis and decrease permeability (Aussenac et al., 2005; Shinoda et al., 2004). Etherlipids might maintain membrane integrity and rigidity, while *Trypanosoma brucei* faces oxidative and alkaline pH stress in the proventriculus of the tsetse fly and oxidative stress in the mammalian host (Brunet, 2001; Hao et al., 2003). In the tsetse fly, a pH gradient exists starting with pH 7.9 in the posterior midgut up to pH 10.6 in the proventriculus (Liniger et al., 2003). As the IDHg differentiation phenotype was also observed in culture upon RBP6 overexpression, the developmental defect seems to be cell autonomous. A defective defence of oxidative and pH stress introduced by the host as cause for the block in differentiation can be excluded. Variations in the etherlipid content between WT and the ΔIDHg mutant are currently analysed by GC-MS.

IDHg is also providing α-ketoglutarate (α-KG) in the glycosome. Possible α-KG consuming reactions are dioxygenases. The α-ketoglutarate dehydrogenase complex (KDH) subunit E_1 catalysing the oxidative decarboxylation of α-KG in the mitochondrion

was found to be essential in BSFs. Interestingly, in BSFs, which have a minimal TCA cycle activity, α-KG decarboxylase E_1 is localised to the glycosomes, whereas in PCFs it is mitochondrial and non-essential (Bochud-Allemann and Schneider, 2002; Sykes et al., 2015). The role of this unusual localisation of E_1 in BSFs has not been identified. A moonlighting function of another subunit of α-ketoglutarate dehydrogenase complex has been described for subunit E_2. E_2 dihydrolipoamid-succinyltransferase was found to be essential for mitochondrial kDNA inheritance in BSFs and PCFs (Sykes and Hajduk, 2013). Stumpy BSFs take up α-KG and maintain motility for more than three hours (Vickerman, 1965). However, external α-KG supplementation of *in vitro* differentiating ΔIDHg RBP6$^+$ mutants did not re-establish metacyclogenesis. Assuming α-KG enters the glycosome, a developmental phenotype based on a lack α-KG in the glycosome may rather be unlikely.

In order to determine which reduced coenzyme is functionally relevant for the process of fly-stage differentiation, a complementation of the ΔIDHg mutant with an IDH isoform specific for one coenzyme could be performed. For the introduction of NADP$^+$-dependent IDH activity, the *T. cruzi* IDH (*Tc*IDHc) is a good candidate gene (Leroux et al., 2011). Eukaryotic NAD$^+$ -dependent IDH isoforms found in the mitochondrion are usually hetero-oligomeric and thus not suitable. Instead bacterial type I IDHs or the recently identified type II algal IDH are potential candidate genes (Wang et al., 2015). The codon usage needs to be optimized for expression in *T. brucei* and a peroxisomal targeting sequence needs to be added to the C-terminus to ensure glycosomal localisation. The correct subcellular localisation will be controlled by digitonin titration and enzyme activities will be assayed. Eventually, a rescue of the developmental phenotype of the *Tb*IDHg null mutant in the RBP6 differentiation system (Kolev et al., 2012) will tell, if glycosomal NADH or NADPH is necessary for successful differentiation.

4.4 Hydroxyglutarate is not a xenometabolite in *Trypanosoma brucei*

In the past decade the xenometabolite 2-hydroxyglutarate (2-HG) became the focus of attention, as it was found to be involved in tumorigenesis and neuronal diseases (Engqvist et al., 2014). In the cellular metabolism, both stereoisomers L-2-HG and D-2-HG are produced, though by distinct enzymatic reactions. All our data do not discriminate between the stereoisomers and represent the racemate of total 2-HG. 2-HG is known to be a competitive inhibitor of many α-ketoglutarate (α-KG)- dependent dioxygenases. Generally, L-2-HG is a more potent inhibitor than D-2-HG with prolyl hydroxylase being an exception. Epigenetic regulators among others TET proteins and

histone demethylases belong to the dioxygenases (Xu et al., 2011). Trypanosomes express TET family members, JBP1 and JBP2, that control polymerase II transcription initiation by means of baseJ (Cliffe et al., 2012). Recently it was shown in various cancer cell lines, that $NADP^+$ -dependent isocitrate dehydrogenase (IDH) IDH1 and IDH2 harbour a distinct missense mutation at the R132 and R140/R172, respectively (Yan et al., 2009). This gain-of-function mutation at the active site enables the mutant IDH to catalyse a neomorphic enzymatic reaction converting α-KG into 2-HG. However, the ability to catalyse the interconversion of isocitrate and α-KG got lost in the IDH mutants (Dang et al., 2009; Zhao et al., 2009). Previously it seemed likely, that neither wild type (WT) IDH1 nor WT IDH2 is able to generate 2-HG from α-KG (Leonardi et al., 2012; Ward et al., 2010). Though, recently Smolková et al. published that WT IDH2 contributes ~50 % to the 2-HG pool in breast and adenocarcinoma cells (Smolkova et al., 2015). In contrast to isocitrate, 2-HG cannot be metabolised by aconitase (Engqvist et al., 2014). Considering our gas chromatography/ mass spectrometry (GC/MS) and ^{13}C-enrichment profile from [U-^{13}C] proline, it seems that neither glycosomal IDH (IDHg) nor mitochondrial (IDHm) contribute to the 2-HG pool in trypanosomes. No significant changes in cellular total 2-HG metabolite concentration or formation could be detected in the *Tb*IDHg and *Tb*IDHm null mutants. Thus it seems that 2-HG in *Trypanosoma brucei* is unlikely to be derived from IDHg or IDHm. Even though D-2-HG is an oncometabolite in mammalians, in bacteria D-2-HG is a precursor for butyrate biosynthesis from α-KG (Szafrański et al., 2015; Vital et al., 2014). In contrast to D-2-HG, there has been no cellular function identified for L-2-HG, yet. In mammals L-2-HG is produced by a side activity of malate dehydrogenase (MDH) (Rzem et al., 2007). The *Trypanosoma brucei* genome encodes three MDH isoforms with distinct subcellular localisations in the cytosol (MDHc), glycosomes (MDHg) and mitochondrion (MDHm). The three isoforms are differentially expressed within the parasite life cycle. BSFs only express MDHc, whereas PCFs express all three isoforms (Aranda et al., 2006). In case any MDH isoform is the source for 2-HG, it is more likely to be MDHc, since 2-HG is produced in PCFs and BSFs (Kim et al., 2015). As L-2-HG seems to be an undesired side product of MDH, a "metabolite repair" mechanism was identified to remove L-2-HG in human. The mitochondrial membrane associated FAD- dependent L-2-hydroxyglutarate dehydrogenase (L-2-HGDH) specifically catalyzes the conversion of L-2-HG to α-KG (Rzem et al., 2004). Lack of L-2-HGDH causes L-2-hydroxyglutaric aciduria, which is associated to a neurometabolic disorder and increased risk of developing tumours (Van Schaftingen et al., 2009). In *Trypanosoma brucei* Opperdoes recently annotated a L-2-

HGDH in TriTryp database with 33 % sequence homology to the human enzyme (Tb927.10.9360).

To investigate the role of 2-HG in trypanosomes it would be important to track down the source of 2-HG. Our data correspond to the racemate of total 2-HG. An advisable pre-experiment could be the discrimination between L- and D-2- hydroxyglutarate using chiral derivatisation combined with LC-MS/MS to preselect potential sources for 2-HG (Fig. 4.2) (Dang et al., 2009; Struys, 2013). Further analyses could include silencing of the potential 2-HG producing enzyme and subsequent metabolite analyses with MS. Another interesting experiment could elucidate the impact of 2-HG on base-J abundance in the nucleus.

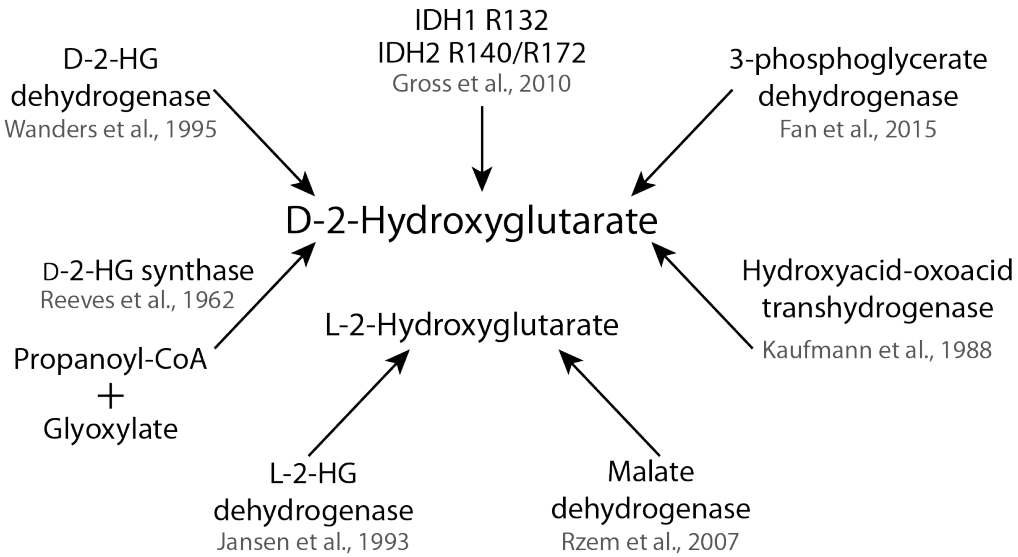

Figure 19 Overview of 2-hydroxyglutarate producing/consuming reactions. Unless otherwise indicated hydroxyglutarate is formed from α-ketoglutarate. 2-HG, 2-hydroxyglutarate; IDH, isocitrate dehydrogenase

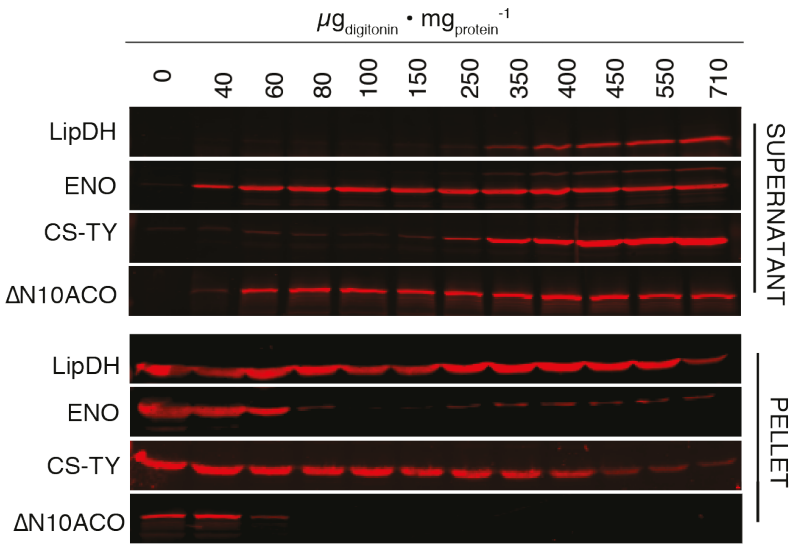

Figure A 1 Subcellular localisation of ΔN10ACO and *Tb*CS-TY. AnTat 1.1 1313 ΔN10ACO TbCS-TY^{Ti} was induced with 0.01 µg/ml tetracycline for 2 days. Digitonin fractionation with increasing concentrations of digitonin. Western blot analysis of supernatants and washed pellets probed with specific antibodies against lipoamide dehydrogenase (LipDH) as mitochondrial marker, enolase (ENO) as cytosolic marker, citrate synthase (CS) and aconitase (ACO).

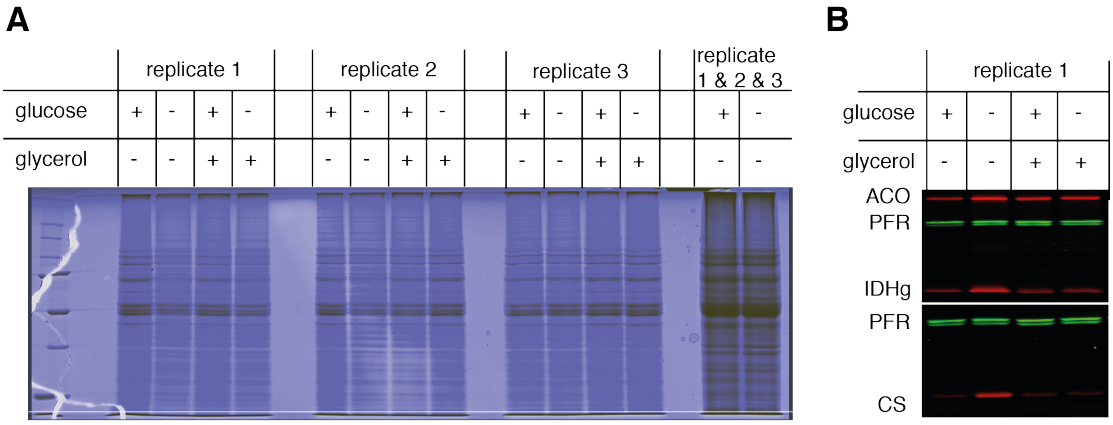

Figure A 2 Quality controls of proteome samples. [A] Coomassie stain to quantify total protein concentrations prior mass spectrometry analysis (Dupuy, Université de Bordeaux). [B] Western blot analysis to control glucose- and glycerol-dependent protein regulation in aconitase (ACO), citrate synthase (CS) and glycosomal isocitrate dehydrogenase (IDHg) of samples analysed by mass spectrometry. Paraflagellar rod protein (PFR) served as loading control.

Table A 1 High confidence proteome for procyclic EATRO 1125 cells. Cells were grown for ten days in SDM79 in presence and/or absence of glycerol or glucose. NanoLC MS/MS peptide detection and label-free quantitative data analysis with Progenesis® QI software. Proteins involved in metabolism are shown sorted according to their pathway. Ratios of expression levels of cells grown in absence of glucose and glycerol normalised against cells cultured in presence of either glycerol or glucose or the presence of both. (Data analysis by Allmann and Dupuy (Bordeaux).

ID	Protein name	Pathway	Peptide count	Unique peptides	Confidence score	WT +Glu-Gly mean	WT +Glu-Gly ±SD	WT +Glu-Gly ±SD	WT -Glu-Gly mean	WT -Glu-Gly ±SD	WT -Glu-Gly ±SD	WT +Glu+Gly mean	WT +Glu+Gly ±SD	WT +Glu+Gly ±SD	WT -Glu+Gly mean	WT -Glu+Gly ±SD	WT -Glu+Gly ±SD	-glc-glyc/ +glc-glyc	-glc-glyc/ -glc+glyc	-glc-glyc/ +glc+glyc
Tb927.10.2010	hexokinase (HK1)	glycolysis	70	3	3789	346691	169173	49%	1631523	354700	22%	209949	40581	19%	255430	25611	10%	4.706	6.387	7.771
Tb927.10.2020	hexokinase (HK2)		69	3	3950	1793125	603771	34%	2081056	248345	12%	1094257	258750	24%	1492521	116457	8%	1.161	1.394	1.902
Tb927.1.3830	glucose-6-phosphate isomerase, glycosomal (PGI)		27	21	914	4065361	2292435	56%	4654642	648781	14%	2542234	76534	3%	2676126	85635	3%	1.145	1.739	1.831
Tb927.3.3270	ATP-dependent phosphofructokinase (PFK)		47	36	1812	9555697	935470	10%	10918021	2501461	23%	8033248	986473	12%	7434467	789583	11%	1.143	1.469	1.359
Tb927.10.5620	fructose-bisphosphate aldolase, glycosomal (ALD)		68	63	3201	82600752	9226265	11%	109029316	4725043	4%	78578559	3425160	4%	88253503	5755072	7%	1.320	1.235	1.388
Tb927.11.5520	triosephosphate isomerase (TIM)		36	30	1987	81961701	3035788	4%	112937944	14866033	13%	72415968	6073297	8%	75031697	8731297	12%	1.378	1.505	1.560
Tb927.6.4280	glyceraldehyde 3-phosphate dehydrogenase, glycosomal (GAPDH)		120	92	5790	140709662	21040557	15%	218540998	14575520	7%	110583102	2830306	3%	113879259	3734580	3%	1.553	1.919	1.976
Tb927.8.3530	glycerol-3-phosphate dehydrogenase [NAD+], glycosomal		64	53	3678	39405762	3526868	9%	84483753	5758655	7%	42342056	3047728	7%	47485690	5390543	11%	2.144	1.779	1.995
Tb927.10.6880	glyceraldehyde 3-phosphate dehydrogenase, cytosolic (GAP)		21	15	1255	13323064	632747	5%	16280454	897600	6%	12623205	848291	7%	13616969	712722	5%	1.222	1.196	1.290
Tb927.9.12570	glycerol kinase, glycosomal (glk1)		114	99	6362	34676919	4006558	12%	67171258	3029990	5%	28901996	4440382	15%	31003193	4263553	14%	1.937	2.167	2.324
Tb927.1.710	phosphoglycerate kinase (PGKB)		54	5	2721	14489779	760668	5%	19957339	751858	4%	11463426	2508103	22%	10867599	2656082	24%	1.377	1.836	1.741
Tb927.1.720	phosphoglycerate kinase (PGKA)		41	15	1654	2979902	897643	30%	6197924	278228	4%	2587601	51666	2%	2636843	90268	3%	2.080	2.351	2.395
Tb927.10.7930	2,3-bisphosphoglycerate-independent phosphoglycerate mutase (PGAM)		47	40	1769	15032246	4110959	27%	13686497	753094	6%	11208062	163256	1%	11376163	509422	4%	0.910	1.203	1.221
Tb927.10.2890	enolase		89	64	4546	240016497	33373130	14%	197501170	35044753	18%	159177173	8865278	6%	200739675	45883263	23%	0.823	0.984	1.241
Tb927.10.14140;Tb11.v5.0605	pyruvate kinase 1 (PYK1)		50	42	1995	24892489	233211	1%	17464369	2985711	17%	19015930	1092894	6%	17204790	1402946	8%	0.702	1.015	0.918
Tb927.11.6280	pyruvate phosphate dikinase (PPDK)		184	154	8297	63744846	5867624	9%	83433573	3806171	5%	51078588	1984181	4%	48356718	3523964	7%	1.309	1.725	1.633
Tb927.10.15410	glycosomal malate dehydrogenase (gMDH)	succinate branch	49	43	2467	105491055	15300032	15%	170485495	14645071	9%	98093377	7220393	7%	102093440	12345976	12%	1.616	1.670	1.738
Tb927.2.4210	glycosomal phosphoenolpyruvate carboxykinase (PEPCK)		133	109	6540	41572176	648689	2%	69348930	7599254	11%	41716586	1357522	3%	41347522	3785067	9%	1.668	1.677	1.662
Tb927.11.11250	cytosolic malate dehydrogenase (cMDH)		19	14	860	14758873	1593997	11%	11970628	293944	2%	9568838	878001	9%	10548807	1315291	12%	0.811	1.135	1.251
Tb927.3.4500;Tb11.v5.0629	fumarate hydratase, class I (FHc)		49	41	2221	13499616	1779851	13%	9016135	1288715	14%	10845214	665044	6%	9859056	213112	2%	0.668	0.915	0.831
Tb927.5.930;Tb11.v5.0613	NADH-dependent fumarate reductase (FRDg)		68	23	2914	11363298	612641	5%	13499718	1674129	12%	9970474	1629044	16%	10603586	516481	5%	1.188	1.273	1.354
Tb927.3.1790	pyruvate dehydrogenase E1 beta subunit, putative	acetate branch	40	30	1923	42088907	555654	1%	45202676	3541143	8%	37231435	2046332	5%	36392871	3214667	9%	1.074	1.242	1.214
Tb927.10.12700	pyruvate dehydrogenase E1 alpha subunit, putative		76	63	3571	28789522	3698440	13%	38151443	2659296	7%	26296530	411774	2%	24832512	2021896	8%	1.325	1.536	1.451
Tb927.10.7570;Tb11.v5.0774	dihydrolipoamide acetyltransferase E2 subunit, putative		37	34	1685	44453325	7179090	16%	55461667	9161030	17%	40692440	1746575	4%	38244696	9982105	26%	1.248	1.450	1.363
Tb927.10.2350	pyruvate dehydrogenase complex E3 binding protein, putative		13	7	960	1079834	473519	44%	347095	98971	29%	445766	137404	31%	294486	89262	30%	0.321	1.179	0.779
Tb927.11.2690	succinyl-coA:3-ketoacid-coenzyme A transferase, mitochondrial precursor, putative		43	32	2013	18708197	409276	2%	25043985	3825830	15%	12607927	1394221	11%	13241066	1973059	15%	1.339	1.891	1.986
Tb927.3.4260	thioesterase superfamily		3	2	106	544616	222023	41%	1008125	599768	59%	1726930	811141	47%	2217294	228107	10%	1.851	0.455	0.584
Tb927.10.13430	citrate synthase, putative	TCA cycle	41	38	2022	18468353	1117534	6%	41651609	4162154	10%	12568077	1792207	14%	15306090	3075413	20%	2.255	2.721	3.314
Tb927.10.14000	aconitase (ACO)		76	61	3992	23759487	4640055	20%	40768013	2314242	6%	19877344	1435437	7%	19160326	1547894	8%	1.716	2.128	2.051
Tb927.8.3690	isocitrate dehydrogenase [NADP], mitochondrial precursor		26	24	1057	5216571	506491	10%	5165018	240903	5%	4489991	338053	8%	3890049	346891	9%	0.990	1.328	1.150
Tb927.11.9980	2-oxoglutarate dehydrogenase E1 component, putative		111	80	5479	47447163	10305272	22%	46116567	2917075	6%	42829992	2442572	6%	45418688	765273	2%	0.972	1.015	1.077
Tb927.11.1450	2-oxoglutarate dehydrogenase E1 component, putative		140	114	5693	42633028	6489849	15%	37579674	2030499	5%	33844146	2414054	7%	36728372	6086058	17%	0.881	1.023	1.110
Tb927.11.11680	2-oxoglutarate dehydrogenase E2 component, putative		54	35	2509	74135123	8070652	11%	83508635	10482677	13%	63994051	1632999	3%	67327030	9366124	14%	1.126	1.240	1.305
Tb927.10.7410	succinyl-CoA ligase [GDP-forming] beta-chain, putative		68	59	3605	66873624	12910935	19%	55419780	4997124	9%	49927679	5643126	11%	54160772	1152566	2%	0.829	1.023	1.110
Tb927.3.2230	succinyl-CoA synthetase alpha subunit, putative		40	34	1932	52970322	4002260	8%	68809482	9695309	14%	58615858	3116867	5%	63698702	4435828	7%	1.299	1.080	1.174
Tb927.8.6580	succinate dehydrogenase flavoprotein, putative		32	27	1443	6070518	1062256	17%	8144987	1303929	16%	4381916	863856	20%	4666517	741040	16%	1.342	1.745	1.859
Tb927.9.5960	succinate dehydrogenase, putative		13	11	434	2761834	231758	8%	7279682	1720044	24%	3083016	414731	13%	4518625	228320	5%	2.636	1.611	2.361
Tb927.11.5050	fumarate hydratase, class I (FHm)		20	16	735	3053386	692906	23%	4576207	307192	7%	4266060	67685	2%	6408879	978620	15%	1.499	0.714	1.073
Tb927.10.2560	mitochondrial malate dehydrogenase (mMDH)		45	42	2098	211328566	43982549	21%	224635019	3608891	2%	172616268	11155336	6%	185880278	23854424	13%	1.063	1.208	1.301
Tb927.10.2490	glucose-6-phosphate 1-dehydrogenase (G6PD)	Pentose phosphate pathway	18	13	338	3225196	640741	20%	3279937	188633	6%	3468716	138989	4%	3584418	185469	5%	1.017	0.915	0.946
Tb927.11.6330	6-phosphogluconolactonase (6PGL)		5	3	148	1762014	514751	29%	1818743	128970	7%	1591829	217999	14%	1002011	61526	6%	1.032	1.815	1.143
Tb927.9.12110	6-phosphogluconate dehydrogenase, decarboxylating (gnD)		12	10	685	3278227	271143	8%	4283110	207877	5%	2526414	470637	19%	2748697	393702	14%	1.307	1.558	1.695
Tb927.10.12210	ribulose-5-phosphate 3-epimerase, putative		4	3	104	1197857	107806	9%	1427778	309222	22%	1662102	193081	12%	1558101	296727	19%	1.192	0.916	0.859
Tb927.11.8970	ribose 5-phosphate isomerase, putative		17	16	926	40403043	2771461	7%	45002891	2580587	6%	34802110	2764806	8%	39593696	2043268	5%	1.114	1.137	1.293
Tb927.8.6170	transketolase, putative (TK)		58	42	2353	51157685	5404542	11%	39123334	5227338	13%	43049306	3808036	9%	46260170	3835652	8%	0.765	0.846	0.909
Tb927.8.5600	transaldolase, putative		33	29	1455	15317096	1168063	8%	15101927	2182618	14%	13169592	730442	6%	13111733	1173099	9%	0.986	1.152	1.147
Tb927.11.900	isocitrate dehydrogenase, putative (IDH)	NADPH production	43	39	1962	7796061	239586	3%	27870773	3392053	12%	7262404	1256442	17%	7247267	1028689	14%	3.575	3.846	3.838
Tb927.11.5450	malic enzyme		40	25	1908	10469348	1434331	14%	13462279	682427	5%	7764754	944090	12%	7536852	616177	8%	1.286	1.786	1.734
Tb927.11.5440	malic enzyme		48	34	2102	20469716	861151	4%	23562859	1539081	7%	17330441	569726	3%	19279189	4779223	25%	1.151	1.222	1.360
Tb927.11.15910	iron superoxide dismutase	Oxidative stress defence	23	12	904	22452251	1029972	5%	19299797	1660552	9%	16297209	787869	5%	14906138	1330419	9%	0.860	1.295	1.184
Tb927.10.10390	trypanothione reductase		26	18	1124	11197661	1710774	15%	9342375	806053	9%	9030317	1351994	15%	8928803	809500	9%	0.834	1.046	1.035
Tb927.2.4370	trypanothione synthetase (TRYS)		48	42	2045	14297703	1507946	11%	12165600	1266381	10%	15676554	1190745	8%	12309742	610864	5%	0.851	0.988	0.776
Tb927.9.5750	unspecified product		84	74	2831	47364047	3343789	7%	69446219	3148501	5%	47184286	1347076	3%	52176225	2805693	5%	1.466	1.331	1.472
Tb927.7.1120	trypanothione/tryparedoxin dependent peroxidase 1, cytosolic, GSH peroxidase-like protein 1 (TDPX1)		19	3	692	6280865	1287894	21%	4149632	955325	23%	4359734	740670	17%	3519594	471441	13%	0.661	1.179	0.952
Tb927.7.1130	trypanothione/tryparedoxin dependent peroxidase 2,GSH peroxidase-like 2 (TDPX2)		19	5	727	16307347	1954013	12%	14704702	3749374	25%	13887015	1582060	11%	15013067	2569305	17%	0.902	0.979	1.059
Tb927.10.12370	gamma-glutamylcysteine synthetase (GCS)		12	8	314	2185999	441563	20%	2735494	1098367	40%	1998600	185290	9%	1900549	255209	13%	1.251	1.439	1.369
Tb927.7.7500;Tb927.2.6180; Tb927.2.6230;Tb927.2.6310	thymine-7-hydroxylase, putative (TLP7)		15	13	661	1488498	490655	33%	1429794	115727	8%	743684	116621	16%	761963	113938	15%	0.961	1.876	1.923
Tb927.11.7840	ribonucleoside-diphosphate reductase large chain (RNR1)		35	29	1372	2699029	300867	11%	2953600	243010	8%	3762816	214238	6%	3218155	652295	20%	1.094	0.918	0.785
Tb927.7.4000	glutathione synthetase, putative	Trypanothion synthesis	8	5	233	398837	163780	41%	1112566	376473	34%	585316	356281	61%	364115	53160	15%	2.790	3.056	1.901
Tb927.11.13730	ornithine decarboxylase (ODC)		6	5	71	1894575	217659	11%	1854938	54827	3%	2000826	155960	8%	1829576	277952	15%	0.979	1.014	0.927
Tb927.9.7770	spermidine synthase,SPDSYN (SpSyn)		20	18	816	18757423	1434733	8%	20442926	2584941	13%	15405845	1840358	12%	15503020	1320548	9%	1.090	1.319	1.327
Tb927.7.3500	glutathione-S-transferase/glutaredoxin, putative		16	14	587	12756652	3678669	29%	16410438	557516	3%	10511096	1262422	12%	7800862	235409	3%	1.286	2.104	1.561

.

Figure A 3 Flow cytometry histograms of stage-specific marker analysis. Induction of RBP6 overexpression in WT, ΔIDHg, ΔCS and ΔFBPase cell lines. Trypanosomes were probed with antibodies against procyclin EP, brucei alanine-rich protein (BARP) and calflagin using AlexaFluor488 as secondary antibody. Cells were analysed after 2, 4 and 6 days using flow cytometry (one representative experiment out of three is shown). Uninduced cells (day 0) are shown as reference in red in each histogram. Ranges are indicated as black horizontal line in each diagram dividing the population into high and low expressing subpopulations. Histograms of flow cytometry analysis using the FlowJo software of [A] WT, [B] ΔIDHg, [C] ΔCS and [D] ΔFBPase

A

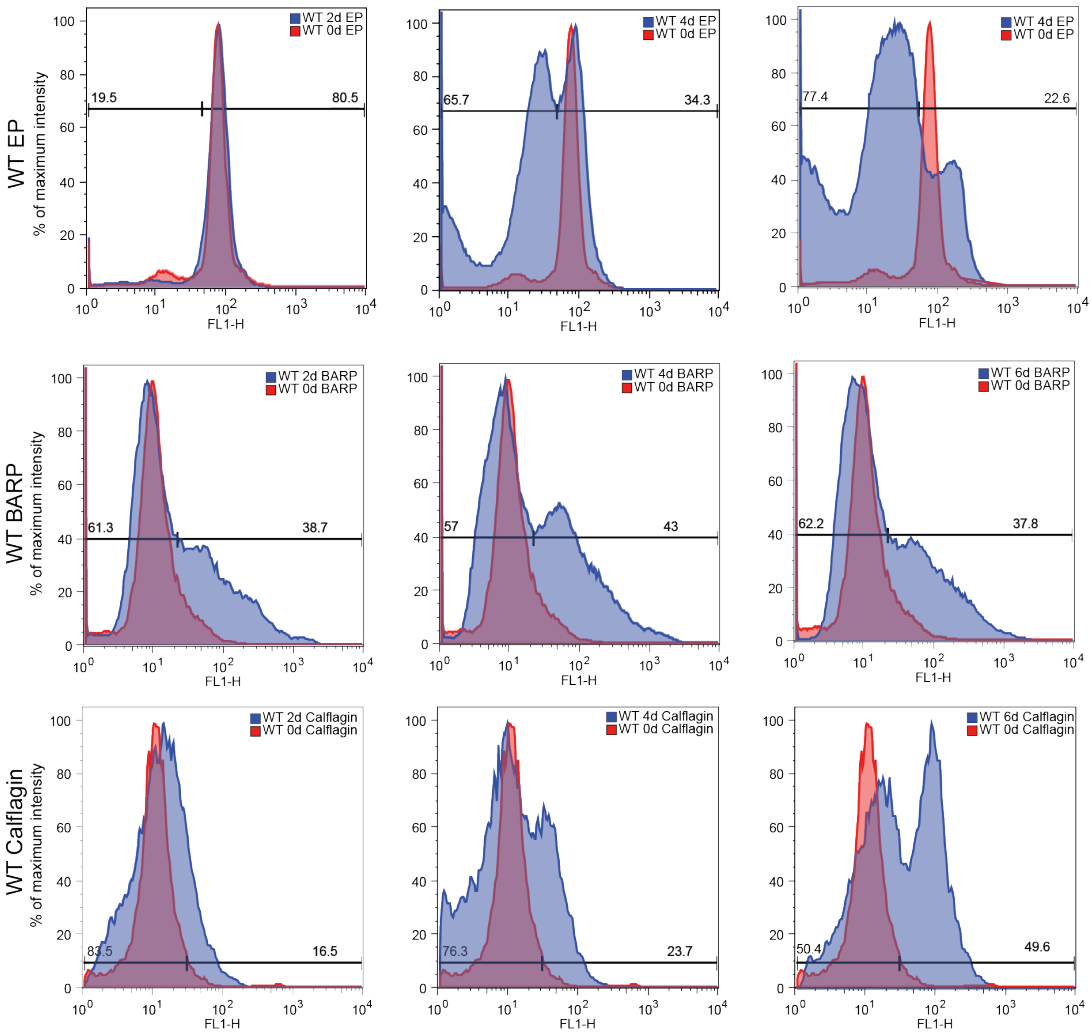

B

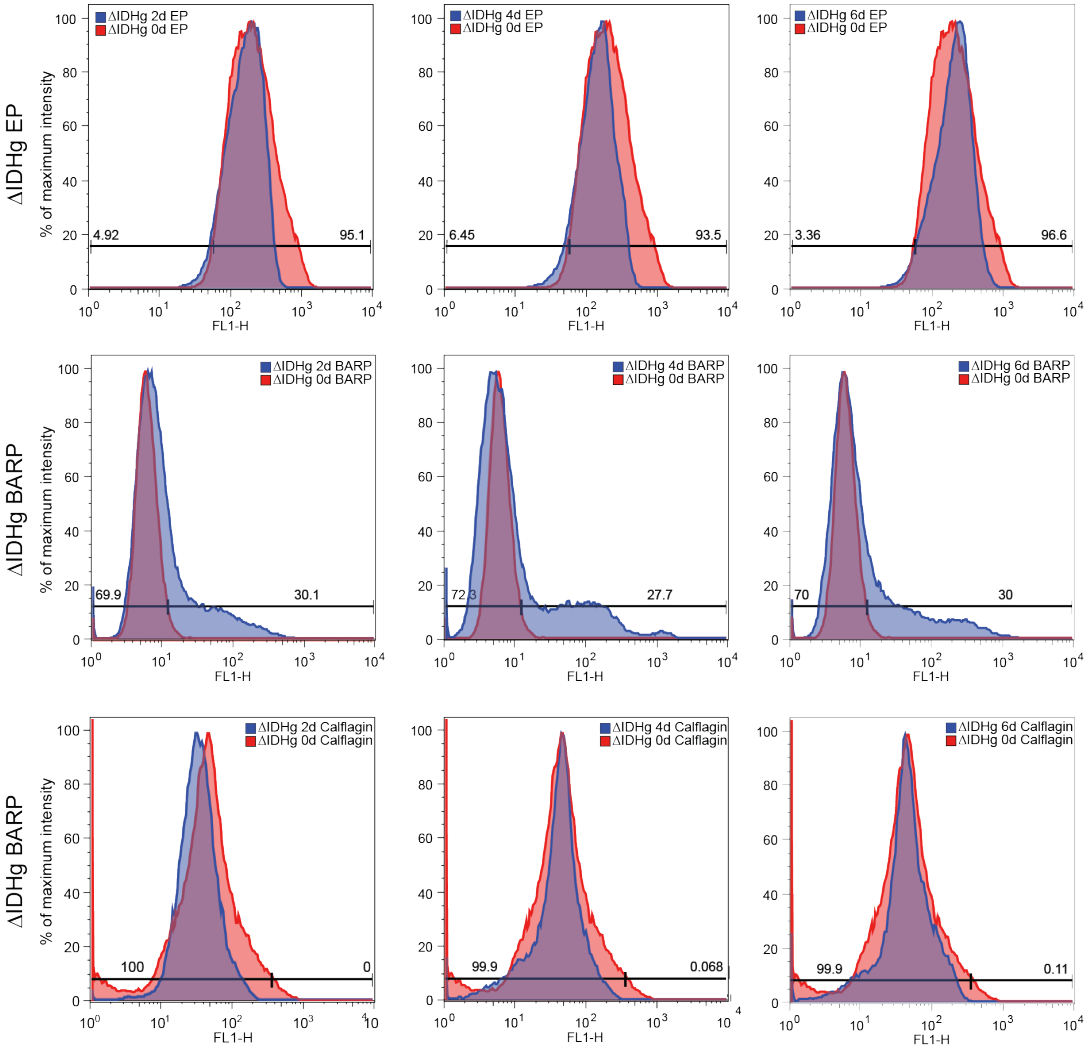
ΔIDHg EP
ΔIDHg BARP
ΔIDHg BARP
% of maximum intensity
FL1-H
ΔIDHg 2d EP
ΔIDHg 0d EP
ΔIDHg 4d EP
ΔIDHg 0d EP
ΔIDHg 6d EP
ΔIDHg 0d EP
ΔIDHg 2d BARP
ΔIDHg 0d BARP
ΔIDHg 4d BARP
ΔIDHg 0d BARP
ΔIDHg 6d BARP
ΔIDHg 0d BARP
ΔIDHg 2d Calflagin
ΔIDHg 0d Calflagin
ΔIDHg 4d Calflagin
ΔIDHg 0d Calflagin
ΔIDHg 6d Calflagin
ΔIDHg 0d Calflagin
4.92
95.1
6.45
93.5
3.36
96.6
69.9
30.1
72.3
27.7
70
30
100
0
99.9
0.068
99.9
0.11

C

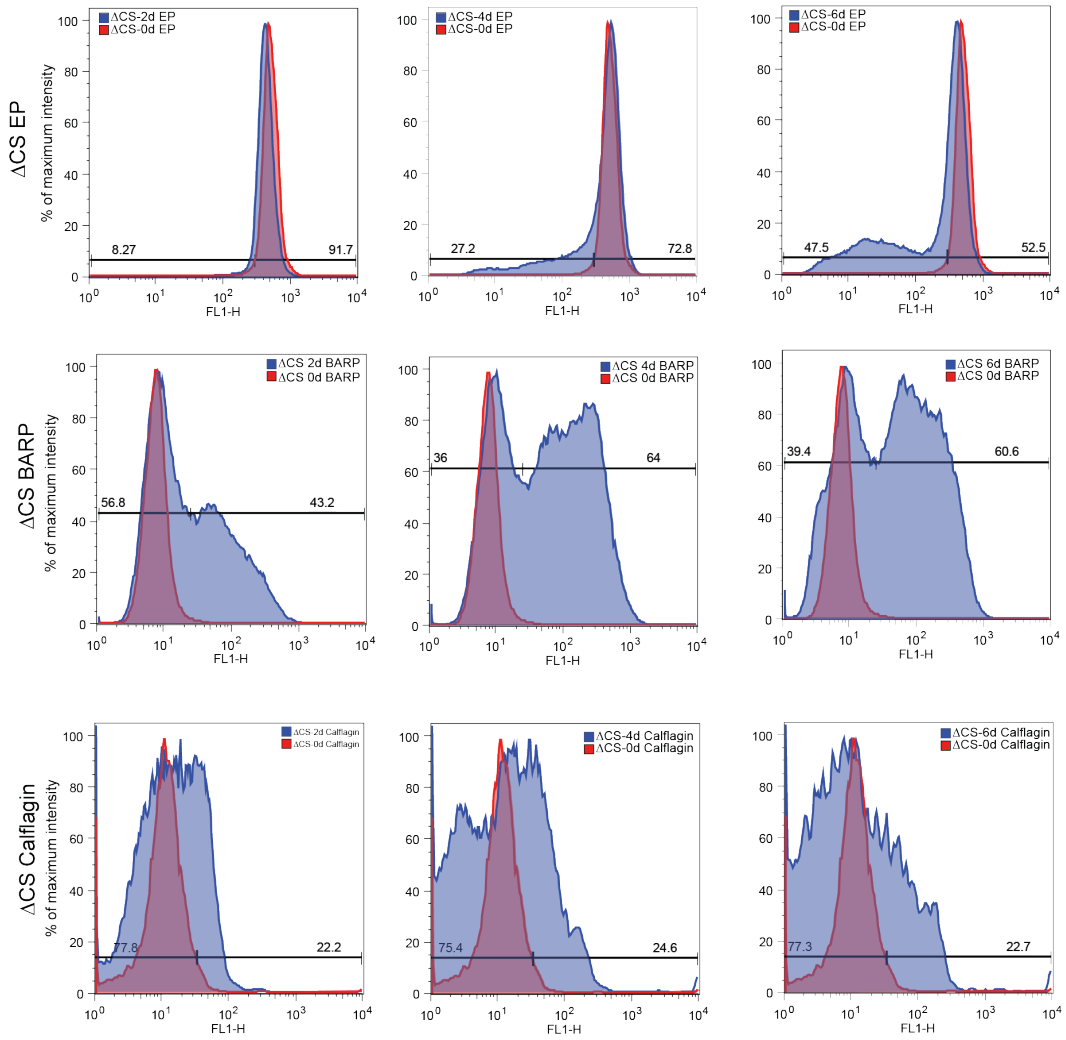
ΔCS EP
ΔCS BARP
ΔCS Calflagin
% of maximum intensity
FL1-H
ΔCS-2d EP
ΔCS-0d EP
8.27
91.7
ΔCS-4d EP
ΔCS-0d EP
27.2
72.8
ΔCS-6d EP
ΔCS-0d EP
47.5
52.5
ΔCS 2d BARP
ΔCS 0d BARP
56.8
43.2
ΔCS 4d BARP
ΔCS 0d BARP
36
64
ΔCS 6d BARP
ΔCS 0d BARP
39.4
60.6
ΔCS-4d Calflagin
ΔCS-0d Calflagin
75.4
24.6
ΔCS-6d Calflagin
ΔCS-0d Calflagin
77.3
22.7

D

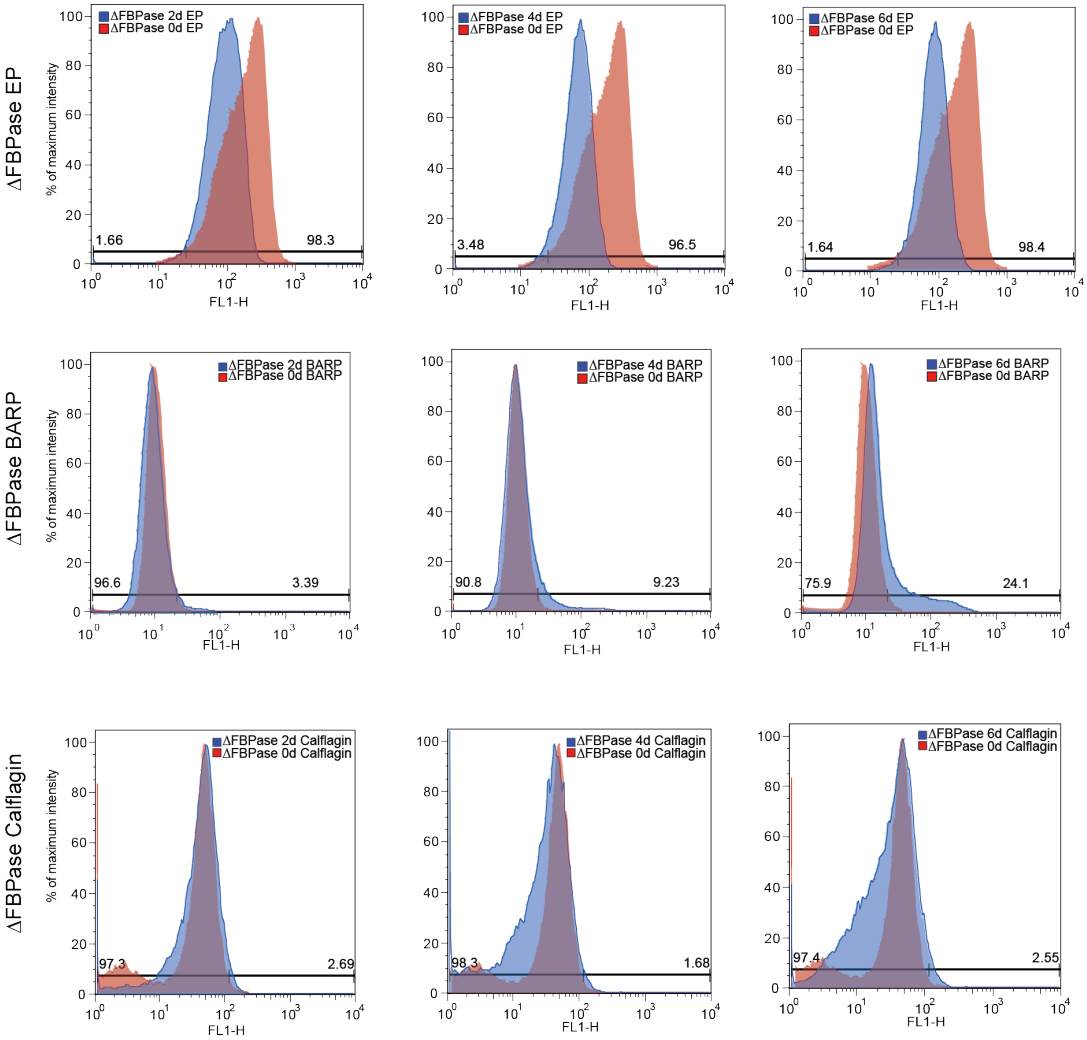
ΔFBPase EP
ΔFBPase 2d EP
ΔFBPase 0d EP
1.66
98.3
ΔFBPase 4d EP
ΔFBPase 0d EP
3.48
96.5
ΔFBPase 6d EP
ΔFBPase 0d EP
1.64
98.4
ΔFBPase BARP
ΔFBPase 2d BARP
ΔFBPase 0d BARP
96.6
3.39
ΔFBPase 4d BARP
ΔFBPase 0d BARP
90.8
9.23
ΔFBPase 6d BARP
ΔFBPase 0d BARP
75.9
24.1
ΔFBPase Calflagin
ΔFBPase 2d Calflagin
ΔFBPase 0d Calflagin
97.3
2.69
ΔFBPase 4d Calflagin
ΔFBPase 0d Calflagin
98.3
1.68
ΔFBPase 6d Calflagin
ΔFBPase 0d Calflagin
97.4
2.55
% of maximum intensity
FL1-H

Figure A 4 Stable isotope enrichment from ^{13}C proline. Procyclic AnTat1.1 WT and null mutants of ΔACO, ΔCS, ΔIDHg, ΔIDHm as well as the ΔACO/ΔCS double knock out were cultured for 10 d in SDM79 medium without glucose. After washing, 2E8 cells/ml were incubated in PBS containing 2 mM [U-^{13}C]proline as sole carbon source. 1E8 cells in 500 µl labelling solution were analysed for each time point (0 min, 15 min, 30 min and 120 min). The proportion of the different isotopologues m0-m7 is shown as heat map. ACO, aconitase; CS, citrate synthase; IDHg, glycosomal iscitrate dehydrogenase; IDHm, mitochondrial isocitrate dehydrogenase; WT, wild type.

A

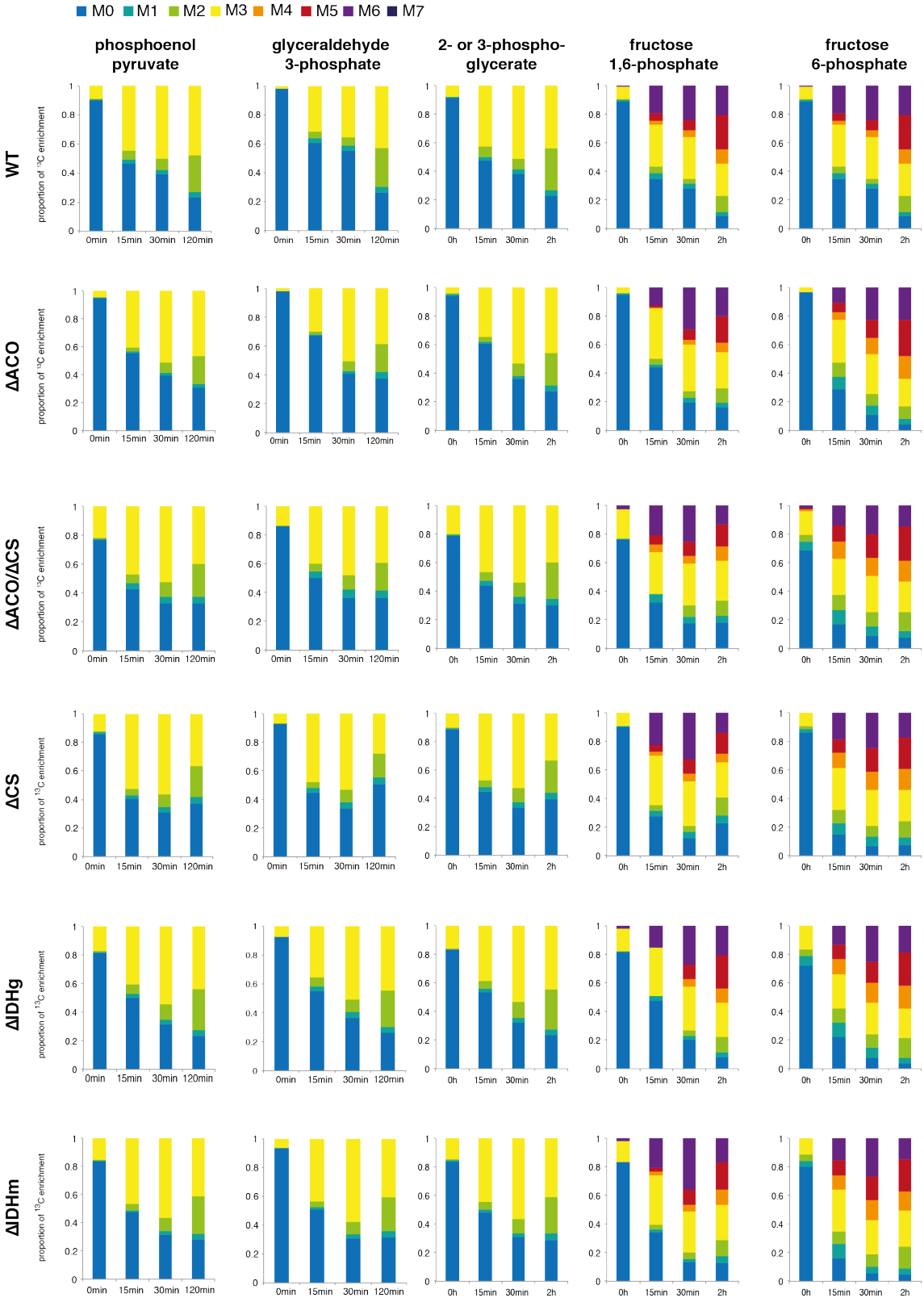

B

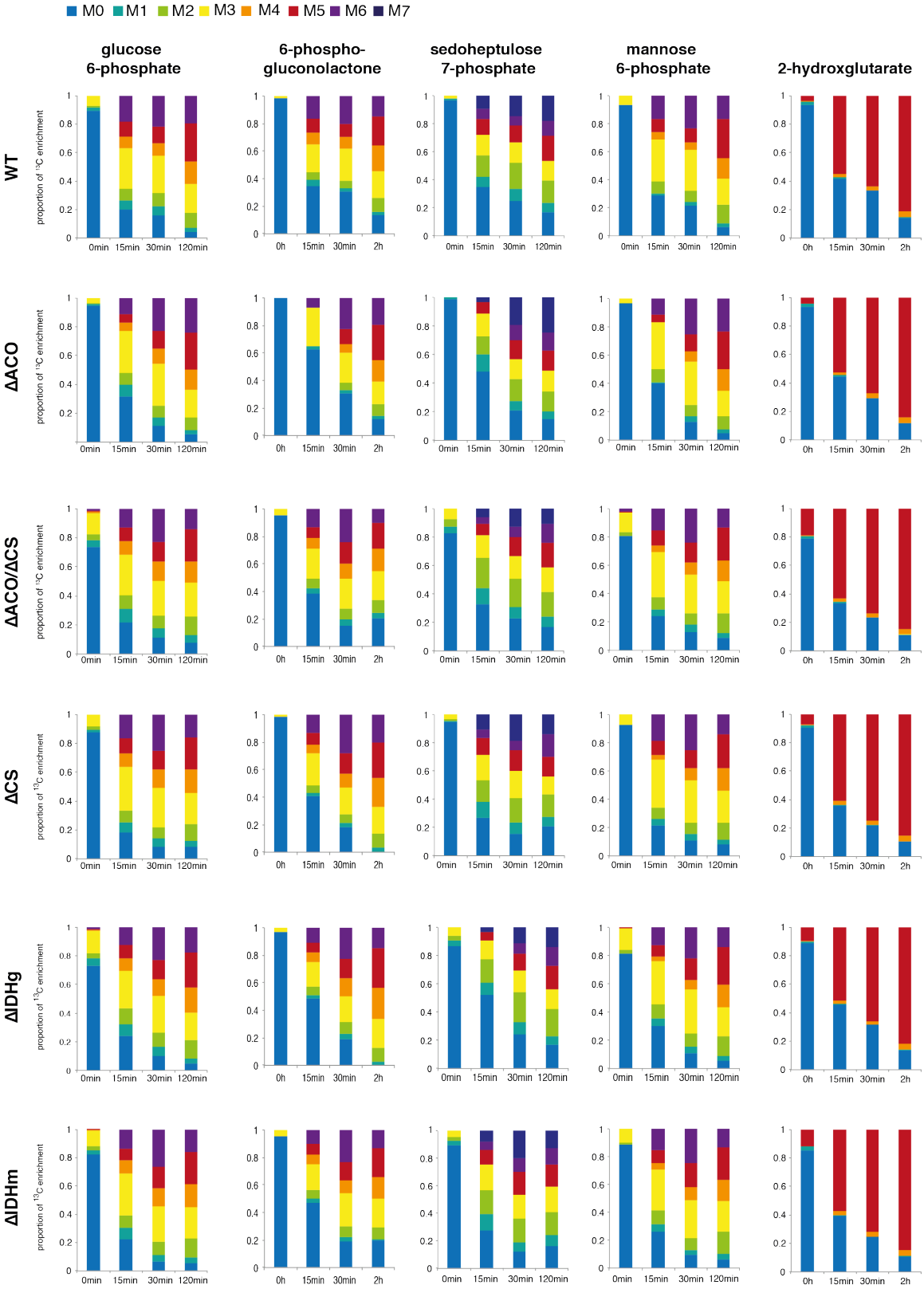
M0 M1 M2 M3 M4 M5 M6 M7
glucose 6-phosphate
6-phospho-gluconolactone
sedoheptulose 7-phosphate
mannose 6-phosphate
2-hydroxglutarate
WT
ΔACO
ΔACO/ΔCS
ΔCS
ΔIDHg
ΔIDHm
proportion of 13C enrichment
0min 15min 30min 120min
0h 15min 30min 2h

C

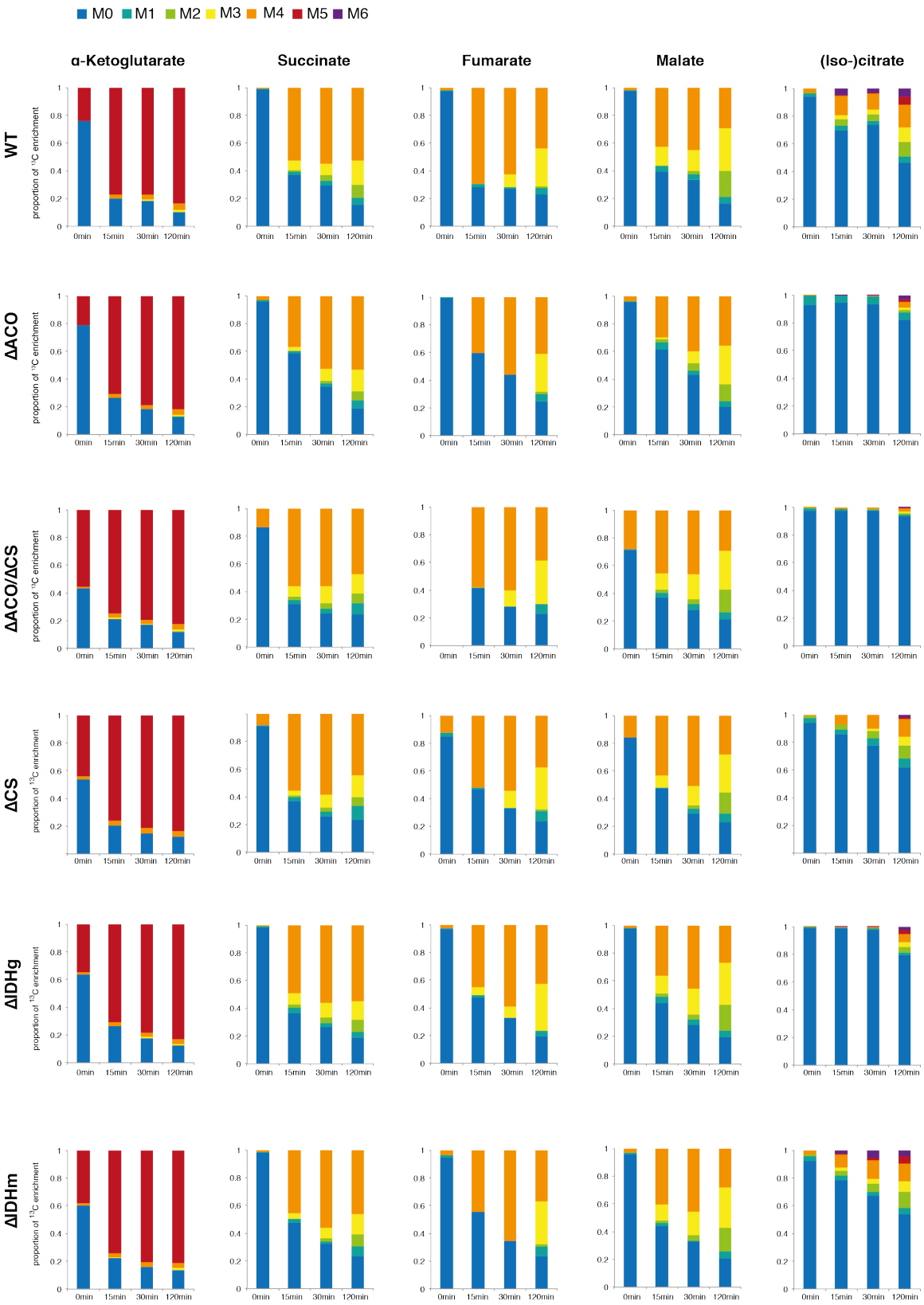
M0 M1 M2 M3 M4 M5 M6
α-Ketoglutarate
Succinate
Fumarate
Malate
(Iso-)citrate
WT
ΔACO
ΔACO/ΔCS
ΔCS
ΔIDHg
ΔIDHm
proportion of 13C enrichment
0min 15min 30min 120min

Figure A 5 The population of cells with high EP surface levels consists mainly of procyclic and some epimastigote cells. EATRO 1125-T7T WT RBP6^{Ti} cells were induced for 4 days. Immunofluorescence images taken with 100x objective at the DeltaVision Elite microscope. Kinetoplasts and nuclei were stained with DAPI (red channel). EP was detected on not permeabilised cells (green channel). Merge of DIC, DAPI and EP signal.

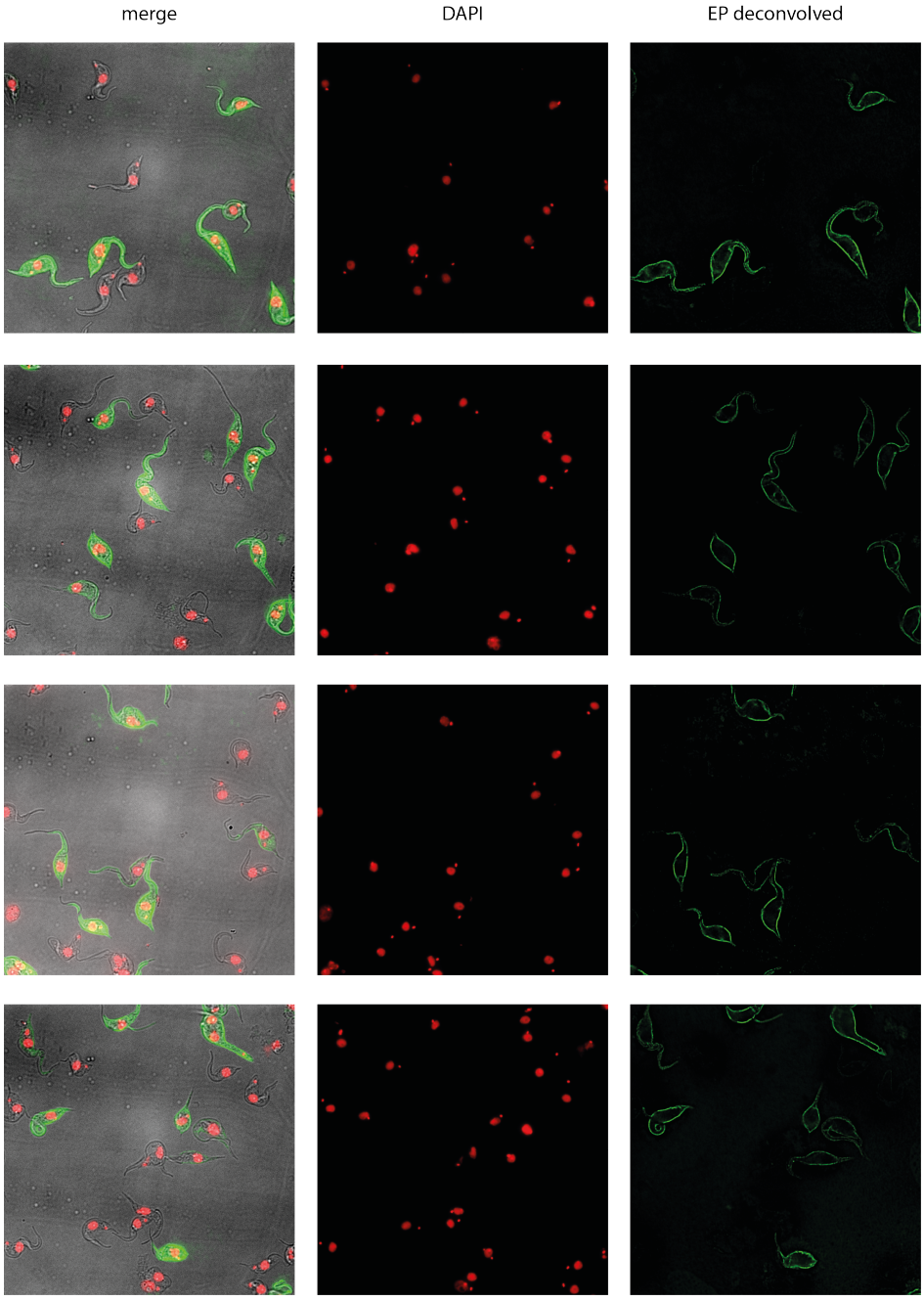

Acestor, N., Zíková, A., Dalley, R.A., Anupama, A., Panigrahi, A.K., and Stuart, K.D. (2011). Trypanosoma brucei Mitochondrial Respiratome: Composition and Organization in Procyclic Form. Molecular & Cellular Proteomics *10*.

Acosta-Serrano, A., Cole, R.N., Mehlert, A., Lee, M.G., Ferguson, M.A., and Englund, P.T. (1999). The procyclin repertoire of Trypanosoma brucei. Identification and structural characterization of the Glu-Pro-rich polypeptides. The Journal of biological chemistry *274*, 29763-29771.

Acosta-Serrano, A., Vassella, E., Liniger, M., Kunz Renggli, C., Brun, R., Roditi, I., and Englund, P.T. (2001). The surface coat of procyclic Trypanosoma brucei: programmed expression and proteolytic cleavage of procyclin in the tsetse fly. Proceedings of the National Academy of Sciences of the United States of America *98*, 1513-1518.

Ahn, C.S., and Metallo, C.M. (2015). Mitochondria as biosynthetic factories for cancer proliferation. Cancer & metabolism *3*, 1.

Alberts, B., Wilson, J., and Hunt, T. (2008). Molecular biology of the cell (New York: Garland Science).

Alibu, V.P., Storm, L., Haile, S., Clayton, C., and Horn, D. (2005). A doubly inducible system for RNA interference and rapid RNAi plasmid construction in Trypanosoma brucei. Molecular and biochemical parasitology *139*, 75-82.

Allmann, S., Mazet, M., Ziebart, N., Bouyssou, G., Fouillen, L., Dupuy, J.W., Bonneu, M., Moreau, P., Bringaud, F., and Boshart, M. (2014). Triacylglycerol Storage in Lipid Droplets in Procyclic Trypanosoma brucei. PloS one *9*, e114628.

Allmann, S., Morand, P., Ebikeme, C., Gales, L., Biran, M., Hubert, J., Brennand, A., Mazet, M., Franconi, J.M., Michels, P.A.*, et al.* (2013). Cytosolic NADPH homeostasis in glucose-starved procyclic Trypanosoma brucei relies on malic enzyme and the pentose phosphate pathway fed by gluconeogenic flux. The Journal of biological chemistry *288*, 18494-18505.

Aranda, A., Maugeri, D., Uttaro, A.D., Opperdoes, F., Cazzulo, J.J., and Nowicki, C. (2006). The malate dehydrogenase isoforms from Trypanosoma brucei: Subcellular localization and differential expression in bloodstream and procyclic forms. International Journal for Parasitology *36*, 295-307.

Aussenac, F., Lavigne, B., and Dufourc, E.J. (2005). Toward Bicelle Stability with Ether-Linked Phospholipids: Temperature, Composition, and Hydration Diagrams by 2H and 31P Solid-State NMR. Langmuir *21*, 7129-7135.

Azema, L., Claustre, S., Alric, I., Blonski, C., Willson, M., Perie, J., Baltz, T., Tetaud, E., Bringaud, F., Cottem, D.*, et al.* (2004). Interaction of substituted hexose analogues with the Trypanosoma brucei hexose transporter. Biochemical pharmacology *67*, 459-467.

Balogun, R. (1974). Amino acids in the excreta of the tsetse fly, Glossina palpalis. Experientia *30*, 239-240.

Berg, J.M., Tymoczko, J.L., and Stryer, L. (2012). Biochemistry (Basingstoke: W.H. Freeman).

Berghammer, H., and Auer, B. (1993). "Easypreps": fast and easy plasmid minipreparation for analysis of recombinant clones in E. coli. BioTechniques *14*, 524, 528.

Berriman, M., Ghedin, E., Hertz-Fowler, C., Blandin, G., Renauld, H., Bartholomeu, D.C., Lennard, N.J., Caler, E., Hamlin, N.E., Haas, B.*, et al.* (2005). The genome of the African trypanosome Trypanosoma brucei. Science (New York, NY) *309*, 416-422.

Besteiro, S., Biran, M., Biteau, N., Coustou, V., Baltz, T., Canioni, P., and Bringaud, F. (2002). Succinate secreted by Trypanosoma brucei is produced by a novel and unique glycosomal enzyme, NADH-dependent fumarate reductase. The Journal of biological chemistry *277*, 38001-38012.

Birsoy, K., Possemato, R., Lorbeer, F.K., Bayraktar, E.C., Thiru, P., Yucel, B., Wang, T., Chen, W.W., Clish, C.B., and Sabatini, D.M. (2014). Metabolic determinants of cancer cell sensitivity to glucose limitation and biguanides. Nature *508*, 108-112.

Blattner, J., Swinkels, B., Dorsam, H., Prospero, T., Subramani, S., and Clayton, C. (1992). Glycosome assembly in trypanosomes: variations in the acceptable degeneracy of a COOH-terminal microbody targeting signal. The Journal of cell biology *119*, 1129-1136.

Bochud-Allemann, N., and Schneider, A. (2002). Mitochondrial substrate level phosphorylation is essential for growth of procyclic Trypanosoma brucei. The Journal of biological chemistry *277*, 32849-32854.

Bradford, M.M. (1976). A rapid and sensitive method for the quantitation of microgram quantities of protein utilizing the principle of protein-dye binding. Analytical Biochemistry *72*, 248-254.

Branduardi, P., Longo, V., Berterame, N.M., Rossi, G., and Porro, D. (2013). A novel pathway to produce butanol and isobutanol in Saccharomyces cerevisiae. Biotechnology for biofuels *6*, 68.

Bringaud, F., Riviere, L., and Coustou, V. (2006). Energy metabolism of trypanosomatids: adaptation to available carbon sources. Molecular and biochemical parasitology *149*, 1-9.

Bringaud, F., Robinson, D.R., Barradeau, S., Biteau, N., Baltz, D., and Baltz, T. (2000). Characterization and disruption of a new Trypanosoma brucei repetitive flagellum protein, using double-stranded RNA inhibition. Molecular and biochemical parasitology *111*, 283-297.

Brown, S.V., Hosking, P., Li, J., and Williams, N. (2006). ATP synthase is responsible for maintaining mitochondrial membrane potential in bloodstream form Trypanosoma brucei. Eukaryot Cell *5*, 45-53.

Brun, R., and Schonenberger (1979). Cultivation and in vitro cloning or procyclic culture forms of Trypanosoma brucei in a semi-defined medium. Short communication. Acta tropica *36*, 289-292.

Brun, R., and Schonenberger, M. (1981). Stimulating effect of citrate and cis-Aconitate on the transformation of Trypanosoma brucei bloodstream forms to procyclic forms in vitro. Zeitschrift fur Parasitenkunde (Berlin, Germany) *66*, 17-24.

Brunet, L.R. (2001). Nitric oxide in parasitic infections. International immunopharmacology *1*, 1457-1467.

Burgess, D.J. (2011). Metabolism: Choose your carbon source. Nat Rev Cancer *11*, 80-81.

Bursell, E. (1977). Synthesis of proline by fat body of the tsetse fly (Glossina morsitans): metabolic pathways. Insect Biochemistry *7*, 427-434.

Bütikofer, P., Ruepp, S., Boschung, M., and Roditi, I. (1997). 'GPEET' procyclin is the major surface protein of procyclic culture forms of Trypanosoma brucei brucei strain 427. Biochemical Journal *326*, 415-423.

Cairns, R.A., Harris, I.S., and Mak, T.W. (2011). Regulation of cancer cell metabolism. Nat Rev Cancer *11*, 85-95.

Ceylan, S., Seidel, V., Ziebart, N., Berndt, C., Dirdjaja, N., and Krauth-Siegel, R.L. (2010). The dithiol glutaredoxins of african trypanosomes have distinct roles and are closely linked to the unique trypanothione metabolism. The Journal of biological chemistry *285*, 35224-35237.

Clarkson, A.B., Jr., Bienen, E.J., Pollakis, G., and Grady, R.W. (1989). Respiration of bloodstream forms of the parasite Trypanosoma brucei brucei is dependent on a plant-like alternative oxidase. The Journal of biological chemistry *264*, 17770-17776.

Clayton, C., Adams, M., Almeida, R., Baltz, T., Barrett, M., Bastien, P., Belli, S., Beverley, S., Biteau, N., Blackwell, J*., et al.* (1998). Genetic nomenclature for Trypanosoma and Leishmania. Molecular and biochemical parasitology *97*, 221-224.

Cliffe, L.J., Hirsch, G., Wang, J., Ekanayake, D., Bullard, W., Hu, M., Wang, Y., and Sabatini, R. (2012). JBP1 and JBP2 Proteins Are Fe(2+)/2-Oxoglutarate-dependent Dioxygenases Regulating Hydroxylation of Thymidine Residues in Trypanosome DNA. The Journal of biological chemistry *287*, 19886-19895.

Colasante, C., Pena Diaz, P., Clayton, C., and Voncken, F. (2009). Mitochondrial carrier family inventory of Trypanosoma brucei brucei: Identification, expression and subcellular localisation. Molecular and biochemical parasitology *167*, 104-117.

Cori, C.F., and Cori, G.T. (1925). THE CARBOHYDRATE METABOLISM OF TUMORS: I. THE FREE SUGAR, LACTIC ACID, AND GLYCOGEN CONTENT OF MALIGNANT TUMORS. Journal of Biological Chemistry *64*, 11-22.

Cosenza, L.W., Bringaud, F., Baltz, T., and Vellieux, F.M. (2000). Crystallization and preliminary crystallographic investigation of glycosomal pyruvate phosphate dikinase from Trypanosoma brucei. Acta crystallographica Section D, Biological crystallography *56*, 1688-1690.

Coustou, V., Besteiro, S., Biran, M., Diolez, P., Bouchaud, V., Voisin, P., Michels, P.A.M., Canioni, P., Baltz, T., and Bringaud, F. (2003). ATP Generation in the Trypanosoma brucei Procyclic Form: CYTOSOLIC SUBSTRATE LEVEL PHOSPHORYLATION IS ESSENTIAL, BUT NOT OXIDATIVE PHOSPHORYLATION. Journal of Biological Chemistry *278*, 49625-49635.

Coustou, V., Besteiro, S., Riviere, L., Biran, M., Biteau, N., Franconi, J.M., Boshart, M., Baltz, T., and Bringaud, F. (2005). A mitochondrial NADH-dependent fumarate reductase involved in the production of succinate excreted by procyclic Trypanosoma brucei. The Journal of biological chemistry *280*, 16559-16570.

Coustou, V., Biran, M., Breton, M., Guegan, F., Riviere, L., Plazolles, N., Nolan, D., Barrett, M.P., Franconi, J.M., and Bringaud, F. (2008). Glucose-induced remodeling of intermediary and energy metabolism in procyclic Trypanosoma brucei. The Journal of biological chemistry *283*, 16342-16354.

Cozzone, A.J., and El-Mansi, M. (2005). Control of isocitrate dehydrogenase catalytic activity by protein phosphorylation in Escherichia coli. Journal of molecular microbiology and biotechnology *9*, 132-146.

Creek, D.J., Mazet, M., Achcar, F., Anderson, J., Kim, D.-H., Kamour, R., Morand, P., Millerioux, Y., Biran, M., Kerkhoven, E.J.*, et al.* (2015). Probing the Metabolic Network in Bloodstream-Form Trypanosoma brucei Using Untargeted Metabolomics with Stable Isotope Labelled Glucose. PLoS Pathogens *11*, e1004689.

Cross, G.A., Klein, R.A., and Linstead, D.J. (1975). Utilization of amino acids by Trypanosoma brucei in culture: L-threonine as a precursor for acetate. Parasitology *71*, 311-326.

Cruz, A.K., Titus, R., and Beverley, S.M. (1993). Plasticity in chromosome number and testing of essential genes in Leishmania by targeting. Proceedings of the National Academy of Sciences of the United States of America *90*, 1599-1603.

Cunningham, I. (1977). New culture medium for maintenance of tsetse tissues and growth of trypanosomatids. The Journal of protozoology *24*, 325-329.

Cunningham, I., and Slater, J.S. (1974). Amino acid analyses of haemolymph of Glossina morsitans morsitans (Westwood). Acta tropica *31*, 83-88.

Czichos, J., Nonnengaesser, C., and Overath, P. (1986). Trypanosoma brucei: cis-aconitate and temperature reduction as triggers of synchronous transformation of bloodstream to procyclic trypomastigotes in vitro. Experimental parasitology *62*, 283-291.

d'Ieteren, G.D., Authie, E., Wissocq, N., and Murray, M. (1998). Trypanotolerance, an option for sustainable livestock production in areas at risk from trypanosomosis. Revue scientifique et technique (International Office of Epizootics) *17*, 154-175.

Dang, L., White, D.W., Gross, S., Bennett, B.D., Bittinger, M.A., Driggers, E.M., Fantin, V.R., Jang, H.G., Jin, S., Keenan, M.C.*, et al.* (2009). Cancer-associated IDH1 mutations produce 2-hydroxyglutarate. Nature *462*, 739-744.

Daye, D., and Wellen, K.E. (2012). Metabolic reprogramming in cancer: Unraveling the role of glutamine in tumorigenesis. Seminars in Cell & Developmental Biology *23*, 362-369.

Dean, S., Marchetti, R., Kirk, K., and Matthews, K.R. (2009). A surface transporter family conveys the trypanosome differentiation signal. Nature *459*, 213-217.

DeBerardinis, R.J., Lum, J.J., Hatzivassiliou, G., and Thompson, C.B. (2008). The Biology of Cancer: Metabolic Reprogramming Fuels Cell Growth and Proliferation. Cell Metabolism *7*, 11-20.

DeBerardinis, R.J., Mancuso, A., Daikhin, E., Nissim, I., Yudkoff, M., Wehrli, S., and Thompson, C.B. (2007). Beyond aerobic glycolysis: transformed cells can engage in glutamine metabolism that exceeds the requirement for protein and nucleotide synthesis. Proceedings of the National Academy of Sciences of the United States of America *104*, 19345-19350.

Deramchia, K., Morand, P., Biran, M., Millerioux, Y., Mazet, M., Wargnies, M., Franconi, J.M., and Bringaud, F. (2014). Contribution of pyruvate phosphate dikinase in the maintenance of the glycosomal ATP/ADP balance in the Trypanosoma brucei procyclic form. The Journal of biological chemistry *289*, 17365-17378.

Dunn, M.F., Ramirez-Trujillo, J.A., and Hernandez-Lucas, I. (2009). Major roles of isocitrate lyase and malate synthase in bacterial and fungal pathogenesis. Microbiology (Reading, England) *155*, 3166-3175.

Durieux, P.O., Schutz, P., Brun, R., and Kohler, P. (1991). Alterations in Krebs cycle enzyme activities and carbohydrate catabolism in two strains of Trypanosoma brucei during in vitro differentiation of their bloodstream to procyclic stages. Molecular and biochemical parasitology *45*, 19-27.

Dyer, N.A., Rose, C., Ejeh, N.O., and Acosta-Serrano, A. (2013). Flying tryps: survival and maturation of trypanosomes in tsetse flies. Trends in parasitology *29*, 188-196.

Ebikeme, C., Hubert, J., Biran, M., Gouspillou, G., Morand, P., Plazolles, N., Guegan, F., Diolez, P., Franconi, J.M., Portais, J.C.*, et al.* (2010). Ablation of succinate production from glucose metabolism in the procyclic trypanosomes induces metabolic switches to the glycerol 3-phosphate/dihydroxyacetone phosphate shuttle and to proline metabolism. The Journal of biological chemistry *285*, 32312-32324.

Ebikeme, C.E., Peacock, L., Coustou, V., Riviere, L., Bringaud, F., Gibson, W.C., and Barrett, M.P. (2008). N-acetyl D-glucosamine stimulates growth in procyclic forms of Trypanosoma brucei by inducing a metabolic shift. Parasitology *135*, 585-594.

Emmer, B.T., Daniels, M.D., Taylor, J.M., Epting, C.L., and Engman, D.M. (2010). Calflagin inhibition prolongs host survival and suppresses parasitemia in Trypanosoma brucei infection. Eukaryot Cell *9*, 934-942.

Emmer, B.T., Souther, C., Toriello, K.M., Olson, C.L., Epting, C.L., and Engman, D.M. (2009). Identification of a palmitoyl acyltransferase required for protein sorting to the flagellar membrane. J Cell Sci *122*, 867-874.

Engqvist, M.K., Esser, C., Maier, A., Lercher, M.J., and Maurino, V.G. (2014). Mitochondrial 2-hydroxyglutarate metabolism. Mitochondrion *19 Pt B*, 275-281.

Engstler, M., and Boshart, M. (2004). Cold shock and regulation of surface protein trafficking convey sensitization to inducers of stage differentiation in Trypanosoma brucei. Genes & development *18*, 2798-2811.

Estévez, A.M., Kempf, T., and Clayton, C. (2001). The exosome of Trypanosoma brucei. The EMBO journal *20*, 3831-3839.

Evans, D.A., and Brown, R.C. (1972). The utilization of glucose and proline by culture forms of Trypanosoma brucei. The Journal of protozoology *19*, 686-690.

Fairlamb, A.H., Blackburn, P., Ulrich, P., Chait, B.T., and Cerami, A. (1985). Trypanothione: a novel bis(glutathionyl)spermidine cofactor for glutathione reductase in trypanosomatids. Science (New York, NY) *227*, 1485-1487.

Fan, J., Teng, X., Liu, L., Mattaini, K.R., Looper, R.E., Vander Heiden, M.G., and Rabinowitz, J.D. (2015). Human phosphoglycerate dehydrogenase produces the oncometabolite D-2-hydroxyglutarate. ACS chemical biology *10*, 510-516.

Fatania, H.R., al-Nassar, K.E., and Thomas, N. (1993). Chemical modification of rat liver cytosolic NADP(+)-linked isocitrate dehydrogenase by N-ethylmaleimide. Evidence for essential sulphydryl groups. FEBS Lett *322*, 245-248.

Ferreira, L.M.R. (2010). Cancer metabolism: The Warburg effect today. Experimental and Molecular Pathology *89*, 372-380.

Filipp, F.V., Scott, D.A., Ronai, Z.A., Osterman, A.L., and Smith, J.W. (2012). Reverse TCA cycle flux through isocitrate dehydrogenases 1 and 2 is required for lipogenesis in hypoxic melanoma cells. Pigment cell & melanoma research *25*, 375-383.

Franco, J.R., Simarro, P.P., Diarra, A., and Jannin, J.G. (2014). Epidemiology of human African trypanosomiasis. Clinical Epidemiology *6*, 257-275.

Furger, A., Schurch, N., Kurath, U., and Roditi, I. (1997). Elements in the 3' untranslated region of procyclin mRNA regulate expression in insect forms of Trypanosoma brucei by modulating RNA stability and translation. Mol Cell Biol *17*, 4372-4380.

Gagnon, D., Foucher, A., Girard, I., and Ouellette, M. (2006). Stage specific gene expression and cellular localization of two isoforms of the serine hydroxymethyltransferase in the protozoan parasite Leishmania. Molecular and biochemical parasitology *150*, 63-71.

Gallagher, S.R. (2006). One-dimensional SDS gel electrophoresis of proteins. Current protocols in molecular biology / edited by Frederick M Ausubel [et al] *Chapter 10*, Unit 10.12A.

Gameiro, Paulo A., Yang, J., Metelo, Ana M., Pérez-Carro, R., Baker, R., Wang, Z., Arreola, A., Rathmell, W.K., Olumi, A., López-Larrubia, P*., et al.* (2013). In Vivo HIF-Mediated Reductive Carboxylation Is Regulated by Citrate Levels and Sensitizes VHL-Deficient Cells to Glutamine Deprivation. Cell Metabolism *17*, 372-385.

Geigy, R., Jenni, L., Kauffmann, M., Onyango, R.J., and Weiss, N. (1975). Identification of T. brucei-subgroup strains isolated from game. Acta tropica *32*, 190-205.

Geisbrecht, B.V., and Gould, S.J. (1999). The human PICD gene encodes a cytoplasmic and peroxisomal NADP(+)-dependent isocitrate dehydrogenase. The Journal of biological chemistry *274*, 30527-30533.

Gibson, W. (2015). Liaisons dangereuses: sexual recombination among pathogenic trypanosomes. Research in microbiology *166*, 459-466.

Gibson, W., and Bailey, M. (2003). The development of Trypanosoma brucei within the tsetse fly midgut observed using green fluorescent trypanosomes. Kinetoplastid Biol Dis *2*, 1.

Grab, D.J., and Kennedy, P.G. (2008). Traversal of human and animal trypanosomes across the blood-brain barrier. Journal of neurovirology *14*, 344-351.

Graham, S.V., and Barry, J.D. (1995). Transcriptional regulation of metacyclic variant surface glycoprotein gene expression during the life cycle of Trypanosoma brucei. Mol Cell Biol *15*, 5945-5956.

Graham, S.V., Matthews, K.R., and Barry, J.D. (1993). Trypanosoma brucei: unusual expression-site-associated gene homologies in a metacyclic VSG gene expression site. Experimental parasitology *76*, 96-99.

Gray, J.P., Alavian, K.N., Jonas, E.A., and Heart, E.A. (2012). NAD kinase regulates the size of the NADPH pool and insulin secretion in pancreatic β-cells. American Journal of Physiology - Endocrinology and Metabolism *303*, E191-E199.

Gross, S., Cairns, R.A., Minden, M.D., Driggers, E.M., Bittinger, M.A., Jang, H.G., Sasaki, M., Jin, S., Schenkein, D.P., Su, S.M*., et al.* (2010). Cancer-associated metabolite 2-hydroxyglutarate accumulates in acute myelogenous leukemia with isocitrate dehydrogenase 1 and 2 mutations. The Journal of experimental medicine *207*, 339-344.

Gualdron-López, M., Vapola, M.H., Miinalainen, I.J., Hiltunen, J.K., Michels, P.A.M., and Antonenkov, V.D. (2012). Channel-Forming Activities in the Glycosomal Fraction from the Bloodstream Form of <italic>Trypanosoma brucei</italic>. PloS one *7*, e34530.

Guerra, D.G., Decottignies, A., Bakker, B.M., and Michels, P.A. (2006). The mitochondrial FAD-dependent glycerol-3-phosphate dehydrogenase of Trypanosomatidae and the glycosomal redox balance of insect stages of Trypanosoma brucei and Leishmania spp. Molecular and biochemical parasitology *149*, 155-169.

Haanstra, J.R., van Tuijl, A., Kessler, P., Reijnders, W., Michels, P.A.M., Westerhoff, H.V., Parsons, M., and Bakker, B.M. (2008). Compartmentation prevents a lethal turbo-explosion of glycolysis in trypanosomes. Proceedings of the National Academy of Sciences *105*, 17718-17723.

Haines, L.R., Lehane, S.M., Pearson, T.W., and Lehane, M.J. (2010). Tsetse EP protein protects the fly midgut from trypanosome establishment. PLoS Pathog *6*, e1000793.

Hannaert, V., Albert, M.A., Rigden, D.J., da Silva Giotto, M.T., Thiemann, O., Garratt, R.C., Van Roy, J., Opperdoes, F.R., and Michels, P.A. (2003a). Kinetic characterization, structure modelling studies and crystallization of Trypanosoma brucei enolase. European journal of biochemistry / FEBS *270*, 3205-3213.

Hannaert, V., Bringaud, F., Opperdoes, F.R., and Michels, P.A. (2003b). Evolution of energy metabolism and its compartmentation in Kinetoplastida. Kinetoplastid Biol Dis *2*, 11.

Hao, Z., Kasumba, I., and Aksoy, S. (2003). Proventriculus (cardia) plays a crucial role in immunity in tsetse fly (Diptera: Glossinidiae). Insect Biochem Mol Biol *33*, 1155-1164.

Hatefi, Y., and Yamaguchi, M. (1996). Nicotinamide nucleotide transhydrogenase: a model for utilization of substrate binding energy for proton translocation. The FASEB Journal *10*, 444-452.

Hatzivassiliou, G., Zhao, F., Bauer, D.E., Andreadis, C., Shaw, A.N., Dhanak, D., Hingorani, S.R., Tuveson, D.A., and Thompson, C.B. (2005). ATP citrate lyase inhibition can suppress tumor cell growth. Cancer Cell *8*, 311-321.

Henke, B., Girzalsky, W., Berteaux-Lecellier, V., and Erdmann, R. (1998). IDP3 encodes a peroxisomal NADP-dependent isocitrate dehydrogenase required for the beta-oxidation of unsaturated fatty acids. The Journal of biological chemistry *273*, 3702-3711.

Hirayama, A., Kami, K., Sugimoto, M., Sugawara, M., Toki, N., Onozuka, H., Kinoshita, T., Saito, N., Ochiai, A., Tomita, M., *et al.* (2009). Quantitative metabolome profiling of colon and stomach cancer microenvironment by capillary electrophoresis time-of-flight mass spectrometry. Cancer research *69*, 4918-4925.

Holmgren, A., Johansson, C., Berndt, C., Lonn, M.E., Hudemann, C., and Lillig, C.H. (2005). Thiol redox control via thioredoxin and glutaredoxin systems. Biochemical Society transactions *33*, 1375-1377.

Hoppe, B. (2010). Evidence of true genotype-phenotype correlation in primary hyperoxaluria type 1. Kidney Int *77*, 383-385.

Horn, D., and McCulloch, R. (2010). Molecular mechanisms underlying the control of antigenic variation in African trypanosomes. Current opinion in microbiology *13*, 700-705.

Hotz, H.R., Hartmann, C., Huober, K., Hug, M., and Clayton, C. (1997). Mechanisms of developmental regulation in Trypanosoma brucei: a polypyrimidine tract in the 3'-untranslated region of a surface protein mRNA affects RNA abundance and translation. Nucleic acids research *25*, 3017-3026.

Hu, Y., and Aksoy, S. (2005). An antimicrobial peptide with trypanocidal activity characterized from Glossina morsitans morsitans. Insect Biochemistry and Molecular Biology *35*, 105-115.

Imabayashi, F., Aich, S., Prasad, L., and Delbaere, L.T. (2006). Substrate-free structure of a monomeric NADP isocitrate dehydrogenase: an open conformation phylogenetic relationship of isocitrate dehydrogenase. Proteins *63*, 100-112.

Inoue, H., Suzuki, F., Fukunishi, K., Adachi, K., and Takeda, Y. (1966). Studies on ATP Citrate Lyase of Rat Liver

I. Purification and Some Properties. The Journal of Biochemistry *60*, 543-553.

Jansen, G.A., and Wanders, R.J.A. (1993). l-2-Hydroxyglutarate dehydrogenase: identification of a novel enzyme activity in rat and human liver. Implications for l-2-hydroxyglutaric acidemia. Biochimica et Biophysica Acta (BBA) - Molecular Basis of Disease *1225*, 53-56.

Jo, S.H., Son, M.K., Koh, H.J., Lee, S.M., Song, I.H., Kim, Y.O., Lee, Y.S., Jeong, K.S., Kim, W.B., Park, J.W.*, et al.* (2001). Control of mitochondrial redox balance and cellular defense against oxidative damage by mitochondrial NADP+-dependent isocitrate dehydrogenase. The Journal of biological chemistry *276*, 16168-16176.

Kaleta, C., de Figueiredo, L.F., Werner, S., Guthke, R., Ristow, M., and Schuster, S. (2011). In silico evidence for gluconeogenesis from fatty acids in humans. PLoS computational biology *7*, e1002116.

Kalhan, S.C., Bugianesi, E., McCullough, A.J., Hanson, R.W., and Kelley, D.E. (2008). Estimates of Hepatic Glyceroneogenesis in Type 2 Diabetes in Humans. Metabolism: clinical and experimental *57*, 305-312.

Kaufman, E.E., Nelson, T., Fales, H.M., and Levin, D.M. (1988). Isolation and characterization of a hydroxyacid-oxoacid transhydrogenase from rat kidney mitochondria. The Journal of biological chemistry *263*, 16872-16879.

Keegan, F.P., and Blum, J.J. (1993). Incorporation of label from acetate and laurate into the mannan of Leishmania donovani via the glyoxylate cycle. The Journal of eukaryotic microbiology *40*, 730-732.

Kelly, S., Reed, J., Kramer, S., Ellis, L., Webb, H., Sunter, J., Salje, J., Marinsek, N., Gull, K., Wickstead, B.*, et al.* (2007). Functional genomics in Trypanosoma brucei: a collection of vectors for the expression of tagged proteins from endogenous and ectopic gene loci. Molecular and biochemical parasitology *154*, 103-109.

Kil, I.S., and Park, J.W. (2005). Regulation of mitochondrial NADP+-dependent isocitrate dehydrogenase activity by glutathionylation. The Journal of biological chemistry *280*, 10846-10854.

Kim, D.H., Achcar, F., Breitling, R., Burgess, K.E., and Barrett, M.P. (2015). LC-MS-based absolute metabolite quantification: application to metabolic flux measurement in trypanosomes. Metabolomics : Official journal of the Metabolomic Society *11*, 1721-1732.

Kim, H., Mozaffar, Z., and Weete, J.D. (1996). A dual cofactor-specific isocitrate dehydrogenase from Pythium ultimum. Canadian Journal of Microbiology *42*, 1241-1247.

Kim, J.-w., Tchernyshyov, I., Semenza, G.L., and Dang, C.V. (2006). HIF-1-mediated expression of pyruvate dehydrogenase kinase: A metabolic switch required for cellular adaptation to hypoxia. Cell Metabolism *3*, 177-185.

Knusel, S., and Roditi, I. (2013). Insights into the regulation of GPEET procyclin during differentiation from early to late procyclic forms of Trypanosoma brucei. Molecular and biochemical parasitology *191*, 66-74.

Kolev, N.G., Ramey-Butler, K., Cross, G.A., Ullu, E., and Tschudi, C. (2012). Developmental progression to infectivity in Trypanosoma brucei triggered by an RNA-binding protein. Science (New York, NY) *338*, 1352-1353.

Kornberg, H.L., and Krebs, H.A. (1957). Synthesis of cell constituents from C2-units by a modified tricarboxylic acid cycle. Nature *179*, 988-991.

Krauth-Siegel, R.L., and Comini, M.A. (2008). Redox control in trypanosomatids, parasitic protozoa with trypanothione-based thiol metabolism. Biochimica et biophysica acta *1780*, 1236-1248.

Kubi, C., van den Abbeele, J., R, D.E.D., Marcotty, T., Dorny, P., and van den Bossche, P. (2006). The effect of starvation on the susceptibility of teneral and non-teneral tsetse flies to trypanosome infection. Medical and veterinary entomology *20*, 388-392.

Kyhse-Andersen, J. (1984). Electroblotting of multiple gels: a simple apparatus without buffer tank for rapid transfer of proteins from polyacrylamide to nitrocellulose. Journal of biochemical and biophysical methods *10*, 203-209.

LaCount, D.J., Gruszynski, A.E., Grandgenett, P.M., Bangs, J.D., and Donelson, J.E. (2003). Expression and function of the Trypanosoma brucei major surface protease (GP63) genes. The Journal of biological chemistry *278*, 24658-24664.

Laemmli, U.K. (1970). Cleavage of structural proteins during the assembly of the head of bacteriophage T4. Nature *227*, 680-685.

Lamour, N., Riviere, L., Coustou, V., Coombs, G.H., Barrett, M.P., and Bringaud, F. (2005). Proline metabolism in procyclic Trypanosoma brucei is down-regulated in the presence of glucose. The Journal of biological chemistry *280*, 11902-11910.

LAZAR, T. (2003). Taiz, L. and Zeiger, E. Plant physiology. 3rd edn. Annals of Botany *91*, 750-751.

Le, A., Lane, Andrew N., Hamaker, M., Bose, S., Gouw, A., Barbi, J., Tsukamoto, T., Rojas, Camilio J., Slusher, Barbara S., Zhang, H.*, et al.* (2012). Glucose-Independent Glutamine Metabolism via TCA Cycling for Proliferation and Survival in B Cells. Cell Metabolism *15*, 110-121.

Lehane, M.J., Aksoy, S., Gibson, W., Kerhornou, A., Berriman, M., Hamilton, J., Soares, M.B., Bonaldo, M.F., Lehane, S., and Hall, N. (2003). Adult midgut expressed sequence tags from the tsetse fly Glossina morsitans morsitans and expression analysis of putative immune response genes. Genome biology *4*, R63.

Leonardi, R., Subramanian, C., Jackowski, S., and Rock, C.O. (2012). Cancer-associated Isocitrate Dehydrogenase Mutations Inactivate NADPH-dependent Reductive Carboxylation. The Journal of biological chemistry *287*, 14615-14620.

Leroux, A.E., Maugeri, D.A., Cazzulo, J.J., and Nowicki, C. (2011). Functional characterization of NADP-dependent isocitrate dehydrogenase isozymes from Trypanosoma cruzi. Molecular and biochemical parasitology *177*, 61-64.

Leterrier, M., Barroso, J.B., Valderrama, R., Palma, J.M., and Corpas, F.J. (2012). NADP-dependent isocitrate dehydrogenase from Arabidopsis roots contributes in the mechanism of defence against the nitro-oxidative stress induced by salinity. TheScientificWorldJournal *2012*, 694740.

Leyland, M.L., Hamblin, M.J., and Kelly, D.J. (1989). Eubacterial isocitrate dehydrogenase with dual specificity for NAD and NADP from Rhodomicrobium vannielii. FEMS Microbiology Letters *58*, 165-169.

Leyland, M.L., and Kelly, D.J. (1991). Purification and characterization of a monomeric isocitrate dehydrogenase with dual coenzyme specificity from the photosynthetic bacterium Rhodomicrobium vannielii. European journal of biochemistry / FEBS *202*, 85-93.

Lin, S., Morris, M.T., Ackroyd, P.C., Morris, J.C., and Christensen, K.A. (2013). Peptide-targeted delivery of a pH sensor for quantitative measurements of intraglycosomal pH in live Trypanosoma brucei. Biochemistry *52*, 3629-3637.

Liniger, M., Acosta-Serrano, A., Van Den Abbeele, J., Kunz Renggli, C., Brun, R., Englund, P.T., and Roditi, I. (2003). Cleavage of trypanosome surface glycoproteins by alkaline trypsin-like enzyme(s) in the midgut of Glossina morsitans. Int J Parasitol *33*, 1319-1328.

Linstead, D.J., Klein, R.A., and Cross, G.A. (1977). Threonine catabolism in Trypanosoma brucei. Journal of general microbiology *101*, 243-251.

Locasale, J.W. (2013). Serine, glycine and one-carbon units: cancer metabolism in full circle. Nat Rev Cancer *13*, 572-583.

Lukeš, J., Lys Guilbride, D., Votýpka, J., Zíková, A., Benne, R., and Englund, P.T. (2002). Kinetoplast DNA Network: Evolution of an Improbable Structure. Eukaryotic Cell *1*, 495-502.

Magni, G., Orsomando, G., and Raffaelli, N. (2006). Structural and functional properties of NAD kinase, a key enzyme in NADP biosynthesis. Mini reviews in medicinal chemistry *6*, 739-746.

Marciano, D., Llorente, C., Maugeri, D.A., de la Fuente, C., Opperdoes, F., Cazzulo, J.J., and Nowicki, C. (2008). Biochemical characterization of stage-specific isoforms of aspartate aminotransferases from Trypanosoma cruzi and Trypanosoma brucei. Molecular and biochemical parasitology *161*, 12-20.

Mazet, M., Morand, P., Biran, M., Bouyssou, G., Courtois, P., Daulouede, S., Millerioux, Y., Franconi, J.M., Vincendeau, P., Moreau, P.*, et al.* (2013). Revisiting the central metabolism of the bloodstream forms of Trypanosoma brucei: production of acetate in the mitochondrion is essential for parasite viability. PLoS neglected tropical diseases *7*, e2587.

McGuinness, E.T., and Butler, J.R. (1985). NAD+ kinase--a review. The International journal of biochemistry *17*, 1-11.

Mehlert, A., Treumann, A., and Ferguson, M.A. (1999). Trypanosoma brucei GPEET-PARP is phosphorylated on six out of seven threonine residues. Molecular and biochemical parasitology *98*, 291-296.

Metallo, C.M., Gameiro, P.A., Bell, E.L., Mattaini, K.R., Yang, J., Hiller, K., Jewell, C.M., Johnson, Z.R., Irvine, D.J., Guarente, L.*, et al.* (2011). Reductive glutamine metabolism by IDH1 mediates lipogenesis under hypoxia. Nature *481*, 380-384.

Mhamdi, A., and Noctor, G. (2015). Analysis of the roles of the Arabidopsis peroxisomal isocitrate dehydrogenase in leaf metabolism and oxidative stress. Environmental and Experimental Botany *114*, 22-29.

Michels, P.A., Bringaud, F., Herman, M., and Hannaert, V. (2006). Metabolic functions of glycosomes in trypanosomatids. Biochimica et biophysica acta *1763*, 1463-1477.

Michels, P.A., Hannaert, V., and Bringaud, F. (2000). Metabolic aspects of glycosomes in trypanosomatidae - new data and views. Parasitology today (Personal ed) *16*, 482-489.

Millard, P., Letisse, F., Sokol, S., and Portais, J.C. (2012). IsoCor: correcting MS data in isotope labeling experiments. Bioinformatics (Oxford, England) *28*, 1294-1296.

Millerioux, Y., Ebikeme, C., Biran, M., Morand, P., Bouyssou, G., Vincent, I.M., Mazet, M., Riviere, L., Franconi, J.-M., Burchmore, R.J.S.*, et al.* (2013). The threonine degradation pathway of the Trypanosoma brucei procyclic form: the main carbon source for lipid biosynthesis is under metabolic control. Molecular microbiology *90*, 114-129.

Millerioux, Y., Morand, P., Biran, M., Mazet, M., Moreau, P., Wargnies, M., Ebikeme, C., Deramchia, K., Gales, L., Portais, J.C.*, et al.* (2012). ATP synthesis-coupled and -uncoupled acetate production from acetyl-CoA by mitochondrial acetate:succinate CoA-transferase and acetyl-CoA thioesterase in Trypanosoma. The Journal of biological chemistry *287*, 17186-17197.

Montal, E.D., Dewi, R., Bhalla, K., Ou, L., Hwang, B.J., Ropell, A.E., Gordon, C., Liu, W.J., DeBerardinis, R.J., Sudderth, J.*, et al.* (2015). PEPCK Coordinates the Regulation of Central Carbon Metabolism to Promote Cancer Cell Growth. Mol Cell.

Morris, J.C., Wang, Z., Drew, M.E., and Englund, P.T. (2002). Glycolysis modulates trypanosome glycoprotein expression as revealed by an RNAi library. The EMBO journal *21*, 4429-4438.

Mowatt, M.R., and Clayton, C.E. (1987). Developmental regulation of a novel repetitive protein of Trypanosoma brucei. Molecular and Cellular Biology *7*, 2838-2844.

Mullen, A.R., Wheaton, W.W., Jin, E.S., Chen, P.-H., Sullivan, L.B., Cheng, T., Yang, Y., Linehan, W.M., Chandel, N.S., and DeBerardinis, R.J. (2012). Reductive carboxylation supports growth in tumour cells with defective mitochondria. Nature *481*, 385-388.

Nayduch, D., and Aksoy, S. (2007). Refractoriness in tsetse flies (Diptera: Glossinidae) may be a matter of timing. Journal of medical entomology *44*, 660-665.

Nishiya, Y., and Imanaka, T. (1998). Purification and characterization of a novel glycine oxidase from Bacillus subtilis. FEBS Lett *438*, 263-266.

Nocito, L., Kleckner, A.S., Yoo, E.J., Jones Iv, A.R., Liesa, M., and Corkey, B.E. (2015). The extracellular redox state modulates mitochondrial function, gluconeogenesis, and glycogen synthesis in murine hepatocytes. PloS one *10*, e0122818.

Nolan, D.P., Jackson, D.G., Biggs, M.J., Brabazon, E.D., Pays, A., Van Laethem, F., Paturiaux-Hanocq, F., Elliott, J.F., Voorheis, H.P., and Pays, E. (2000). Characterization of a novel alanine-rich protein located in surface microdomains in Trypanosoma brucei. The Journal of biological chemistry *275*, 4072-4080.

Nolan, D.P., and Voorheis, H.P. (1992). The mitochondrion in bloodstream forms of Trypanosoma brucei is energized by the electrogenic pumping of protons catalysed by the F1F0-ATPase. European journal of biochemistry / FEBS *209*, 207-216.

Nuttall, F.Q., Ngo, A., and Gannon, M.C. (2008). Regulation of hepatic glucose production and the role of gluconeogenesis in humans: is the rate of gluconeogenesis constant? Diabetes/Metabolism Research and Reviews *24*, 438-458.

Nwagwu, M., and Opperdoes, F.R. (1982). Regulation of glycolysis in Trypanosoma brucei: hexokinase and phosphofructokinase activity. Acta tropica *39*, 61-72.

Oberle, M., Balmer, O., Brun, R., and Roditi, I. (2010). Bottlenecks and the maintenance of minor genotypes during the life cycle of Trypanosoma brucei. PLoS Pathog *6*, e1001023.

Opperdoes, F.R., and Borst, P. (1977). Localization of nine glycolytic enzymes in a microbody-like organelle in Trypanosoma brucei: The glycosome. FEBS Letters *80*, 360-364.

Opperdoes, F.R., and Coombs, G.H. (2007). Metabolism of Leishmania: proven and predicted. Trends in parasitology *23*, 149-158.

Otieno, L.H., and Darji, N. (1979). The abundance of pathogenic African trypanosomes in the salivary secretions of wild Glossina pallidipes. Annals of tropical medicine and parasitology *73*, 583-588.

Overath, P., Czichos, J., and Haas, C. (1986). The effect of citrate/cis-aconitate on oxidative metabolism during transformation of Trypanosoma brucei. European Journal of Biochemistry *160*, 175-182.

Owen, O.E., Kalhan, S.C., and Hanson, R.W. (2002). The Key Role of Anaplerosis and Cataplerosis for Citric Acid Cycle Function. Journal of Biological Chemistry *277*, 30409-30412.

Peacock, L., Bailey, M., Carrington, M., and Gibson, W. (2014). Meiosis and haploid gametes in the pathogen Trypanosoma brucei. Current biology : CB *24*, 181-186.

Peacock, L., Ferris, V., Bailey, M., and Gibson, W. (2012). The influence of sex and fly species on the development of trypanosomes in tsetse flies. PLoS neglected tropical diseases *6*, e1515.

Peacock, L., Ferris, V., Sharma, R., Sunter, J., Bailey, M., Carrington, M., and Gibson, W. (2011). Identification of the meiotic life cycle stage of Trypanosoma brucei in the tsetse fly. Proceedings of the National Academy of Sciences *108*, 3671-3676.

Pey, A.L., Albert, A., and Salido, E. (2013). Protein Homeostasis Defects of Alanine-Glyoxylate Aminotransferase: New Therapeutic Strategies in Primary Hyperoxaluria Type I. BioMed Research International *2013*, 15.

Potter, S. (1993). Evidence for a dual-specificity isocitrate dehydrogenase in the euryarchaeotan Thermoplasma acidophilum. Canadian Journal of Microbiology *39*, 262-264.

Priest, J.W., and Hajduk, S.L. (1994). Developmental regulation of Trypanosoma brucei cytochrome c reductase during bloodstream to procyclic differentiation. Molecular and biochemical parasitology *65*, 291-304.

Pusch, S., Schweizer, L., Beck, A.-C., Lehmler, J.-M., Weissert, S., Balss, J., Miller, A.K., and von Deimling, A. (2014). D-2-Hydroxyglutarate producing neo-enzymatic activity inversely correlates with frequency of the type of isocitrate dehydrogenase 1 mutations found in glioma. Acta Neuropathologica Communications *2*, 19-19.

Quartararo, C.E., Hadi, T., Cahill, S.M., and Blanchard, J.S. (2013). Solvent isotope-induced equilibrium perturbation for isocitrate lyase. Biochemistry *52*, 9286-9293.

Reeves, H.C., and Ajl, S.J. (1962). ALPHA-HYDROXYGLUTARIC ACID SYNTHETASE. Journal of bacteriology *84*, 186-187.

Reshef, L., Hanson, R.W., and Ballard, F.J. (1970). A possible physiological role for glyceroneogenesis in rat adipose tissue. The Journal of biological chemistry *245*, 5979-5984.

Reuner, B., Vassella, E., Yutzy, B., and Boshart, M. (1997). Cell density triggers slender to stumpy differentiation of Trypanosoma brucei bloodstream forms in culture. Molecular and biochemical parasitology *90*, 269-280.

Richardson, J.P., Jenni, L., Beecroft, R.P., and Pearson, T.W. (1986). Procyclic tsetse fly midgut forms and culture forms of African trypanosomes share stage- and species-specific surface antigens identified by monoclonal antibodies. Journal of immunology (Baltimore, Md : 1950) *136*, 2259-2264.

Rico, E., Rojas, F., Mony, B.M., Szoor, B., MacGregor, P., and Matthews, K.R. (2013). Bloodstream form pre-adaptation to the tsetse fly in Trypanosoma brucei. Frontiers in Cellular and Infection Microbiology *3*, 78.

Riviere, L., Moreau, P., Allmann, S., Hahn, M., Biran, M., Plazolles, N., Franconi, J.M., Boshart, M., and Bringaud, F. (2009). Acetate produced in the mitochondrion is the essential precursor for lipid biosynthesis in procyclic trypanosomes. Proceedings of the National Academy of Sciences of the United States of America *106*, 12694-12699.

Riviere, L., van Weelden, S.W., Glass, P., Vegh, P., Coustou, V., Biran, M., van Hellemond, J.J., Bringaud, F., Tielens, A.G., and Boshart, M. (2004). Acetyl:succinate CoA-transferase in procyclic Trypanosoma brucei. Gene identification and role in carbohydrate metabolism. The Journal of biological chemistry *279*, 45337-45346.

Roditi, I., Carrington, M., and Turner, M. (1987). Expression of a polypeptide containing a dipeptide repeat is confined to the insect stage of Trypanosoma brucei. Nature *325*, 272-274.

Roditi, I., Furger, A., Ruepp, S., Schurch, N., and Butikofer, P. (1998). Unravelling the procyclin coat of Trypanosoma brucei. Molecular and biochemical parasitology *91*, 117-130.

Roldán, A., Comini, M.A., Crispo, M., and Krauth-Siegel, R.L. (2011). Lipoamide dehydrogenase is essential for both bloodstream and procyclic Trypanosoma brucei. Molecular microbiology *81*, 623-639.

Rosman, K.J.R.a.T.P.D.P. (1998). Isotopic composition of the elements 1997. IUPAC Pure and Applied Chemistry *70*, 217-235.

Rotureau, B., Subota, I., Buisson, J., and Bastin, P. (2012). A new asymmetric division contributes to the continuous production of infective trypanosomes in the tsetse fly. Development *139*, 1842-1850.

ROTUREAU, B., and VAN DEN ABBEELE, J. (2013). Through the dark continent: African trypanosome developments in the tsetse fly. Frontiers in Cellular and Infection Microbiology *3*.

Rua, J., Soler, J., Busto, F., and de Arriaga, D. (1995). The pH dependence and modification by diethyl pyrocarbonate of isocitrate lyase from Phycomyces blakesleeanus. European journal of biochemistry / FEBS *232*, 381-390.

Ryley, J.F. (1962). Studies on the metabolism of the protozoa. 9. Comparative metabolism of blood-stream and culture forms of Trypanosoma rhodesiense. Biochemical Journal *85*, 211-223.

Rzem, R., Veiga-da-Cunha, M., Noel, G., Goffette, S., Nassogne, M.C., Tabarki, B., Scholler, C., Marquardt, T., Vikkula, M., and Van Schaftingen, E. (2004). A gene encoding a putative FAD-dependent L-2-hydroxyglutarate dehydrogenase is mutated in L-2-hydroxyglutaric aciduria. Proceedings of the National Academy of Sciences of the United States of America *101*, 16849-16854.

Rzem, R., Vincent, M.F., Van Schaftingen, E., and Veiga-da-Cunha, M. (2007). -L 2-hydroxyglutaric aciduria, a defect of metabolite repair. Journal of inherited metabolic disease *30*, 681-689.

Saas, J., Ziegelbauer, K., von Haeseler, A., Fast, B., and Boshart, M. (2000). A developmentally regulated aconitase related to iron-regulatory protein-1 is localized in the cytoplasm and in the mitochondrion of Trypanosoma brucei. The Journal of biological chemistry *275*, 2745-2755.

Schlecker, T., Schmidt, A., Dirdjaja, N., Voncken, F., Clayton, C., and Krauth-Siegel, R.L. (2005). Substrate specificity, localization, and essential role of the glutathione peroxidase-type tryparedoxin peroxidases in Trypanosoma brucei. The Journal of biological chemistry *280*, 14385-14394.

Schnaufer, A., Clark-Walker, G.D., Steinberg, A.G., and Stuart, K. (2005). The F(1)-ATP synthase complex in bloodstream stage trypanosomes has an unusual and essential function. The EMBO journal *24*, 4029-4040.

Schumann Burkard, G., Kaser, S., de Araujo, P.R., Schimanski, B., Naguleswaran, A., Knusel, S., Heller, M., and Roditi, I. (2013). Nucleolar proteins regulate stage-specific gene expression and ribosomal RNA maturation in Trypanosoma brucei. Molecular microbiology *88*, 827-840.

Seed, J.R., and Wenck, M.A. (2003). Role of the long slender to short stumpy transition in the life cycle of the african trypanosomes. Kinetoplastid Biology and Disease *2*, 3-3.

Semenza, G.L. (2010). HIF-1: upstream and downstream of cancer metabolism. Current Opinion in Genetics & Development *20*, 51-56.

Sharma, R., Peacock, L., Gluenz, E., Gull, K., Gibson, W., and Carrington, M. (2008). Asymmetric cell division as a route to reduction in cell length and change in cell morphology in trypanosomes. Protist *159*, 137-151.

Shechter, I., Dai, P., Huo, L., and Guan, G. (2003). IDH1 gene transcription is sterol regulated and activated by SREBP-1a and SREBP-2 in human hepatoma HepG2 cells: evidence that IDH1 may regulate lipogenesis in hepatic cells. Journal of Lipid Research *44*, 2169-2180.

Shin, S.W., Oh, C.J., Kil, I.S., and Park, J.W. (2009). Glutathionylation regulates cytosolic NADP+-dependent isocitrate dehydrogenase activity. Free radical research *43*, 409-416.

Shinoda, K., Shinoda, W., Baba, T., and Mikami, M. (2004). Comparative molecular dynamics study of ether- and ester-linked phospholipid bilayers. The Journal of chemical physics *121*, 9648-9654.

Simon, M.W., Martin, E., and Mukkada, A.J. (1978). Evidence for a functional glyoxylate cycle in the leishmaniae. Journal of bacteriology *135*, 895-899.

Smolkova, K., Dvorak, A., Zelenka, J., Vitek, L., and Jezek, P. (2015). Reductive carboxylation and 2-hydroxyglutarate formation by wild-type IDH2 in breast carcinoma cells. The international journal of biochemistry & cell biology *65*, 125-133.

Smolková, K., and Ježek, P. (2012). The Role of Mitochondrial NADPH-Dependent Isocitrate Dehydrogenase in Cancer Cells. International Journal of Cell Biology *2012*, 12.

Smyth, G.E., and Colman, R.F. (1991). Cysteinyl peptides of pig heart NADP-dependent isocitrate dehydrogenase that are modified upon inactivation by N-ethylmaleimide. The Journal of biological chemistry *266*, 14918-14925.

Someya, S., Yu, W., Hallows, W.C., Xu, J., Vann, J.M., Leeuwenburgh, C., Tanokura, M., Denu, J.M., and Prolla, T.A. (2010). Sirt3 Mediates Reduction of Oxidative Damage and Prevention of Age-Related Hearing Loss under Caloric Restriction. Cell *143*, 802-812.

Spitznagel, D., Ebikeme, C., Biran, M., Nic a' Bhaird, N., Bringaud, F., Henehan, G.T., and Nolan, D.P. (2009). Alanine aminotransferase of Trypanosoma brucei--a key role in proline metabolism in procyclic life forms. The FEBS journal *276*, 7187-7199.

Stark, R., Guebre-Egziabher, F., Zhao, X., Feriod, C., Dong, J., Alves, T.C., Ioja, S., Pongratz, R.L., Bhanot, S., Roden, M.*, et al.* (2014). A role for mitochondrial phosphoenolpyruvate carboxykinase (PEPCK-M) in the regulation of hepatic gluconeogenesis. The Journal of biological chemistry *289*, 7257-7263.

Stijlemans, B., Leng, L., Brys, L., Sparkes, A., Vansintjan, L., Caljon, G., Raes, G., Van Den Abbeele, J., Van Ginderachter, J.A., Beschin, A.*, et al.* (2014). MIF Contributes to <italic>Trypanosoma brucei</italic> Associated Immunopathogenicity Development. PLoS Pathog *10*, e1004414.

Struys, E.A. (2013). 2-Hydroxyglutarate is not a metabolite; d-2-hydroxyglutarate and l-2-hydroxyglutarate are! Proceedings of the National Academy of Sciences *110*, E4939.

Stubbs, M., Veech, R.L., and Krebs, H.A. (1972). Control of the redox state of the nicotinamide–adenine dinucleotide couple in rat liver cytoplasm. Biochemical Journal *126*, 59-65.

Surve, S., Heestand, M., Panicucci, B., Schnaufer, A., and Parsons, M. (2012). Enigmatic presence of mitochondrial complex I in Trypanosoma brucei bloodstream forms. Eukaryot Cell *11*, 183-193.

Sykes, S., Szempruch, A., and Hajduk, S. (2015). The krebs cycle enzyme alpha-ketoglutarate decarboxylase is an essential glycosomal protein in bloodstream African trypanosomes. Eukaryot Cell *14*, 206-215.

Sykes, S.E., and Hajduk, S.L. (2013). Dual Functions of α-Ketoglutarate Dehydrogenase E2 in the Krebs Cycle and Mitochondrial DNA Inheritance in Trypanosoma brucei. Eukaryot Cell *12*, 78-90.

Szafrański, S.P., Deng, Z.-L., Tomasch, J., Jarek, M., Bhuju, S., Meisinger, C., Kühnisch, J., Sztajer, H., and Wagner-Döbler, I. (2015). Functional biomarkers for chronic periodontitis and insights into the roles of Prevotella nigrescens and Fusobacterium nucleatum; a metatranscriptome analysis. Npj Biofilms And Microbiomes *1*, 15017.

Taymaz-Nikerel, H., de Mey, M., Ras, C., ten Pierick, A., Seifar, R.M., van Dam, J.C., Heijnen, J.J., and van Gulik, W.M. (2009). Development and application of a differential method for reliable metabolome analysis in Escherichia coli. Anal Biochem *386*, 9-19.

Thevelein, J.M., and Hohmann, S. (1995). Trehalose synthase: guard to the gate of glycolysis in yeast? Trends in Biochemical Sciences *20*, 3-10.

Treumann, A., Zitzmann, N., Hulsmeier, A., Prescott, A.R., Almond, A., Sheehan, J., and Ferguson, M.A. (1997). Structural characterisation of two forms of procyclic acidic repetitive protein expressed by procyclic forms of Trypanosoma brucei. Journal of molecular biology *269*, 529-547.

Tyler, K.M., Fridberg, A., Toriello, K.M., Olson, C.L., Cieslak, J.A., Hazlett, T.L., and Engman, D.M. (2009). Flagellar membrane localization via association with lipid rafts. Journal of Cell Science *122*, 859-866.

Urwyler, S., Studer, E., Renggli, C.K., and Roditi, I. (2007). A family of stage-specific alanine-rich proteins on the surface of epimastigote forms of Trypanosoma brucei. Molecular microbiology *63*, 218-228.

Urwyler, S., Vassella, E., Van Den Abbeele, J., Renggli, C.K., Blundell, P., Barry, J.D., and Roditi, I. (2005). Expression of procyclin mRNAs during cyclical transmission of Trypanosoma brucei. PLoS Pathog *1*, e22.

Van Den Abbeele, J., Claes, Y., van Bockstaele, D., Le Ray, D., and Coosemans, M. (1999). Trypanosoma brucei spp. development in the tsetse fly: characterization of the post-mesocyclic stages in the foregut and proboscis. Parasitology *118 (Pt 5)*, 469-478.

Van Hellemond, J.J., Opperdoes, F.R., and Tielens, A.G. (1998a). Trypanosomatidae produce acetate via a mitochondrial acetate:succinate CoA transferase. Proceedings of the National Academy of Sciences of the United States of America *95*, 3036-3041.

Van Hellemond, J.J., Opperdoes, F.R., and Tielens, A.G.M. (1998b). Trypanosomatidae produce acetate via a mitochondrial acetate:succinate CoA transferase. Proceedings of the National Academy of Sciences *95*, 3036-3041.

van Roermund, C.W.T., Hettema, E.H., Kal, A.J., van den Berg, M., Tabak, H.F., and Wanders, R.J.A. (1998). Peroxisomal β-oxidation of polyunsaturated fatty acids in Saccharomyces cerevisiae: isocitrate dehydrogenase provides NADPH for reduction of double bonds at even positions. The EMBO journal *17*, 677-687.

Van Schaftingen, E., Rzem, R., and Veiga-da-Cunha, M. (2009). L: -2-Hydroxyglutaric aciduria, a disorder of metabolite repair. Journal of inherited metabolic disease *32*, 135-142.

van Weelden, S.W., Fast, B., Vogt, A., van der Meer, P., Saas, J., van Hellemond, J.J., Tielens, A.G., and Boshart, M. (2003). Procyclic Trypanosoma brucei do not use Krebs cycle activity for energy generation. The Journal of biological chemistry *278*, 12854-12863.

van Weelden, S.W., van Hellemond, J.J., Opperdoes, F.R., and Tielens, A.G. (2005). New functions for parts of the Krebs cycle in procyclic Trypanosoma brucei, a cycle not operating as a cycle. The Journal of biological chemistry *280*, 12451-12460.

Vander Heiden, M.G., Cantley, L.C., and Thompson, C.B. (2009). Understanding the Warburg Effect: The Metabolic Requirements of Cell Proliferation. Science (New York, NY) *324*, 1029-1033.

Vanhamme, L., Paturiaux-Hanocq, F., Poelvoorde, P., Nolan, D.P., Lins, L., Van Den Abbeele, J., Pays, A., Tebabi, P., Van Xong, H., Jacquet, A.*, et al.* (2003). Apolipoprotein L-I is the trypanosome lytic factor of human serum. Nature *422*, 83-87.

Vassella, E., Acosta-Serrano, A., Studer, E., Lee, S.H., Englund, P.T., and Roditi, I. (2001). Multiple procyclin isoforms are expressed differentially during the development of insect forms of Trypanosoma brucei. Journal of molecular biology *312*, 597-607.

Vassella, E., Den Abbeele, J.V., Butikofer, P., Renggli, C.K., Furger, A., Brun, R., and Roditi, I. (2000). A major surface glycoprotein of trypanosoma brucei is expressed transiently during development and can be regulated post-transcriptionally by glycerol or hypoxia. Genes & development *14*, 615-626.

Vassella, E., Probst, M., Schneider, A., Studer, E., Renggli, C.K., and Roditi, I. (2004). Expression of a Major Surface Protein of Trypanosoma brucei Insect Forms Is Controlled by the Activity of Mitochondrial Enzymes. Molecular Biology of the Cell *15*, 3986-3993.

Vickerman, K. (1965). Polymorphism and mitochondrial activity in sleeping sickness trypanosomes. Nature *208*, 762-766.

Vickerman, K. (1985). Developmental cycles and biology of pathogenic trypanosomes. British medical bulletin *41*, 105-114.

Vickerman, K., Tetley, L., Hendry, K.A., and Turner, C.M. (1988). Biology of African trypanosomes in the tsetse fly. Biology of the cell / under the auspices of the European Cell Biology Organization *64*, 109-119.

Villas-Bôas, S.G., and Bruheim, P. (2007). Cold glycerol–saline: The promising quenching solution for accurate intracellular metabolite analysis of microbial cells. Analytical Biochemistry *370*, 87-97.

Villas-Boas, S.G., Kesson, M., and Nielsen, J. (2005). Biosynthesis of glyoxylate from glycine in Saccharomyces cerevisiae. FEMS yeast research *5*, 703-709.

Vincent, Emma E., Sergushichev, A., Griss, T., Gingras, M.-C., Samborska, B., Ntimbane, T., Coelho, Paula P., Blagih, J., Raissi, Thomas C., Choinière, L.*, et al.* Mitochondrial Phosphoenolpyruvate Carboxykinase Regulates Metabolic Adaptation and Enables Glucose-Independent Tumor Growth. Molecular Cell *60*, 195-207.

Vincent, I.M., Creek, D.J., Burgess, K., Woods, D.J., Burchmore, R.J., and Barrett, M.P. (2012). Untargeted metabolomics reveals a lack of synergy between nifurtimox and eflornithine against Trypanosoma brucei. PLoS neglected tropical diseases *6*, e1618.

Visser, N., and Opperdoes, F.R. (1980). Glycolysis in Trypanosoma brucei. European journal of biochemistry / FEBS *103*, 623-632.

Visser, W.F., van Roermund, C.W., Ijlst, L., Hellingwerf, K.J., Waterham, H.R., and Wanders, R.J. (2006). First identification of a 2-ketoglutarate/isocitrate transport system in mammalian peroxisomes and its characterization. Biochemical and biophysical research communications *348*, 1224-1231.

Vital, M., Howe, A.C., and Tiedje, J.M. (2014). Revealing the bacterial butyrate synthesis pathways by analyzing (meta)genomic data. mBio *5*, e00889.

Walshe, D.P., Lehane, M.J., and Haines, L.R. (2011). Post eclosion age predicts the prevalence of midgut trypanosome infections in Glossina. PloS one *6*, e26984.

Wang, P., Lv, C., and Zhu, G. (2015). Novel Type II and Monomeric NAD(+) Specific Isocitrate Dehydrogenases: Phylogenetic Affinity, Enzymatic Characterization, and Evolutionary Implication. Sci Rep *5*.

Warburg, O. (1925). The Metabolism of Carcinoma Cells. The Journal of Cancer Research *9*, 148-163.

Ward, P.S., Patel, J., Wise, D.R., Abdel-Wahab, O., Bennett, B.D., Coller, H.A., Cross, J.R., Fantin, V.R., Hedvat, C.V., Perl, A.E.*, et al.* (2010). The Common Feature of Leukemia-Associated IDH1 and IDH2 Mutations Is a Neomorphic Enzyme Activity Converting α-Ketoglutarate to 2-Hydroxyglutarate. Cancer Cell *17*, 225-234.

Weiss, B.L., Wang, J., Maltz, M.A., Wu, Y., and Aksoy, S. (2013). Trypanosome Infection Establishment in the Tsetse Fly Gut Is Influenced by Microbiome-Regulated Host Immune Barriers. PLoS Pathog *9*, e1003318.

Wilkinson, S.R., Prathalingam, S.R., Taylor, M.C., Ahmed, A., Horn, D., and Kelly, J.M. (2006). Functional characterisation of the iron superoxide dismutase gene repertoire in Trypanosoma brucei. Free radical biology & medicine *40*, 198-209.

Wirtz, E., Leal, S., Ochatt, C., and Cross, G.A. (1999). A tightly regulated inducible expression system for conditional gene knock-outs and dominant-negative genetics in Trypanosoma brucei. Molecular and biochemical parasitology *99*, 89-101.

Wise, D.R., Ward, P.S., Shay, J.E.S., Cross, J.R., Gruber, J.J., Sachdeva, U.M., Platt, J.M., DeMatteo, R.G., Simon, M.C., and Thompson, C.B. (2011). Hypoxia promotes isocitrate dehydrogenase-dependent carboxylation of α-ketoglutarate to citrate to support cell growth and viability. Proceedings of the National Academy of Sciences *108*, 19611-19616.

Woods, A., Sherwin, T., Sasse, R., MacRae, T.H., Baines, A.J., and Gull, K. (1989). Definition of individual components within the cytoskeleton of Trypanosoma brucei by a library of monoclonal antibodies. Journal of Cell Science *93*, 491-500.

Wu, Y., Deford, J., Benjamin, R., Lee, M.G., and Ruben, L. (1994). The gene family of EF-hand calcium-binding proteins from the flagellum of Trypanosoma brucei. Biochemical Journal *304 (Pt 3)*, 833-841.

Xu, W., Yang, H., Liu, Y., Yang, Y., Wang, P., Kim, S.H., Ito, S., Yang, C., Wang, P., Xiao, M.T.*, et al.* (2011). Oncometabolite 2-hydroxyglutarate is a competitive inhibitor of alpha-ketoglutarate-dependent dioxygenases. Cancer Cell *19*, 17-30.

Xu, X., Zhao, J., Xu, Z., Peng, B., Huang, Q., Arnold, E., and Ding, J. (2004). Structures of human cytosolic NADP-dependent isocitrate dehydrogenase reveal a novel self-regulatory mechanism of activity. The Journal of biological chemistry *279*, 33946-33957.

Yan, H., Parsons, D.W., Jin, G., McLendon, R., Rasheed, B.A., Yuan, W., Kos, I., Batinic-Haberle, I., Jones, S., Riggins, G.J.*, et al.* (2009). IDH1 and IDH2 Mutations in Gliomas. New England Journal of Medicine *360*, 765-773.

Yu, W., Dittenhafer-Reed, K.E., and Denu, J.M. (2012). SIRT3 protein deacetylates isocitrate dehydrogenase 2 (IDH2) and regulates mitochondrial redox status. The Journal of biological chemistry *287*, 14078-14086.

Zamze, S.E., Ferguson, M.A., Collins, R., Dwek, R.A., and Rademacher, T.W. (1988). Characterization of the cross-reacting determinant (CRD) of the glycosyl-phosphatidylinositol membrane anchor of Trypanosoma brucei variant surface glycoprotein. European journal of biochemistry / FEBS *176*, 527-534.

Zhang, J., Pierick, A.t., van Rossum, H.M., Maleki Seifar, R., Ras, C., Daran, J.-M., Heijnen, J.J., and Aljoscha Wahl, S. (2015). Determination of the Cytosolic NADPH/NADP Ratio in Saccharomyces cerevisiae using Shikimate Dehydrogenase as Sensor Reaction. Scientific Reports *5*, 12846.

Zhao, S., Lin, Y., Xu, W., Jiang, W., Zha, Z., Wang, P., Yu, W., Li, Z., Gong, L., Peng, Y., *et al.* (2009). Glioma-Derived Mutations in IDH1 Dominantly Inhibit IDH1 Catalytic Activity and Induce HIF-1α. Science (New York, NY) *324*, 261-265.

Zhu, G., Golding, G.B., and Dean, A.M. (2005). The Selective Cause of an Ancient Adaptation. Science (New York, NY) *307*, 1279-1282.

Ziegelbauer, K., Quinten, M., Schwarz, H., Pearson, T.W., and Overath, P. (1990). Synchronous differentiation of Trypanosoma brucei from bloodstream to procyclic forms in vitro. European journal of biochemistry / FEBS *192*, 373-378.

Zikova, A., Schnaufer, A., Dalley, R.A., Panigrahi, A.K., and Stuart, K.D. (2009). The F(0)F(1)-ATP synthase complex contains novel subunits and is essential for procyclic Trypanosoma brucei. PLoS Pathog *5*, e1000436.

Acknowledgements

Zuallererst möchte ich mich herzlich bei Prof. Dr. Michael Boshart für das interessante Projekt und die hervorragende Betreuung bedanken. Sehr schätzte ich die gemeinsame Planung und Ausarbeitung des Projekts und die Möglichkeit auch eigene Hypothesen zu verfolgen. Vielen Dank für die Gelegenheit das Projekt auch auf internationalen Kongressen vorzustellen.

Prof. Dr. Kai Papenfort möchte ich dafür danken, meine Thesis als zweiter Gutachter zu bewerten und das Gutachten zu verfassen.

I would like to express my sincere gratitude to our cooperation partners for the numerous fruitful discussions, their expertise and planning joint projects. I would like to gratefully acknowledge the scientific support and collaboration with the lab of Dr. Jean-Charles Portais and Prof. Dr. Wolfgang Eisenreich. I would like to give special thanks to Dr. Frédéric Bringaud and Dr. Daniel Inaoka for the exchange of data and cell lines.

Special thanks goes to the former and present lab members of the AG Boshart for being so friendly and creating a very nice working atmosphere. Namely I would like to thank Eleni, Sabine, Flo, Ana, George, Matt and Yuri. Special thanks goes to Stefan for his continuous support in continuing his project. A big thank you goes to Larissa for making life in lab easier.

Zu guter Letzt möchte ich mich herzlich bei meinen Eltern, meiner Oma und meinem Bruder für ihre stetige Unterstützung, Rückhalt und ihre Geduld bedanken. Auch meinem Freund Michael und seiner Familie möchte ich hier ausdrücklich danken, sowie meinen Freunden, ganz besonders Paulina, dafür, dass sie immer für mich da sind.

Curriculum Vitae

Personal Information

Name	Nicole Emmy Ziebart
Date of Birth	12th November, 1987
Place of Birth	Dresden
Nationality	Germany

Education

10/2012-4/2016	Ph.D. student at the lab of Prof. Boshart Ludwig-Maximilians Universität München (LMU), Germany Enrolled in the LMU Graduate School of Life Sciences (LSM) Project: Metabolism and Differentiation in Trypanosoma brucei
9/2010- 9/2012	M.Sc. Molecular Biosciences- Major Infectious Diseases Ruprecht-Karls Universität, Heidelberg, Germany Majors: Immunology, Parasitology, Microbiology and Virology
9/2007-8/2010	B.Sc. Molecular Cell Biology Ruprecht-Karls Universität, Heidelberg, Germany Majors: Biochemistry, Molecular and Cellular Biology
7/2007	German Abitur (Secondary high school diploma) Biotechnological Gymnasium, Heidelberg, Germany

Publications

2010 Ceylan S, Seidel V, Ziebart N, Berndt C, Dirdjaja N, and Krauth-Siegel RL The Dithiol Glutaredoxins of African Trypanosomes Have Distinct Roles and Are Closely Linked to the Unique Trypanothione Metabolism J. Biol. Chem. 285: 35224-35237 doi:10.1074/jbc.M110.165860

2014 Allmann S, Mazet M, Ziebart N, Bouyssou G, Fouillen L, et al. Triacylglycerol Storage in Lipid Droplets in Procyclic Trypanosoma brucei. PLoS ONE 9(12): e114628. doi:10.1371/journal.pone.0114628